

สเปกโทรสโกปีการทะลุผ่านของรอยต่อระหว่างตัวนำวดยิ่งกับ
แก๊สอิเล็กตรอนสองมิติที่มีคู่ควบของสปินและออร์บิทัลแบบรัศนา

นางสาวเบญจมาศ ศรีสองเมือง

วิทยานิพนธ์นี้เป็นส่วนหนึ่งของการศึกษาตามหลักสูตรปริญญาวิทยาศาสตรดุษฎีบัณฑิต
สาขาวิชาฟิสิกส์
มหาวิทยาลัยเทคโนโลยีสุรนารี
ปีการศึกษา 2550

**TUNNELING SPECTROSCOPY OF
SUPERCONDUCTOR/TWO-DIMENSIONAL ELECTRON
GAS WITH RASHBA SPIN-ORBIT COUPLING
JUNCTION**

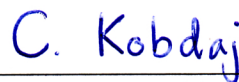
Benjamat Srisongmuang

**A Thesis Submitted in Partial Fulfillment of the Requirements for the
Degree of Doctor Philosophy in Physics
Suranaree University of Technology
Academic Year 2007**

TUNNELING SPECTROSCOPY OF SUPERCONDUCTOR/TWO-DIMENSIONAL ELECTRON GAS WITH RASHBA SPIN-ORBIT COUPLING JUNCTIONS

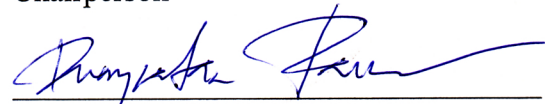
Suranaree University of Technology has approved this thesis submitted in partial fulfillment of the requirements for the Degree of Doctor of Philosophy.

Thesis Examining Committee



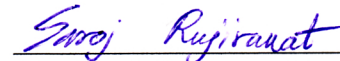
(Asst. Prof. Dr. Chinorat Kobdaj)

Chairperson



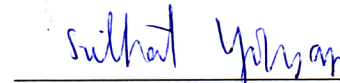
(Asst. Prof. Dr. Puangratana Pairor)

Member (Thesis Advisor)



(Dr. Saroj Rujirawat)

Member



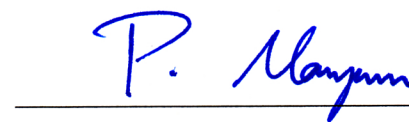
(Prof. Dr. Suthat Yoksan)

Member

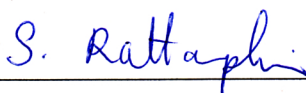


(Assoc. Prof. Dr. Udomsilp Pinsook)

Member



(Assoc. Prof. Dr. Prapun Manyum)



(Assoc. Prof. Dr. Saowanee Rattanaphani)

Vice Rector for Academic Affairs

Dean of Institute of Science

เบญจมาศ ศรีสองเมือง : สเปกโทรสโกปีการทะลุผ่านของรอยต่อระหว่างตัวนำยวดยิ่งกับ
แก๊สอิเล็กตรอนสองมิติที่มีคู่ควบของสปินและออร์บิตแบบรัชบา (TUNNELING
SPECTROSCOPY OF SUPERCONDUCTOR/TWO-DIMENSIONAL ELECTRON
GAS WITH RASHBA SPIN-ORBIT COUPLING JUNCTIONS)

อาจารย์ที่ปรึกษา : รองศาสตราจารย์ ดร.พวงรัตน์ ไพเราะ, 111 หน้า.

วิทยานิพนธ์นี้เป็นการศึกษาเชิงทฤษฎีเกี่ยวกับสเปกโทรสโกปีการทะลุผ่านของรอยต่อ 3
แบบของแก๊สอิเล็กตรอนสองมิติที่มีคู่ควบของสปินและออร์บิตแบบรัชบา ได้แก่ รอยต่อกับโลหะ
รอยต่อกับตัวนำยวดยิ่งแบบ-เอส-เวฟ และรอยต่อกับตัวนำยวดยิ่งแบบ-ดี-เวฟ วิธีการกระเจิงถูก
นำมาใช้ในการคำนวณความน่าจะเป็นของการสะท้อนกลับและการส่งผ่านในรอยต่อ ซึ่งค่าความ
น่าจะเป็นดังกล่าวถูกนำไปคำนวณหาค่าสภาพนำไฟฟ้าที่เป็นฟังก์ชันของความต่างศักย์ที่อุณหภูมิ
ศูนย์องศาสัมบูรณ์ ในรอยต่อระหว่างแก๊สอิเล็กตรอนสองมิติกับโลหะพบว่าสภาพนำไฟฟ้าของ
อิเล็กตรอนสปินอัพและของอิเล็กตรอนสปินดาวน์มีความแตกต่างกัน ความแตกต่างดังกล่าวสูงสุด
ที่พลังงานเท่ากับจุดตัดกันของแถบพลังงานทั้งสองของแก๊สอิเล็กตรอนสองมิติ สเปกตรัมสภาพนำ
ไฟฟ้ามักมีลักษณะเด่นที่สังเกตได้ 2 ลักษณะ ซึ่งระยะห่างระหว่างสองลักษณะนี้มีขนาดเท่ากับขนาด
ของพลังงานรัชบา

ในรอยต่อระหว่างแก๊สอิเล็กตรอนสองมิติกับตัวนำยวดยิ่งแบบ-เอส-เวฟ พบว่าผลของ
คู่ควบของสปินและออร์บิตแบบรัชบาต่อสเปกตรัมสภาพนำไฟฟ้าขึ้นอยู่กับระดับพลังงานเฟอร์มี
ของแก๊สอิเล็กตรอนสองมิติ เมื่อระดับพลังงานเฟอร์มีสูงกว่าจุดตัดกันของแถบพลังงานของแก๊ส
อิเล็กตรอนสองมิติ สภาพนำไฟฟ้าของรอยต่อที่พลังงานต่ำกว่าช่องว่างพลังงานของตัวนำยวดยิ่ง
ลดลงเมื่อความแรงของคู่ควบเพิ่มขึ้น ในกรณีที่ระดับพลังงานเฟอร์มีอยู่ต่ำกว่าหรืออยู่ที่จุดตัดกัน
ของแถบพลังงานของแก๊สอิเล็กตรอนสองมิติ การเพิ่มความแรงของคู่ควบสามารถเพิ่มสภาพนำ
ไฟฟ้าของรอยต่อได้จนถึงค่าวิกฤตค่าหนึ่ง แต่หลังจากนั้นการเพิ่มความแรงของคู่ควบจะทำให้
สภาพนำไฟฟ้าลดลง ในทุกกรณีของระดับพลังงานเฟอร์มีของแก๊สอิเล็กตรอนสองมิติ พบว่ายอด
สูงสุดของสภาพนำไฟฟ้าที่พลังงานเท่ากับช่องว่างพลังงานของตัวนำยวดยิ่ง เพิ่มขึ้นตามความแรง
ของคู่ควบและไม่เปลี่ยนแปลงตามขนาดของกำแพงศักย์ของรอยต่อ

ผลของความแตกต่างกันของมวลยังผลของอิเล็กตรอนต่อสภาพนำไฟฟ้า มีความแตกต่าง
กันตามระดับพลังงานเฟอร์มีของแก๊สอิเล็กตรอนสองมิติ กล่าวคือ เมื่อระดับพลังงานเฟอร์มีอยู่สูง
กว่าจุดตัดกันของแถบพลังงานในแก๊สอิเล็กตรอนสองมิติ ผลของความแตกต่างระหว่างมวลยังผล
ของอิเล็กตรอนต่อสภาพนำไฟฟ้าทั้งที่พลังงานต่ำกว่าและสูงกว่าช่องว่างพลังงานในตัวนำยวดยิ่ง
เทียบเท่ากับผลของการเปลี่ยนแปลงขนาดของกำแพงศักย์ตรงรอยต่อ กล่าวคือ การเพิ่มขึ้นของทั้ง

ความแตกต่างของมวลยังผลและกำแพงศักย์ ทำให้สภาพนำไฟฟ้าลดลง อย่างไรก็ตามที่พลังงานเท่ากับช่องว่างพลังงาน ผลของความแตกต่างของมวลยังผลกับกำแพงศักย์ของรอยต่อ ไม่ได้เป็นไปในทางเดียวกัน กล่าวคือ การเปลี่ยนขนาดของกำแพงศักย์ไม่มีผลต่อสภาพนำไฟฟ้า แต่ความแตกต่างกันของมวลยังผลของอิเล็กตรอนทำให้สภาพนำไฟฟ้าของรอยต่อลดต่ำลง ในกรณีที่ระดับพลังงานเฟอร์มีอยู่ต่ำกว่าหรืออยู่ที่จุดตัดกันของแถบพลังงาน ผลของความแตกต่างของมวลยังผลของอิเล็กตรอนเทียบเท่าได้กับผลของความแรงของกลุ่มควมทั้งที่พลังงานต่ำกว่าและสูงกว่าช่องว่างพลังงานของตัวนำเวดจ์ และเทียบเท่าได้กับการเปลี่ยนขนาดของกำแพงศักย์ตรงรอยต่อที่พลังงานเท่ากับช่องว่างพลังงานของตัวนำเวดจ์

สเปกตรัมสภาพนำไฟฟ้าของรอยต่อของแก๊สอิเล็กตรอนสองมิติกับตัวนำเวดจ์แบบดี-เวฟ มีการเปลี่ยนแปลงตามการวางตัวของผิวรอยต่อ ในกรณีที่ผิวรอยต่อวางตัวแบบ {100} พบลักษณะเด่นเพิ่มที่พลังงานต่ำกว่าจุดสูงสุดของช่องว่างพลังงานของตัวนำเวดจ์ ซึ่งตำแหน่งที่พบลักษณะเด่นนี้เปลี่ยนแปลงตามขนาดความแรงของกลุ่มควมของสปีนและออร์บิท ลักษณะเด่นดังกล่าวพบเฉพาะในรอยต่อที่มีความโปร่งเท่านั้น สำหรับกรณีผิวรอยต่อวางตัวเบี่ยงเบนไปจากแบบ {100} สเปกตรัมสภาพนำไฟฟ้าประกอบด้วยยอดสูงสุดที่ความต่างศักย์เป็นศูนย์ และยอดสูงสุดที่พลังงานเท่ากับช่องว่างพลังงานของตัวนำเวดจ์ในทิศทางตั้งฉากกับผิวรอยต่อ

ยอดสูงสุดที่ความต่างศักย์เป็นศูนย์เพิ่มขึ้นตามความแรงของกลุ่มควมของสปีนและออร์บิทในรอยต่อที่โปร่งในทุกระดับพลังงานเฟอร์มี สำหรับรอยต่อที่มีกำแพงศักย์สูง ยอดสูงสุดที่ความต่างศักย์เป็นศูนย์ลดลงเมื่อเพิ่มความแรงของกลุ่มควมในกรณีที่ระดับพลังงานเฟอร์มีอยู่สูงกว่าจุดตัดกันของแถบพลังงานทั้งสองของแก๊สอิเล็กตรอนสองมิติ แต่เมื่อระดับพลังงานเฟอร์มีอยู่ที่จุดตัดกันของแถบพลังงาน พบว่ายอดสูงสุดที่ความต่างศักย์เป็นศูนย์ลดลงจนถึงค่าวิกฤติค่าหนึ่งของความแรงกลุ่มควม หลังจากนั้นยอดสูงสุดที่ความต่างศักย์เป็นศูนย์จะเพิ่มขึ้นเมื่อเพิ่มความแรงของกลุ่มควม

BENJAMAT SRISONGMUANG : TUNNELING SPECTROSCOPY OF SUPERCONDUCTOR/TWO-DIMENSIONAL ELECTRON GAS WITH RASHBA SPIN-ORBIT COUPLING JUNCTIONS. THESIS ADVISOR : ASSOC. PROF. PUANGRATANA PAIROR, Ph.D. 111 PP.

TUNNELING SPECTROSCOPY OF SUPERCONDUCTOR/TWO-DIMENSIONAL ELECTRON GAS WITH RASHBA SPIN-ORBIT COUPLING JUNCTIONS

In this thesis, the conductance spectra of 3 types of junctions containing two-dimensional electron gas (2DEG) with Rashba spin-orbit coupling (RSOC): 2DEG/metal (2DEG/M), 2DEG/s-wave superconductor (2DEG/S), 2DEG/ $d_{a^2-b^2}$ -wave superconductor (2DEG/D) are theoretically studied. The scattering method is applied to obtain reflection and transmission probabilities, which are used to obtain the zero-temperature conductance spectrum. In 2DEG/M junction, there is a difference between the conductance of electron with up spin and that of with down spin. This difference is maximum at the voltage corresponding to the crossing of the two energy branches of 2DEG. The total conductance of 2DEG/M junction contains 2 distinguished features, the distance between which is equal to the Rashba energy.

In 2DEG/S junction, the effect of RSOC is different for different Fermi levels of 2DEG. When the Fermi level lies above the crossing between the two energy branches of 2DEG, the conductance below the energy gap is suppressed with increasing RSOC strength. When the Fermi level is located at or below the crossing, increasing RSOC strength enhances the conductance below the energy gap up to a critical value, but suppresses the conductance beyond this value. In all cases of the

Fermi levels, the conductance at the energy gap is increased with the RSOC strength, but is unaffected by the change in the potential barrier

The effect of the difference in effective masses on the conductance is also different for different Fermi levels of 2DEG. When the Fermi level lies above the crossing, the effect of mismatch of effective mass is equivalent to that of potential barrier for applied voltage both below and above the energy gap, i.e., they both suppresses the conductance. However, at the energy gap, the mismatch and the barrier affect the conductance in a different way, i.e, the conductance is unaffected by the barrier but is suppressed by the mismatch. When Fermi level is located at or below the crossing, the effect of the mismatch is also equivalent to that of RSOC for applied voltage both below and above the gap, but at the energy gap the effect of the mismatch is the same as that of barrier.

In 2DEG/D junction, the conductance spectrum of $\{100\}$ junction is found to contain an additional feature at energy less than the maximum gap. This feature depends strongly on the RSOC strength and only appear when the junction is in the Andreev limit. For junction away from $\{100\}$ orientation, the conductance spectrum contains a zero-bias conductance peak (ZBCP) and a peak at the energy equal to the superconducting gap along the direction of the interface normal.

In Andreev limit, ZBCP is enhanced by the RSOC for all Fermi levels. In tunneling limit, ZBCP is suppressed when Fermi level lies above the crossing, but when it is at the crossing, ZBCP is decreased with the RSOC strength up to a critical value of RSOC, but it is increased after this value.

School of Physics

Academic Year 2007

Student's Signature Benjamat Srisongmuang

Advisor's Signature Prayada Pan

ACKNOWLEDGEMENTS

I would like to thank the various people who provided a useful and helpful assistance. Without their care and consideration, this thesis would likely not have been completed. First of all, I would like to express my sincere gratitude to my supervisor, Assoc. Prof. Dr. Paungratana Pairor, for her support and providing an excellent forum to discuss the ideas and shaping it up to ultimately become a thesis. Her patient reading and editing are also appreciated.

My second supervisor, Assoc. Prof. Dr. Mona Berciu, who supervised and taken care of me in Vancouver, her patience, kind guidance and support are greatly appreciated.

I wish to especially thank Asst. Prof. Dr. Chinorat Kobdaj, Dr. Saroj Rujirawat, Prof. Dr. Suthat Yoksan and Assoc. Prof. Dr. Udomsilp Pinsook for being my supervisory thesis committee, and for helpful comments and suggestions.

My sincere thanks are due to all teachers in school of physics, who gave me the good education throughout my study here.

In my daily study, I have been blessed with a friendly and cheerful group of our physics students. My warmly thank are due to all my friends who shared and discussed all kind of problem with me.

I wish to also thank my parents, my sister and my brother for their love and encouragement.

Finally, I wish to thank the Commission on Higher Education for its financial support since my graduate years.

Benjamat Srisongmuang

CONTENTS

	Page
ABSTRACT IN THAI.....	I
ABSTRACT IN ENGLISH.....	III
ACKNOWLEDGEMENTS.....	V
CONTENTS.....	VI
LIST OF FIGURES.....	VIII
 CHAPTER	
I INTRODUCTION.....	1
1.1 Two-Dimensional electron gas with Rashba Spin-Orbit Coupling.....	2
1.2 Methods and Assumptions.....	5
1.3 Outline of Thesis.....	7
II 2DEG-METAL JUNCTION.....	9
2.1 Model and Method of Calculation.....	9
2.2 Results and Discussion.....	17
2.3 Conclusions.....	23
III 2DEG/S JUNCTION.....	24
3.1 Model and method of calculation.....	24
3.1.1 Case 1: E_F is located above the crossing of the two branches.....	29
3.1.2 Case 2: E_F is located at the crossing of the two branches	32

CONTENTS (Continued)

	Page
3.1.3 Case 3: E_F is located below the crossing of the two branches.....	34
3.2 Results and Discussion.....	41
3.2.1 Case 1: E_F is located above the crossing of the two branches	41
3.2.2 Case 2: E_F is located at the crossing of the two branches	48
3.2.3 Case 3: E_F is located below the crossing of the two branches	55
3.3. Conclusions.....	58
IV 2DEG/D JUNCTION.....	60
4.1 Assumptions and Method of Calculation.....	61
4.2 Results and Discussion.....	65
4.2.1 Case 1: E_F is located above the crossing	65
4.2.2 Case 2: E_F is located at the crossing.....	74
4.3 Conclusions.....	81
V CONCLUSION.....	83
REFERENCES.....	87
APPENDICES	
APPENDIX A 8×8 equations of the 2DEG/S junction.....	92
APPENDIX B Average tunneling probabilities	95
CURRICULUM VITAE.....	111

LIST OF FIGURES

Figure		Page
1.1	<p>(a) The sketch of energy dispersion of the 2DEG with RSOC (b) The energy contours of the plus and minus branches. \vec{k}^+ and \vec{k}^- are the wave vectors of the same k_z. The thick arrows show the direction of the spins for each \vec{k}^--state along the energy contours.....</p>	3
1.2	<p>The plot of DOS of the 2DEG with RSOC. The solid line is the total DOS. The upper and lower dashed line are the DOS of the minus and plus branches for $E > 0$ respectively. The inset is energy dispersion of the 2DEG for zero and finite q_0</p>	4
2.1	<p>The upper panel shows the energy contours plot of the electron in 2DEG (left) and metal (right). The sketches of excitation energies of 2DEG and metal are shown in the lower panel. The dashed line is the line of the same E. The arrows show the \vec{k} states of the electrons on each side with the same E</p>	12
2.2	<p>The transmission probabilities of up - (C_1) and down - (C_2) spin states for different $k_z = 0$ and $0.05 k_F$. The horizontal arrow line indicates the energy range over which the spin polarization is large. The inset in the upper panel is the plot of the energy vs k_x at a particular k_z. The range of the energy between the two dashed line correspond to the energy</p>	

LIST OF FIGURES (Continued)

Figure	Page
range indicates by the arrow lines.....	19
2.3 The tunneling conductance of up-(G_1) and down-(G_2) spin, the different between up-and down-spin conductance (G_2-G_1) and the total conductance (G_1+G_2), for $q_0 = 0.2 k_F$ and $m/m^* = 10$ for $z = 0$ and 1. $E_F = E_{F,2DEG} = E_{F,M}$ for simplicity.....	20
2.4. The difference of the conductance of spin-up and spin-down at $eV = E_{F,2DEG}$ as a function of q_0 for different $z = 0, 0.5, 1, 2$ and 3	21
2.5 The conductance spectra of 2DEG/M junction for a fixed $q_0 = 0.1 k_F$, $0.2 k_F$, $0.3 k_F$ and $0.4 k_F$ at $E = E_{F,2DEG}$. (G_1 , G_2 , G_1+G_2 and G_2-G_1 same as defined in Fig. 2.3).....	22
2.6 The conductance as a function of z for different q_0 at $eV = E_{min}$. The inset shows the close up of the conductance near $z = 0$ where $q_0 = 0.6 k_F$	22
2.7 The conductance as a function of bias voltage for different $q_0 = 0.1 k_F$, $0.15 k_F$ and $0.2 k_F$. The arrows in the case of $q_0 = 0.2 k_F$ indicates the two features occurs at $eV = E_{F,2DEG}$ and $E_{F,2DEG} + E_\lambda$	22
3.1 The sketch of the 2DEG-s-wave superconductor junction.....	25
3.2 The sketch of the excitation energy of the quasiparticles in the superconductor.....	26

LIST OF FIGURES (Continued)

Figure	Page
3.3	(a) The sketch of energy dispersion of 2DEG with RSOC. (b) The energy contours of the electrons in 2DEG. (q_1^+ and q_2^+ are the x -component of wave vector \bar{q}_1 (plus branch) and \bar{q}_2 (minus branch)).....28
3.4	The sketch of excitation energy of 2DEG/S junction.....30
3.5	The sketch of excitation energy on 2DEG side.....32
3.6	The sketch of excitation energy on 2DEG side when voltage V is applied34
3.7	The conductance spectra (normalized by $e^2 L^2 / 2\pi\hbar$) as a function of bias voltage for different $q_0 = 0, 0.3 k_F, 0.5 k_F$ and $0.7 k_F$ where $r_m = 1$ (a) $z = 0$ (b) $z = 1$42
3.8	The conductance spectra (normalized by $e^2 L^2 / 2\pi\hbar$) of 2DEG/S junction: $r_m = 10$, (a) $z = 0$ (b) $z = 1$. The arrows indicate the feature at the voltage below the superconducting gap.....43
3.9	The conductance spectra (normalized by $e^2 L^2 / 2\pi\hbar$) of 2DEG/S junction for different value of z , $q_0 = 0.2 k_F$: (a) $r_m = 1$ (b) $r_m = 10$. The arrows indicate the feature at the voltage below the superconducting gap.....44

LIST OF FIGURES (Continued)

Figure	Page
3.10 The q_0 dependence conductance (normalized by $e^2 L^2 / 2\pi\hbar$) at $eV = 0$ where $r_m = 1$ (a) $z = 0, 0.1$ and 0.5 (b) $z = 1$ and 2 (c) $r_m = 10, z = 0$ and 1	46
3.11 The q_0 dependence conductance (normalized by $e^2 L^2 / 2\pi\hbar$) at $eV = \Delta$ where $r_m = 1$ and 10	47
3.12 The z dependence conductance (normalized by $e^2 L^2 / 2\pi\hbar$) for $q_0 = 0.2 k_F$, $r_m = 1$ and 10 at $eV = 0$ and Δ	47
3.13 The r_m dependence conductance (normalized by $e^2 L^2 / 2\pi\hbar$) for $q_0 = 0.2$, $z = 0$, at $eV = 0$ and Δ	48
3.14 The conductance spectra (normalized by $e^2 L^2 / 2\pi\hbar$) of 2DEG/S junction for different value of q_0 , $r_m = 1$ (a) $z = 0$ (b) $z = 1$	49
3.15 The conductance spectra (normalized by $e^2 L^2 / 2\pi\hbar$) of 2DEG/S junction for $r_m = 10$ and different value of q_0 (a) $z = 0$ (b) $z = 1$	50
3.16 The conductance (normalized by $e^2 L^2 / 2\pi\hbar$) as a function of q_0 for different $z = 0, 0.5, 1$ and 2 at $eV = 0$ and $r_m = 1$	51
3.17 The conductance (normalized by $e^2 L^2 / 2\pi\hbar$) as a function of q_0 for different $z = 0, 0.5, 1$ and 2 at $eV = 0$ and $r_m = 10$	51

LIST OF FIGURES (Continued)

Figure	Page
3.18	The conductance spectra (normalized by $e^2 L^2 / 2\pi\hbar$) of 2DEG/S junction for different value of z , where $q_0 = 0.4 k_F$ (a) $r_m = 1$ (b) $r_m = 10$52
3.19	The conductance (normalized by $e^2 L^2 / 2\pi\hbar$) as a function of q_0 at $eV = \Delta$ and different $z = 0, 0.5, 1$, $r_m = 1$ and 1053
3.20	The conductance (normalized by $e^2 L^2 / 2\pi\hbar$) as a function of z , $q_0 = 0.2$, $r_m = 1$ and 10 , at $eV = 0$ and Δ54
3.21	The conductance (normalized by $e^2 L^2 / 2\pi\hbar$) as a function of r_m where $z = 0$ and $q_0 = 0.2$ at $eV = 0$ and Δ54
3.22	The conductance spectra (normalized by $e^2 L^2 / 2\pi\hbar$) of 2DEG/S junction: for different $q_0 = 0.2 k_F$, $0.3 k_F$ and $0.4 k_F$ (a) $z = 0$ and (b) $z = 1$. The arrows indicate the feature at the crossing of the two energy branches.....55
3.23	The conductance spectra (normalized by $e^2 L^2 / 2\pi\hbar$) of 2DEG/S junction: $r_m = 10$, $q_0 = 0.2, 0.3, 0.4$ (a) $z = 0$ (b) $z = 1$. The arrows indicate the feature at the crossing of the two energy branches.....56
3.24	The conductance (normalized by $e^2 L^2 / 2\pi\hbar$) as a function of q_0 at $eV = \Delta$, $r_m = 1$ and 1057

LIST OF FIGURES (Continued)

Figure	Page
3.25	The conductance (normalized by $e^2 L^2 / 2\pi\hbar$) as a function of z for fix $q_0 = 0.2 k_F$, $r_m = 1$ and 10 , at $eV = 0$ and Δ57
3.26	The conductance (normalized by $e^2 L^2 / 2\pi\hbar$) as a function of r_m where $z = 0$ and $q_0 = 0.2$ at $eV = 0$ and Δ58
4.1	The sketch of the 2DEG-d-wave superconductor junction.....62
4.2	The sketch of $d_{x^2-y^2}$ - wave superconducting gap function. Plus and minus sign represent the phase of the gap.....62
4.3	The conductance spectra of 2DEG/D junction with various q_0 when $\alpha = 0$, $r_m = 10$ (a) $z = 0$ (b) $z = 0.3$ (c) $z = 2$. The arrows indicate the feature at $eV < \Delta$66
4.4	The conductance spectra of 2DEG/D junction with various z , $r_m = 10$ (a) $\alpha = 0$ (b) $\alpha = \frac{\pi}{16}$67
4.5	The conductance spectra of 2DEG/D junction with various α , $z = 0$, $r_m = 10$ and $q_0 = 0.3k_F$68
4.6	The conductance spectra of 2DEG/D junction with various $z = 0, 0.3, 1$ and 2 , $\alpha = 0$, $r_m = 10$ (a) $q_0 = 0.1k_F$ (b) $q_0 = 0.4k_F$68

LIST OF FIGURES (Continued)

Figure	Page
4.7 The conductance spectra with various RSOC, $\alpha = \frac{\pi}{4}$, (a) $z = 0$ (b) $z = 2$. The inset is the close up plot of the conductance spectra near $eV = 0$	70
4.8 The conductance spectra of 2DEG/D junction with various $z = 0, 0.5, 1$ and 2 , $\alpha = \frac{\pi}{4}$, $r_m = 10$ (a) $q_0 = 0.1k_F$ (b) $q_0 = 0.4k_F$	71
4.9 The conductance spectra with various RSOC, $\alpha = \frac{\pi}{8}$, (a) $z = 0$ (b). $z = 2$. The arrows indicate the feature at $eV = \Delta_0 \cos 2\alpha$. The inset is the close up plot of the conductance spectra near $eV = 0$	72
4.10 The conductance spectra of 2DEG/D junction with various $z = 0, 0.5, 1$ and 2 , $\alpha = \frac{\pi}{8}$, $r_m = 10$ (a) $q_0 = 0.1k_F$ (b) $q_0 = 0.4k_F$. The inset is the close up plot of the conductance spectra near $eV = 0$	73
4.11 The conductance spectra with various RSOC, $\alpha = 0$, (a) $z = 0$ (b) $z = 1$	75
4.12 The conductance spectra of 2DEG/D junction with various $z = 0, 0.5, 1$ and 2 , $\alpha = 0$, $r_m = 10$ (a) $q_0 = 0.1k_F$ (b) $q_0 = 0.4k_F$	76
4.13 The conductance spectra with various RSOC, $\alpha = \frac{\pi}{4}$, (a) $z = 0$ (b) $z = 1$ (c) $z = 2$	77

LIST OF FIGURES (Continued)

Figure	Page
4.14	The conductance spectra with various RSOC, $\alpha = \frac{\pi}{8}$, (a) $z = 0$ (b) $z = 1$ (c) $z = 2$78
4.15	The conductance spectra of 2DEG/D junction with various $z = 0, 0.5, 1$ and 2, $\alpha = \frac{\pi}{4} = 0$, $r_m = 10$ (a) $q_0 = 0.1k_F$ (b) $q_0 = 0.4k_F$79
4.16	The conductance spectra of 2DEG/D junction with various $z = 0, 0.5, 1$ and 2, $\alpha = \frac{\pi}{8} = 0$, $r_m = 10$ (a) $q_0 = 0.1k_F$ (b) $q_0 = 0.4k_F$ The inset is the close up plot of the conductance spectra near $eV = 0$80

CHAPTER I

INTRODUCTION

In the past decade, the advent of spintronics has motivated the study of spin transport in solid state systems (Žutić, Fabian and Das Sarma, 2004) and two-dimensional electron gas (2DEG) with the Rashba spin-orbit coupling RSOC is among the systems of interest. RSOC is known to lift spin degeneracy of 2DEG. This system can be potentially used as a part of the spin-polarized field-effect transistor (Spin-FET) (Datta and Das, 1990), spin interference device (Aronov and Lyanda-Geller, 1993), and spin filters (Koga, Nitta, Takayanagi and Datta, 2002; Cummings, Akis and Ferry, 2006). In general, RSOC is present in a system with structure inversion asymmetry (Bychkov and Rashba, 1984) as in III-V semiconductor heterostructure. For example, InGaAs/InAlAs, GaSb/InAs/GaSb, GaAs/AlGaAs, InAs/AlSb, InAl/AlSb (Luo, Munekata, Fang and Stiles, 1988; Das, Miller, Datta, Reifenberger, Hong, Bhattacharya, Singh and Jaffe, 1989; Das and Datta, 1990; Luo, Munekata, Fang and Stiles, 1990; Nitta, Akazaki and Takayanagi, 1997; Miller, Zumbühl, Marcus, Lyanda-Geller, Goldhaber-Gordon, Campman and Gossard, 2003).

The possibility of creating new devices made from 2DEG motivated this thesis work, which is a theoretical study of the tunneling spectroscopy of three types of junctions containing 2DEG with the RSOC, i.e. 2DEG/metal (2DEG/M), 2DEG/s-wave superconductor (2DEG/S) and 2DEG/d-wave superconductor (2DEG/D).

The effect of the RSOC on the differential conductance spectrum of each junction is the main focus of this thesis.

1.1 Two-Dimensional Electron Gas with Rashba Spin-Orbit Coupling

The Hamiltonian that describes the RSOC in 2DEG can be written in terms of the 2D electron momentum (\vec{p}) and the Pauli matrices ($\vec{\sigma}$) as (Bychkov and Rashba, 1984),

$$\hat{H}_e = \frac{\hat{p}^2}{2m^*} - \lambda \vec{\sigma} \cdot (\hat{y} \times \vec{p}). \quad (1.1)$$

Here, λ represents the strength of RSOC, or known as Rashba parameter, m^* is effective mass of the electron in 2DEG and \hat{y} is the direction perpendicular to the 2D plane.

The eigenenergies of 2DEG with RSOC are

$$E^\pm = \frac{\hbar^2 k^2}{2m^*} \pm \lambda \hbar k \quad (1.2)$$

where $k = |\vec{k}| = \sqrt{k_x^2 + k_z^2}$. The splitting eigenenergy in equation (1.2) can also be rewritten as

$$E^\pm = \frac{\hbar^2}{2m^*} (k \pm q_0)^2 - \frac{\hbar^2 q_0^2}{2m^*}, \quad (1.3)$$

where $q_0 = \frac{m^* \lambda}{\hbar}$ representing the RSOC strength in units of momentum. The

eigenstates corresponding to the eigenenergy in equation (1.2) are

$$|\bar{k}, +\rangle = \begin{pmatrix} \cos \frac{\phi_k^+}{2} \\ -\sin \frac{\phi_k^+}{2} \end{pmatrix} e^{i\bar{k}\cdot\bar{r}}, \quad \text{and} \quad |\bar{k}, -\rangle = \begin{pmatrix} \sin \frac{\phi_k^-}{2} \\ \cos \frac{\phi_k^-}{2} \end{pmatrix} e^{i\bar{k}\cdot\bar{r}}, \quad (1.4)$$

where $\phi_k^{+,-}$ are the angles between the wave vector $\bar{k}^{+,-}$ and wave vector \bar{k}_x as shown in Fig. 2.1 (b). As can be seen in equation (1.4), the spin states in both plus and minus branches are not completely up or down, when $\phi_k^{+,-}$ is away from zero.

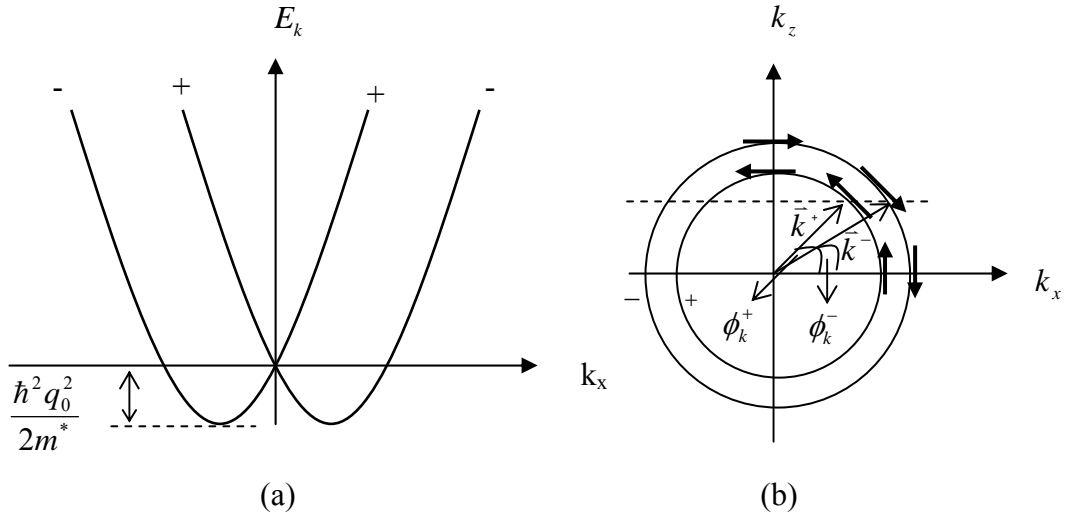


Figure 1.1 (a) The sketch of energy dispersion of the 2DEG with RSOC (b) The energy contours of the plus and minus branches. \bar{k}^+ and \bar{k}^- are the wave vectors of the same k_z . The thick arrows show the direction of the spins for each \bar{k} -state along the energy contours.

The density of states (DOS) of each branch for $E > 0$ is

$$D_{\pm}(E) = \frac{L_x L_z}{2\pi} \cdot \frac{m^*}{\hbar^2} \left[1 \mp \frac{q_0}{\sqrt{(2m^* E / \hbar^2) + q_0^2}} \right] \quad E \geq 0, \quad (1.5)$$

where D_+ and D_- are DOS of plus and minus branches respectively, L_x and L_z are the dimensions of 2DEG. The total DOS for $E > 0$ is

$$D(E) = D_+(E) + D_-(E) = \frac{L_x L_z}{\pi} \cdot \frac{m^*}{\hbar^2}, \quad (1.6)$$

which is a constant equal to the DOS of 2DEG without RSOC.

For $E < 0$, there is only one branch (minus branch) and the DOS is

$$D_-(E) = \frac{L_x L_z}{\pi} \cdot \frac{m^*}{\hbar^2} \left(\frac{q_0}{\sqrt{(2m^* E / \hbar^2) + q_0^2}} \right) \quad E < 0, \quad (1.7),$$

which becomes singular at $E = -E_\lambda \equiv -\frac{\hbar^2 q_0^2}{2m^*}$ or the bottom of the energy band. This

singularity occurs due to the point-like energy spectrum for 2DEG with no RSOC becomes ring-like (see inset of Fig. 2.2).

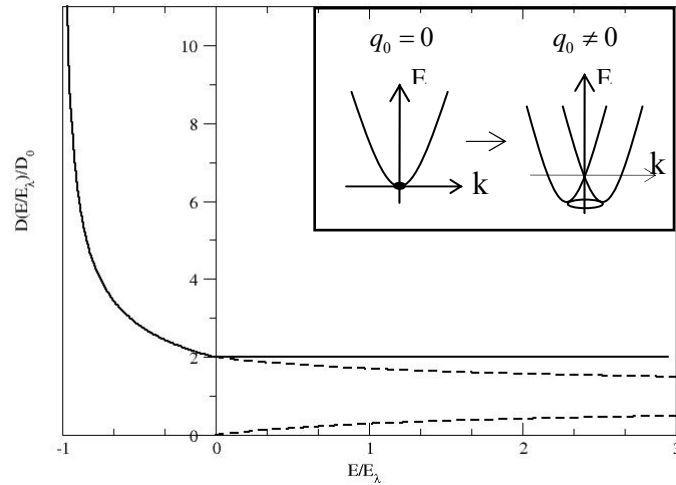


Figure 1.2 The plot of DOS of the 2DEG with RSOC. The solid line is the total DOS. The upper and lower dashed line are the DOS of the minus and plus branches for $E > 0$ respectively. The inset is the sketch of energy dispersions of the 2DEG with and without RSOC.

The RSOC strength can be measured from the analysis of the beating pattern in the magnetoresistance oscillations in small magnetic field (Luo, Munekata, Fang and Stiles, 1988; 1990; Das, Miller, Datta, Reifenberger, Hong, Bhattacharya, Singh and Jaffe, 1989). It was found to be in the range of 10^{-12} - 10^{-7} eV.m. The strength of the spin-orbit coupling λ was shown to be controlled by applying a gate voltage perpendicular to the 2D plane (Chen, Han, Huang, Datta and Janes, 1993; Knap, Skierbiszewski, Zduniak, Litwin-Staszewska, Bertho, Kobbi and Robert, 1996; Nitta, Akazaki, Takayanagi and Enoki, 1997).

1.2 Methods and Assumptions

A simple method called the scattering method is used to study all the junctions. This method was first used by Griffin and Demer in 1971 in study of quasiparticle transport of metal-insulator-superconductor (MIS) junction, where the insulator is represented by a square barrier potential (Griffin and Demer, 1971). Later, by modeling the insulating layer as a delta-function potential, Blonder, Tinkham and Klapwijk adopted this scattering method to calculate the current in MIS junction and predicted an excess current in the limit where the insulating potential is small (Blonder, Tinkham and Klapwijk, 1982). Since then, this method has been used to study the tunneling spectroscopy of MIS junction and became well-known as the BTK formalism. In this approach, the junction of interest in this thesis are modeled as 2D infinite systems. The interface is at $x = 0$. The $x < 0$ region is occupied by the 2DEG. The metal or superconductor occupied the $x > 0$ region. The Hamiltonian of the system is written as

$$\hat{H} = \hat{H}_L + \hat{H}_R + H_S \delta(x), \quad (1.8)$$

where \hat{H}_L is the Hamiltonian of the 2DEG with an adjustable Fermi level, \hat{H}_R is the Hamiltonian of the metal and/or the superconductor, and $H_S\delta(x)$ is the scattering potential at the interface (H_S represents the strength of the barrier potential). In general, the effective masses of all regions are assumed to be different. Note that in the case of the junction containing the superconductor, one needs to consider both electron and hole states. Therefore, the Rashba Hamiltonian for holes is also considered:

$$\hat{H}_h = \frac{-\hat{p}^2}{2m^*} - \lambda\vec{\sigma} \cdot (\hat{y} \times \vec{p}),$$

which lead to the following eigenenergies and eigenstates.

$$E^\pm = -\frac{\hbar^2 k^2}{2m^*} \mp \lambda\hbar k,$$

$$|\bar{k}, +\rangle = \begin{pmatrix} -\sin\frac{\phi_k^+}{2} \\ -\cos\frac{\phi_k^+}{2} \end{pmatrix} e^{i\bar{k}\cdot\bar{r}}, \quad \text{and} \quad |\bar{k}, -\rangle = \begin{pmatrix} \cos\frac{\phi_k^-}{2} \\ -\sin\frac{\phi_k^-}{2} \end{pmatrix} e^{i\bar{k}\cdot\bar{r}}.$$

From the Hamiltonian, one can obtain the eigenstates and eigenenergy for the electrons/holes in each region. For the ballistic transport, the wave function of the electron in the 2DEG is the linear combination of the incoming and reflected eigenstates of the same energy and the momentum with the same component parallel to the interface. Similarly, the wave function of the electron or the quasiparticle in the metal or superconductor is a linear combination of all the suitable outgoing eigenstates. These wave functions are matched by the appropriate boundary conditions at the interface to obtain the reflection and transmission probabilities. These probabilities are then used to calculate the differential conductance of the

junction as a function of applied voltage. For simplicity, only the conductance spectra at zero temperature are considered in this thesis. The effect of finite temperature is expected to smear off the features in the spectra. For the junction with both kinds of superconductors, the effect of both the suppression of the superconducting gap near the interface and the proximity effect are ignored.

1.3 Outline of Thesis

Various types of junctions between these RSOC systems and other materials have been theoretically studied in many aspects. For instance, Matsuyama et al. investigated the ballistic spin transport in ferromagnet/2DEG with RSOC (F/2DEG) junction. They found that the spin-injection rate across the interface depends on the carrier density of the 2DEG (Matsuyama, Hu, Grundler, Meier and Merkt, 2001). Jiang and Jalil studied the heterostructure F/2DEG/F and found the insulating barrier at each F/2DEG interface enhances the spin-polarization of the system (Jiang and Jalil, 2003). They also found the spin-polarization has an almost linear dependence with the strength of RSOC (Jiang and Jalil, 2003). In addition to the junction with ferromagnetic metal, the junction with s-wave superconductor was also recently studied by Yokoyama et al. (Yokoyama, Tanaka and Inoue, 2006). They calculated the tunneling conductance of the junction in comparison with that of F/S junction. The main results of this work are related to the Andreev reflection, which is the process in which two electrons are transported across the metal/superconductor junction at a time (Andreev, 1964; Blonder, Tinkham and Klapwijk, 1982). It was found that in F/S junction, the Andreev reflection is suppressed by the exchange field causing both band splitting and the imbalance of up- and down-spin electrons in F. On the contrary,

in 2DEG/S such suppression does not occur, because the Rashba splitting never causes the imbalance (Yokoyama, Tanaka and Inoue, 2006). In these studies, the Fermi level of 2DEG is usually considered to be much higher than the Rashba energy.

The main focus of this thesis is to theoretically study the tunneling spectroscopy of 3 types of junctions involving the 2DEG with RSOC, i. e., 2DEG/metal (2DEG/M), 2DEG/S and 2DEG/d-wave superconductor (2DEG/D) junction. The mismatch effective mass, the insulating barrier potential at the interface and the level of the Fermi energy of the 2DEG are considered.

The organization of this thesis is as follows. In Chapter II, tunneling conductance spectrum of 2DEG/M junction is examined. The effect of the RSOC and the interfacial scattering on the conductance spectrum is considered. In Chapter III, the tunneling conductance spectrum of 2DEG/S junction is investigated. The effect of the difference in effective mass is considered. Also, the effect of different Fermi levels of the 2DEG is included. The tunneling spectroscopy of 2DEG/D junction is addressed in Chapter IV. In addition to the effect of the interfacial scattering and the different Fermi levels of the 2DEG, the effect of the crystal orientation of the d-wave superconductor with respect to the normal interface is considered. Finally, the conclusions of this thesis are addressed in Chapter V.

CHAPTER II

2DEG/M JUNCTION

In this chapter, the tunneling conductance spectrum of 2DEG/M junction is investigated. The energy levels of the 2DEG are assumed to be occupied up to the energy above the crossing of two energy branches. The effect of barrier potential and the RSOC on the differential conductance spectrum is examined. The work in this chapter is motivated by the previous work of Jiang and Jalil on the junction of F/I/2DEG/I/F, in which the barrier potential can greatly improve the spin-polarization (Jiang and Jalil, 2003).

2.1 Model and Method of Calculation

The 2DEG/M junction is modeled as a 2D infinite system. The plane of the junction is on xz plane. The interface is at $x = 0$. The $x < 0$ region is occupied by the 2DEG, and the $x > 0$ region by the metal. The insulating barrier at the interface is described by a delta function, $H_S \delta(x)$, where H_S represents the strength barrier potential.

The Hamiltonian of the junction can be written as (Zulicke and Schroll, 2002)

$$\hat{H} = \hat{p} \frac{1}{2m(x)} \hat{p} - \frac{\hat{y}}{2} [\lambda(x)(\vec{p} \times \vec{\sigma}) + (\vec{p} \times \vec{\sigma})\lambda(x)] + H_S \delta(x) - E_{F,2DEG} \Theta(-x) - E_{F,M} \Theta(x) \quad (2.1)$$

where $\frac{1}{m(x)} = \frac{1}{m^*} \Theta(-x) + \frac{1}{m} \Theta(x)$ describing the mismatch of the effective mass (m^*

is the electron mass in the 2DEG and m is the mass in the metal), $\Theta(x)$ is the Heaviside step function, $\lambda(x) = \lambda\Theta(-x)$, and $E_{F,2DEG}$ and $E_{F,M}$ are the Fermi energies of the 2DEG and the metal respectively.

In the $x < 0$ (2DEG) region, the excitation energy dispersion relation is

$$E_k^\pm = \frac{\hbar^2 k^2}{2m^*} \pm \hbar\lambda k - E_{F,2DEG} \quad (2.2)$$

The excitation energy dispersion of the system is depicted in Fig. 2.1. There are two equal possibilities for an incident electron:

- 1) from the state with wave vector \vec{q}_1 , where

$$q_1 = -q_0 + \sqrt{q_0^2 + \frac{2m^*}{\hbar^2}(E + E_{F,2DEG})} \quad \text{for } E > -E_{F,2DEG}$$

$$q_1 = q_0 - \sqrt{q_0^2 + \frac{2m^*}{\hbar^2}(E + E_{F,2DEG})} \quad \text{for } E < -E_{F,2DEG}$$

- 2) from the state with wave vector \vec{q}_2 ,

$$q_2 = q_0 + \sqrt{q_0^2 + \frac{2m^*}{\hbar^2}(E + E_{F,2DEG})} \quad \text{for all } E\text{'s.}$$

When the incoming eigenstate is from the E_k^+ branch, the wave function of the electron from the 2DEG, for the energy above the crossing of the two branches is

$$\psi_{2DEG}(x < 0, z) = \left(\begin{bmatrix} \cos \varphi_1 \\ -\sin \varphi_1 \end{bmatrix} e^{iq_{1x}x} + b_1 \begin{bmatrix} \sin \varphi_1 \\ \cos \varphi_1 \end{bmatrix} e^{-iq_{1x}x} + b_2 \begin{bmatrix} \cos \varphi_2 \\ \sin \varphi_2 \end{bmatrix} e^{-iq_{2x}x} \right) e^{ik_z z}, \quad (2.3)$$

where $\varphi_{1(2)} = \frac{\phi_{1(2)}}{2}$, $\phi_{1(2)}$ is the angle between the wave vector $\vec{q}_{1(2)}$ and k_x as shown in

Fig. 2.1, q_{1x} and q_{2x} are the x -components of wave vectors \vec{q}_1 and \vec{q}_2 respectively.

b_1 and b_2 are the amplitudes of the two reflected eigenstates with the wave vectors \vec{q}_1 and \vec{q}_2 .

Similarly, when the incoming eigenstate is from the E_k^- branch, the wave function of the electron from the 2DEG for the energy above the crossing is written as

$$\psi_{2DEG}(x < 0, z) = \left(\begin{bmatrix} \sin \varphi_2 \\ \cos \varphi_2 \end{bmatrix} e^{iq_2 x} + b_1' \begin{bmatrix} \sin \varphi_1 \\ \cos \varphi_1 \end{bmatrix} e^{-iq_1 x} + b_2' \begin{bmatrix} \cos \varphi_2 \\ \sin \varphi_2 \end{bmatrix} e^{-iq_2 x} \right) e^{ik_z z}, \quad (2.4)$$

where b_1' and b_2' are the amplitudes of the reflected eigenstates with the wave vectors \bar{q}_1 and \bar{q}_2 respectively.

For the energy below the crossing, both incoming eigenstates are from the E_k^- branch. Only the wave function of the electron with the incoming eigenstate \bar{q}_1 is modified to

$$\psi_{2DEG}(x < 0, z) = \left(\begin{bmatrix} \cos \varphi_1 \\ \sin \varphi_1 \end{bmatrix} e^{iq_1 x} + b_1 \begin{bmatrix} \sin \varphi_1 \\ \cos \varphi_1 \end{bmatrix} e^{-iq_1 x} + b_2 \begin{bmatrix} \cos \varphi_2 \\ \sin \varphi_2 \end{bmatrix} e^{-iq_2 x} \right) e^{ik_z z}. \quad (2.5)$$

First consider the $x > 0$ (metal) region. In this region, the excitation energy dispersion relation is $E_k = \frac{\hbar^2 k^2}{2m} - E_{F,M}$ and the wave function of the electron is the linear combination of the two transmitted eigenstates: one with spin up and the other with spin down. These two states have the same energy and k_z .

$$\psi_M(x > 0, z) = \left(c_1 \begin{bmatrix} 1 \\ 0 \end{bmatrix} e^{ik_x x} + c_2 \begin{bmatrix} 0 \\ 1 \end{bmatrix} e^{ik_x x} \right) e^{ik_z z}, \quad (2.6)$$

where k_x and k_z are the x - and z -component of the transmitted wave vector \vec{k} , c_1 and c_2 are the transmission amplitudes for spin up and spin down eigenstates respectively.

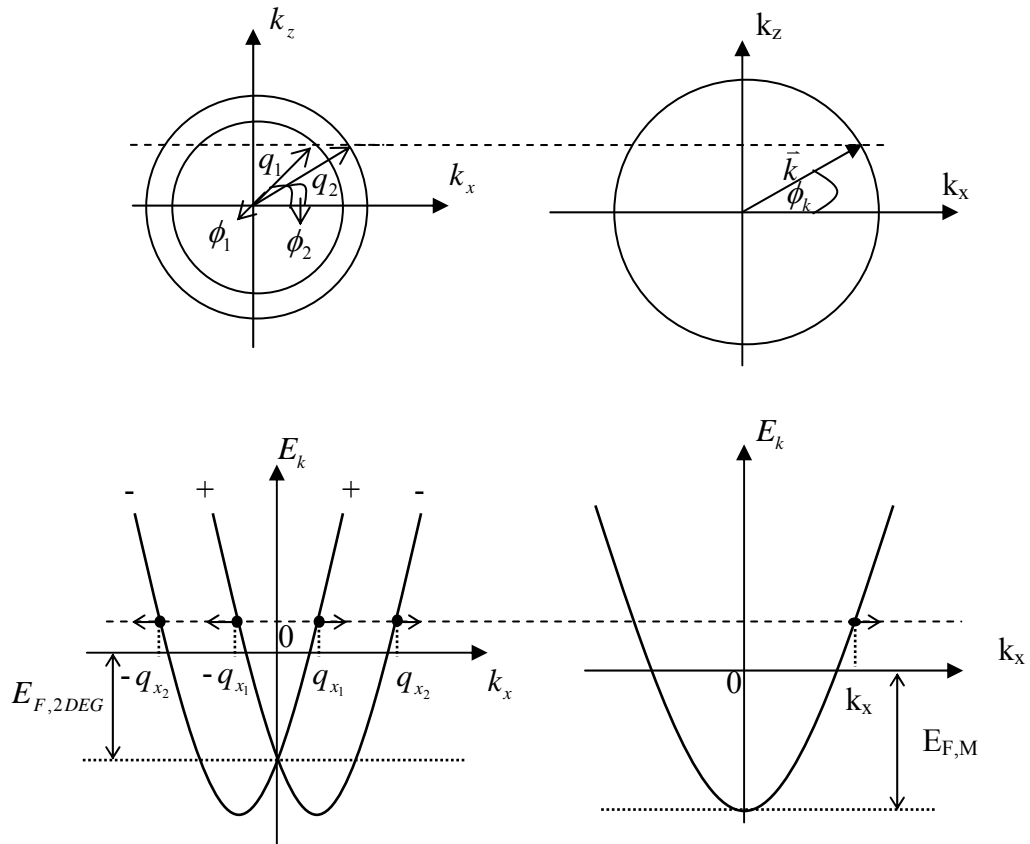


Figure 2.1 The upper panel shows the energy contours plot of the electron in 2DEG (left) and metal (right). The sketches of excitation energies of 2DEG and metal are shown in the lower panel. The dashed line is the line of the same E . The arrows show the \vec{k} states of the electrons on each side with the same E .

The appropriate matching conditions for the wave functions are

- (i) Continuity of the wave function at the interface

$$\psi_{2DEG}(0) = \psi_M(0) = \psi(0), \quad (2.7)$$

- (ii) The discontinuity of the slope of the wave function at the interface are (Schnittler and Kirilov, 1993; Zulicke and Schroll, 2002)

$$\frac{\partial \psi_M}{\partial x} \Big|_{x=0^+} - \frac{m}{m^*} \frac{\partial \psi_{2DEG}}{\partial x} \Big|_{x=0^-} = \begin{bmatrix} 2k_F z + i \frac{m}{m^*} q_0 & 0 \\ 0 & 2k_F z - i \frac{m}{m^*} q_0 \end{bmatrix} \psi(0), \quad (2.8)$$

where $z = \frac{mH}{\hbar^2 k_F}$ is the unitless parameter that characterizes the barrier strength, k_F is

the Fermi wave vector of the metal.

After the substitution of wave functions into the matching conditions, the following equations for incident state with wave vector \vec{q}_1 are obtained.

$$\begin{bmatrix} \sin \varphi_1 & \cos \varphi_2 & -1 & 0 \\ -\cos \varphi_1 & \sin \varphi_2 & 0 & -1 \\ q_{1x} r_m \sin \varphi_1 & q_{2x} r_m \cos \varphi_2 & k_x + 2iz - r_m q_0 & 0 \\ -q_{1x} r_m \cos \varphi_1 & q_{2x} r_m \sin \varphi_2 & 0 & k_x + 2iz + r_m q_0 \end{bmatrix} \begin{bmatrix} b_1 \\ b_2 \\ c_1 \\ c_2 \end{bmatrix} = \begin{bmatrix} -\cos \varphi_1 \\ \sin \varphi_1 \\ q_{1x} r_m \cos \varphi_1 \\ -q_{1x} r_m \sin \varphi_1 \end{bmatrix}, \quad (2.9)$$

$$\begin{bmatrix} \sin \varphi_1 & \cos \varphi_2 & -1 & 0 \\ \cos \varphi_1 & \sin \varphi_2 & 0 & -1 \\ -q_{1x} r_m \sin \varphi_1 & q_{2x} r_m \cos \varphi_2 & k_x + 2iz - r_m q_0 & 0 \\ -q_{1x} r_m \cos \varphi_1 & q_{2x} r_m \sin \varphi_2 & 0 & k_x + 2iz + r_m q_0 \end{bmatrix} \begin{bmatrix} b_1 \\ b_2 \\ c_1 \\ c_2 \end{bmatrix} = \begin{bmatrix} -\cos \varphi_2 \\ -\sin \varphi_2 \\ -q_{1x} r_m \sin \varphi_1 \\ -q_{1x} r_m \cos \varphi_1 \end{bmatrix}, \quad (2.10)$$

where $r_m = \frac{m}{m^*}$, equations (2.9) and (2.10) are for $E > -E_{F,2DEG}$ and for $E < -E_{F,2DEG}$

respectively. In case of the incident state with wave vector \vec{q}_2 , the following equation

for $E > -E_{F,2DEG}$ and for $E < -E_{F,2DEG}$ are obtained respectively.

$$\begin{bmatrix} \sin \varphi_1 & \cos \varphi_2 & -1 & 0 \\ -\cos \varphi_1 & \sin \varphi_2 & 0 & -1 \\ q_{1x} r_m \sin \varphi_1 & q_{2x} r_m \cos \varphi_2 & k_x + 2iz - r_m q_0 & 0 \\ -q_{1x} r_m \cos \varphi_1 & q_{2x} r_m \sin \varphi_2 & 0 & k_x + 2iz + r_m q_0 \end{bmatrix} \begin{bmatrix} b_1 \\ b_2 \\ c_1 \\ c_2 \end{bmatrix} = \begin{bmatrix} -\sin \varphi_2 \\ -\cos \varphi_2 \\ q_{2x} r_m \sin \varphi_2 \\ q_{2x} r_m \cos \varphi_2 \end{bmatrix}, \quad (2.11)$$

$$\begin{bmatrix} \sin \varphi_1 & \cos \varphi_2 & -1 & 0 \\ \cos \varphi_1 & \sin \varphi_2 & 0 & -1 \\ -q_{1x} r_m \sin \varphi_1 & q_{2x} r_m \cos \varphi_2 & k_x + 2iz - r_m q_0 & 0 \\ -q_{1x} r_m \cos \varphi_1 & q_{2x} r_m \sin \varphi_2 & 0 & k_x + 2iz + r_m q_0 \end{bmatrix} \begin{bmatrix} b_1 \\ b_2 \\ c_1 \\ c_2 \end{bmatrix} = \begin{bmatrix} -\sin \varphi_2 \\ -\cos \varphi_2 \\ q_{2x} r_m \sin \varphi_2 \\ q_{2x} r_m \cos \varphi_2 \end{bmatrix}, \quad (2.12)$$

These 4×4 equations above are used to obtain the reflection and transmission coefficients and then the reflection and transmission probabilities which are defined as follows.

$$B_{1(2)}(E, kz) = \left| b_{1(2)}(E, kz) \right|^2 \frac{|v_r^{1(2)}|}{|v_{in}|}, \quad (2.13)$$

$$C_{1(2)}(E, kz) = \left| c_{1(2)}(E, kz) \right|^2 \frac{|v_t^{1(2)}|}{|v_{in}|}, \quad (2.14)$$

where $v_{in}^{1(2)} = \frac{1}{\hbar} \frac{\partial E^{+(-)}}{\partial q_x} \Big|_{q_x=q_{1x(2x)}}$, $v_r^{1(2)} = \frac{1}{\hbar} \frac{\partial E^{+(-)}}{\partial q_x} \Big|_{q_x=-q_{1x(2x)}}$ are the group velocities of

the incoming and reflected eigenstates in the 2DEG respectively, and $v_t = \frac{1}{\hbar} \frac{\partial E}{\partial k_x} \Big|_{k_x}$ is

the group velocity of transmitted eigenstates in the metal. The superscript 1(2) indicates the state with wave vector \bar{q}_1 (\bar{q}_2). The magnitude of these group velocities are defined as follows.

$$v_{in}^1 = \frac{\hbar}{m^*} (q_{1x} + q_0 \cos 2\varphi_1), \quad \text{for } E > -E_{F,2DEG},$$

$$v_{in}^1 = \frac{\hbar}{m^*} (-q_{1x} + q_0 \cos 2\varphi_1), \quad \text{for } E < -E_{F,2DEG},$$

$$v_{in}^2 = \frac{\hbar}{m^*} (q_{2x} - q_0 \cos 2\varphi_2) = v_r^2, \quad \text{for all } E,$$

$$v_r^1 = \frac{\hbar}{m^*} (-q_{1x} - q_0 \cos 2\varphi_1), \quad \text{for } E > -E_{F,2DEG},$$

$$v_r^1 = \frac{\hbar}{m^*} (q_{1x} - q_0 \cos 2\varphi_1), \quad \text{for } E < -E_{F,2DEG},$$

$$v_t^{1(2)} = \frac{\hbar k_x}{m}, \quad \text{for all } E.$$

The conservation of probability requires

$$B_1(E, k_z) + B_2(E, k_z) + C_1(E, k_z) + C_2(E, k_z) = 1 \quad (2.15)$$

In the 2D system, the general expression for the current density in x -direction across the junction is given by

$$J = \sum_{k_x, k_z} n_k v_k e \quad (2.16)$$

where v_k is the group velocities and e is the electron charge, the electron concentration, $n_k = (C_1(E) + C_2(E))f(E)$ where $f(E)$ is the Fermi Dirac distribution function. The current flowing to the right across junction from 2DEG to metal with applied voltage, V is

$$I_{2DEG \rightarrow M} = \frac{L^2 e}{4\pi^2} \iint dk_x dk_z v_k (C_1(E, k_z) + C_2(E, k_z)) f(E - eV), \quad (2.17)$$

where L represent the dimension of the interface. The current flowing to the left across junction from metal to 2DEG is

$$I_{M \rightarrow 2DEG} = \frac{L^2 e}{4\pi^2} \iint dk_x dk_z v_k (C_1(E, k_z) + C_2(E, k_z)) f(E), \quad (2.18)$$

Thus, the net current crossing the junction is

$$\begin{aligned} I(eV) &= I_{2DEG \rightarrow M} - I_{M \rightarrow 2DEG} \\ &= \frac{L^2 e}{4\pi^2} \iint dk_x dk_z v_k (C_1(E, k_z) + C_2(E, k_z)) [f(E - eV) - f(E)] \\ &= \frac{L^2 e}{4\pi^2 \hbar} \iint dk_z dE (C_1(E, k_z) + C_2(E, k_z)) [f(E - eV) - f(E)]. \end{aligned} \quad (2.19)$$

The tunneling conductance of the 2DEG/M junction is the derivative of the current flows across junction with respect to the applied voltage

$$G_{2DEG/M}(eV) = \frac{dI_{2DEG/M}(eV)}{dV}. \quad (2.20)$$

At zero temperature, the tunneling conductance becomes

$$G(eV) = \frac{L^2 e^2}{4\pi^2 \hbar} \int dk_z (C_1(eV, k_z) + C_2(eV, k_z)), \quad (2.21)$$

2.2 Results and Discussion

The tunneling probabilities (C_1 , C_2) of up- and down-spin eigenstates of 2DEG/M junction depend on the incident angle (or k_z) as shown in Fig. 2.2. It is found that for normal incident ($k_z = 0$), the transmission probabilities of spin up and

spin down states are equal due to the fact that for $k_z = 0$ the spin states in the plus and minus branches are completely up- and down-spin. However, when k_z is non-zero the tunneling probability of transmitted electron up- and down-spin are not equal and spin polarization can be generated. It is found that for each k_z within some energy range, the spin is strongly polarized as shown by the arrow-headed line in Fig. 2.2.

The energy range where the spin polarization is large for each k_z consistent with the splitting of two branches at $k_x = 0$, $E^\pm(0, k_z)$ (see the inset of Fig. 2.2). This splitting, caused by the two dimensionality, is similar to the splitting due to magnetic field in the previous work by Středa and Šeba's on the junction of two 2DEGs with RSOC in one dimension (Středa and Šeba, 2003).

Fig. 2.3 contains the spectra of spin-up (G_1), spin-down (G_2) and the net conductance. The difference in G_1 and G_2 defines the spin polarization of the system. The spin polarization depends on the applied voltage. It is maximum at the bias voltage equal to the crossing of two energy branches. The spin polarization is not always increased with RSOC strength (q_0) as one may expect. The difference between the conductance of electron spin up and spin down ($G_2 - G_1$) at $eV = E_{F,2DEG}$ is only increased with q_0 until it reaches a maximum value and then steadily decreased as shown in Fig. 2.4.

Fig. 2.5 shows the conductance spectra at $eV = E_{F,2DEG}$ as a function of barrier potential(z). It is found that the effect of the z on the spin-up and spin-down conductance at $eV = E_{F,2DEG}$ is different. For the spin down conductance z suppresses the conductance, while the spin-up is enhanced up to a critical value z^* and is then decreased with z . Thus, the increase in the potential barrier decreases the difference

between the conductance of spin up and spin down electrons. These results are different from those of 2DEG/F junction previously studied by Jiang and Jalil (Jiang and Jalil, 2003).

Fig. 2.6 shows the plots of conductance spectra at $eV = E_{F,2DEG}$ as a function of z at different values of q_0 . It is found that conductance is slightly enhanced within a range of small z and is then decreased with z .

The plot of conductance as a function of bias voltage for different values of q_0 is shown in Fig. 2.7. It suggests that one can use the tunneling spectroscopy to measure the strength of RSOC. The distance of the two distinguished features as indicated in the Fig. 2.7 is equal to the Rashba energy.

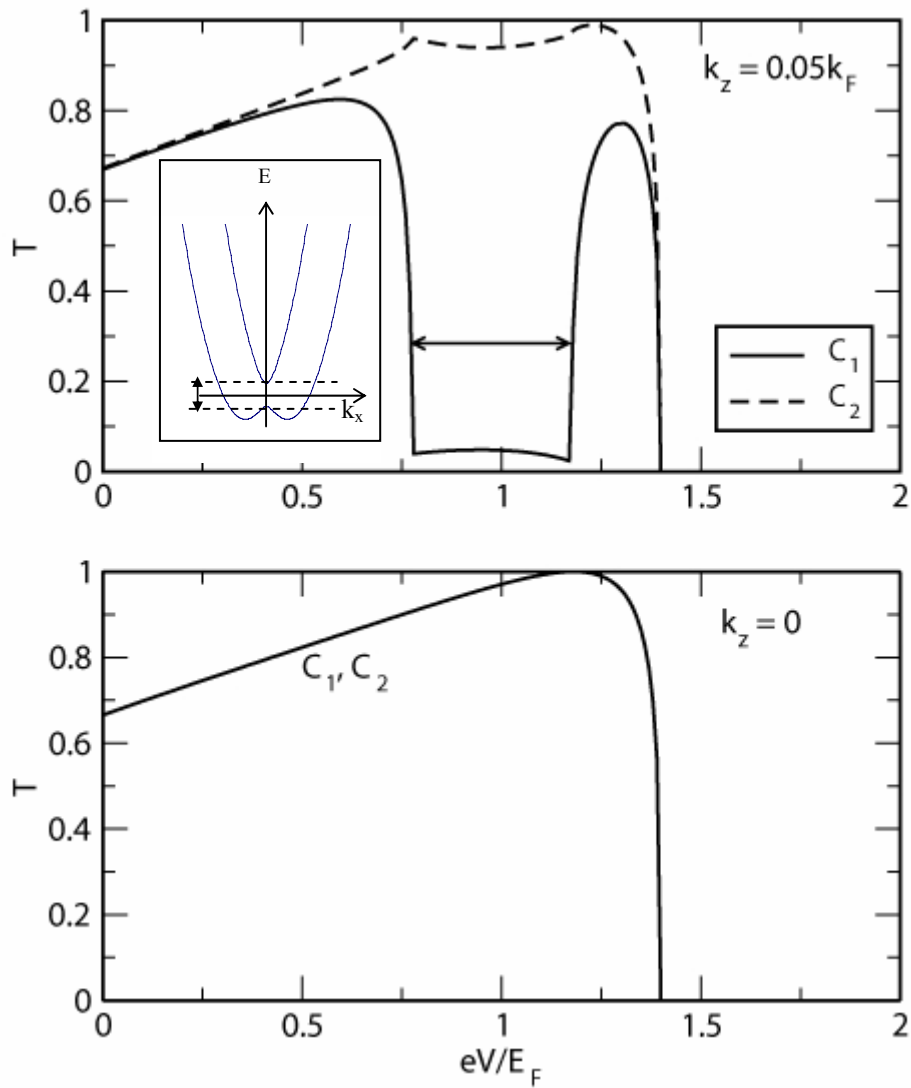


Figure 2.2 The transmission probabilities of up- (C_1) and down- (C_2) spin states for different $k_z = 0$ and $0.05 k_F$, $m/m^* = 10$. The horizontal arrow line indicates the energy range over which the spin polarization is large. The inset in the upper panel is the plot of the energy vs k_x at a particular k_z . The range of the energy between the two dashed line correspond to the energy range indicates by the arrow lines.

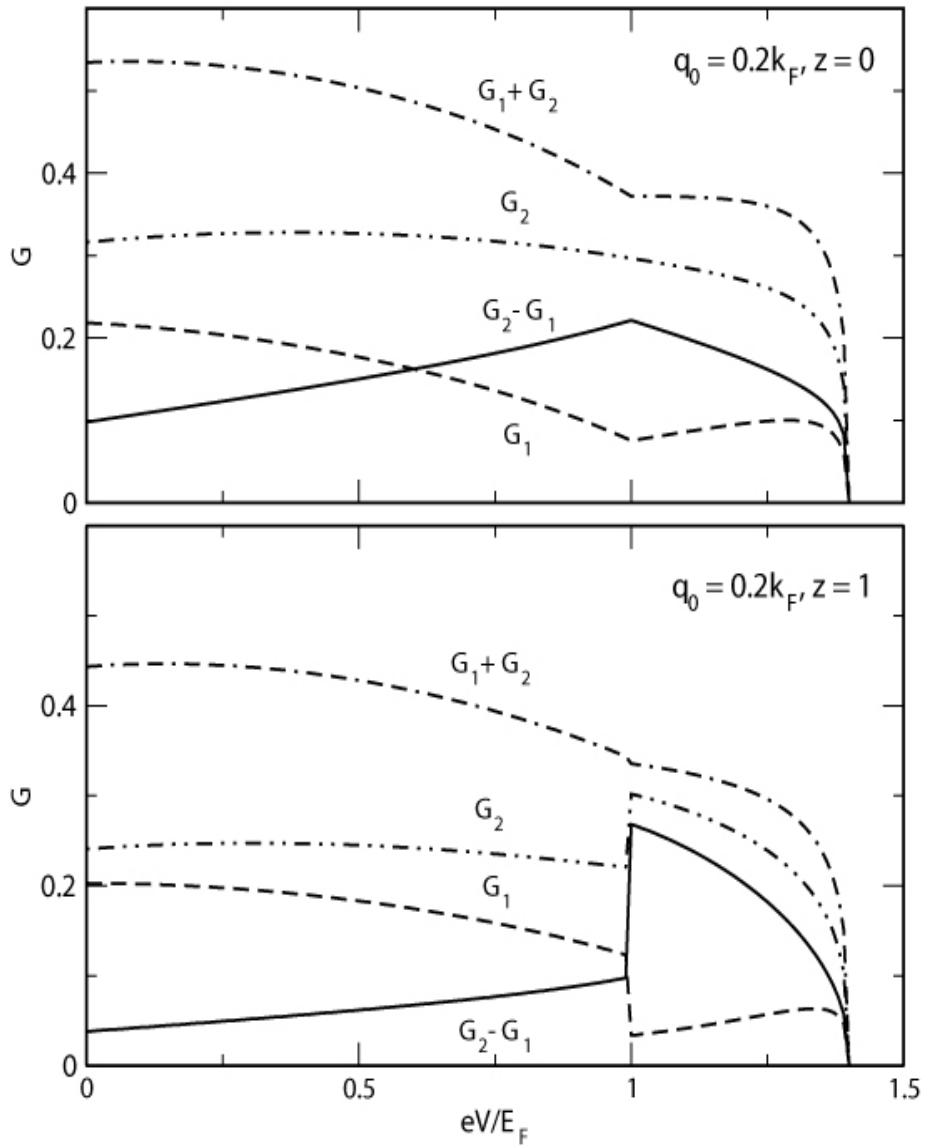


Figure 2.3 The tunneling conductance of up- (G_1) and down- (G_2) spin, the difference between up- and down-spin conductance ($G_2 - G_1$) and the total conductance ($G_1 + G_2$), for $q_0 = 0.2k_F$ and $m/m^* = 10$ for $z = 0$ and 1 . $E_F = E_{F,2DEG} = E_{F,M}$ for simplicity.

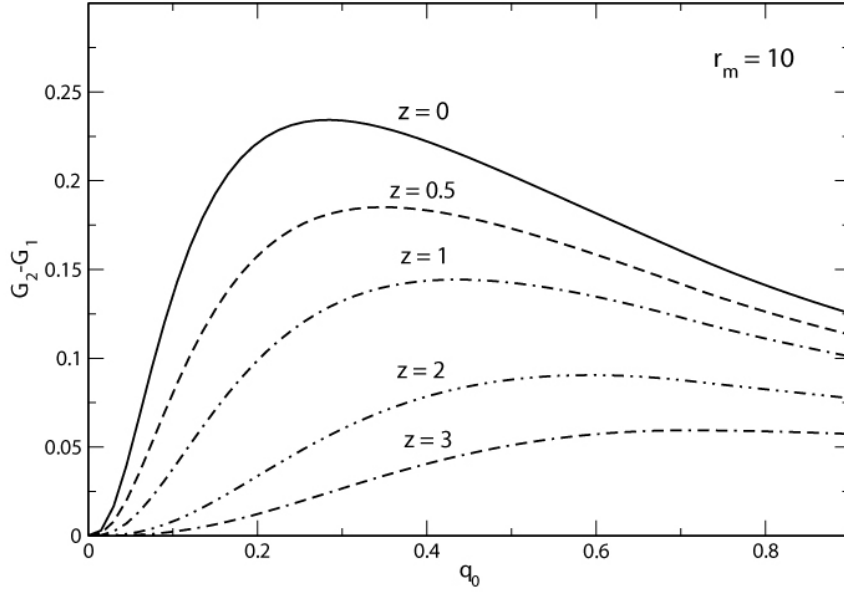


Figure 2.4 The difference of the conductance of spin-up and spin-down at $eV = E_{F,2DEG}$ as a function of q_0 for different $z = 0, 0.5, 1, 2$ and 3 , $m/m^* = 10$.

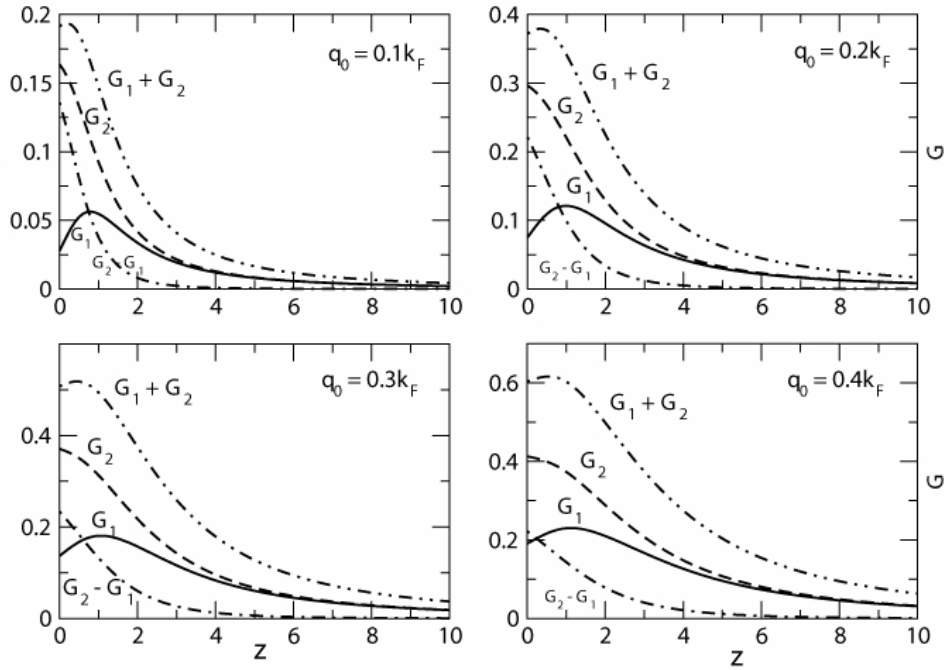


Figure 2.5 The conductance spectra of 2DEG/M junction for a fixed $q_0 = 0.1k_F, 0.2k_F, 0.3k_F$ and $0.4k_F$ at $eV = E_{F,2DEG}$. $m/m^* = 10$ (G_1, G_2, G_1+G_2 and G_2-G_1 same as defined in Fig. 2.3)

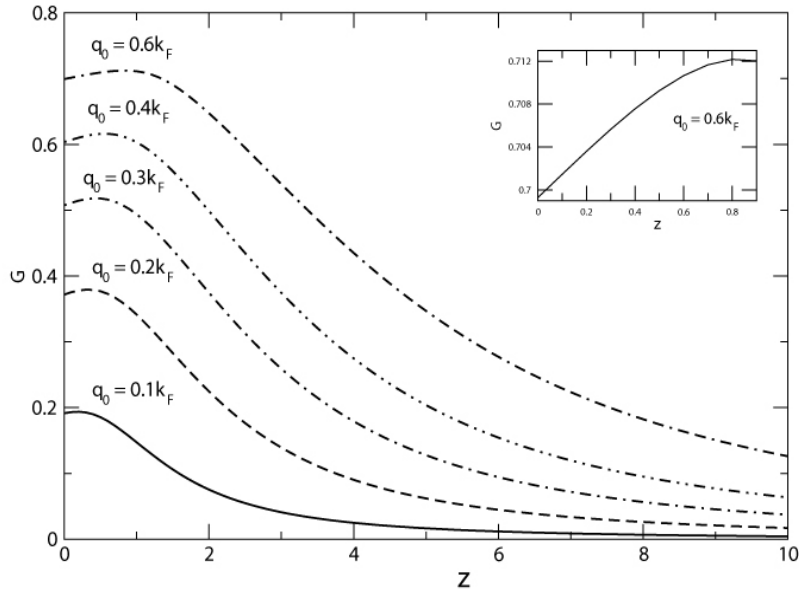


Figure 2.6 The conductance as a function of z for different q_0 at $eV = E_{F,2DEG}$. The inset shows the close up of the conductance near $z = 0$ where $q_0 = 0.6k_F$, $m/m^* = 10$.

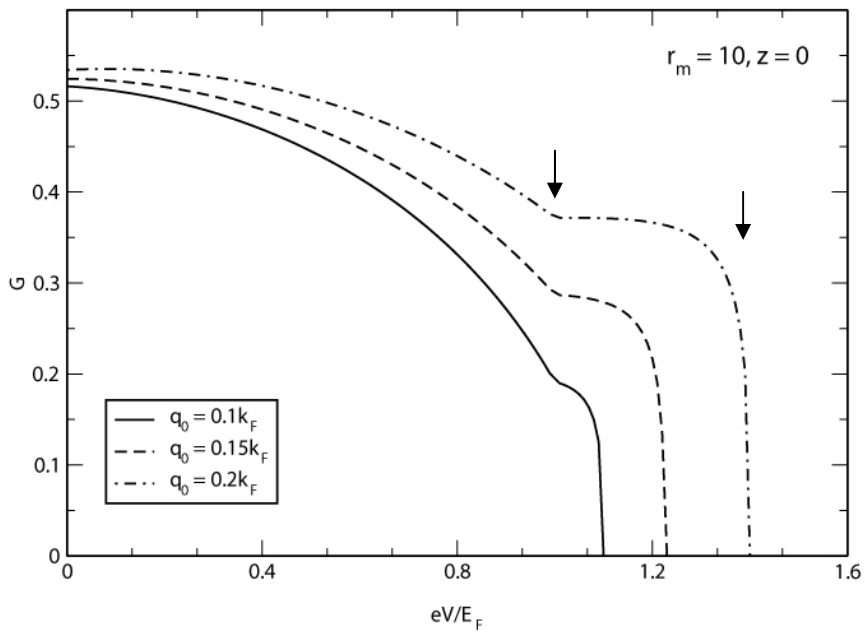


Figure 2.7 The conductance as a function of bias voltage for different $q_0 = 0.1k_F$, $0.15k_F$ and $0.2k_F$, $m/m^* = 10$. The arrows in the case of $q_0 = 0.2k_F$ indicates the two features occurs at $eV = E_{F,2DEG}$ and $E_{F,2DEG} + E_\lambda$.

2.3 Conclusion

In this chapter, the tunneling conductance spectra of 2DEG/M junction are examined. It is found that the injection from 2DEG can generate the spin polarization in the metal which is caused by the two-dimensionality. The spin polarization depends on the applied voltage. It is maximum at the crossing of two energy branches. The increase in the barrier potential decreases the spin polarization and also suppress the conductance except in a range of small barrier, which the conductance is slightly enhanced.

The increase in RSOC strength enhances the conductance spectra. However, the difference between the conductance of spin up and spin down electrons is not increased with RSOC strength as one may expect. It is just enhanced over some range of RSOC strength and then steadily decreased. From the plot of conductance as a function of bias voltage, it suggests that one can use the tunneling spectroscopy to measure the strength of RSOC.

CHAPTER III

2DEG/S JUNCTION

Recently, 2DEG/S junction was studied by Yokoyama et al. (Yokoyama, Tanaka and Inoue, 2006). They calculated the tunneling conductance of the junction in comparison with that of F/S junction. In their study, they considered only when the Fermi level of the 2DEG is much higher than the Rashba energy and they did not show explicitly the effect of the different effective mass of both sides. In general, one can control the Fermi level of the 2DEG by adjusting the number of carriers. One can study how the lower Fermi level will affect the charge transport in 2DEG/S junctions.

In this chapter, the tunneling spectroscopy of 2DEG/S junction is investigated. The Fermi level of the 2DEG will be set arbitrarily. The effect of RSOC strength, barrier potential and the mismatch of effective masses will be studied in details.

3.1 Model and Method of Calculation

The junction is modeled as a 2D infinite system in the xz plane. The interface is at $x = 0$. The 2DEG occupies the $x < 0$ region and the superconductor occupies the $x > 0$ region as depicted in Fig. 3.1. The potential barrier at the interface is described by a delta function, $V(x) = H_s \delta(x)$ where H_s represents the strength of barrier. The gap function is taken to be zero in the 2DEG and to be finite and independent of position on the superconductor, i.e. $\Delta(\vec{k}) = \Delta \Theta(x)$ where $\Theta(x)$ is the Heaviside step function and Δ is a constant.

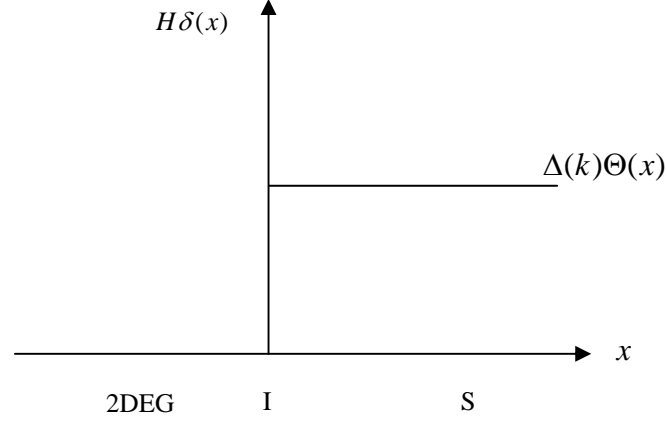


Figure 3.1 The sketch of the 2DEG/S junction.

In the study of 2DEG/M junction in Chapter II, only the Hamiltonian of electrons is used. However, in 2DEG/S junction, the Hamiltonian of hole needs to be included, because a quasiparticle in the superconductor is a combination of both electron and hole. Therefore, the Schrödinger equations describing the system is written as

$$\begin{pmatrix} \hat{H}_0 + \hat{H}_{R\uparrow} + H_S \delta(x) & 0 & \Delta \Theta(x) & 0 \\ 0 & \hat{H}_0 + \hat{H}_{R\downarrow} + H_S \delta(x) & 0 & \Delta \Theta(x) \\ \Delta \Theta(x) & 0 & -\hat{H}_0 + \hat{H}_{R\uparrow} - H_S \delta(x) & 0 \\ 0 & \Delta \Theta(x) & 0 & -\hat{H}_0 + \hat{H}_{R\downarrow} - H_S \delta(x) \end{pmatrix} \psi(x, z) = E \psi(x, z), \quad (3.1)$$

where \hat{H}_0 and $\hat{H}_{R\uparrow, \downarrow}$ are the Hamiltonian of the free electron and Rashba Hamiltonian of electron and/or hole with spin up and spin down respectively. That is,

$$\hat{H}_0 = \hat{p} \frac{1}{2m(x)} \hat{p} - E_{F,S} \Theta(x) - E_{F,2DEG} \Theta(-x),$$

$$\hat{H}_{R\uparrow} = \frac{\lambda}{2} (\Theta(-x)(\sigma_{z(11)}\hat{p}_x - \sigma_{x(12)}\hat{p}_z) + (\sigma_{z(11)}\hat{p}_x - \sigma_{x(12)}\hat{p}_z)\Theta(-x)),$$

$$\hat{H}_{R\downarrow} = \frac{\lambda}{2} (\Theta(-x)(\sigma_{z(22)}\hat{p}_x - \sigma_{x(12)}\hat{p}_z) + (\sigma_{z(22)}\hat{p}_x - \sigma_{x(12)}\hat{p}_z)\Theta(-x)),$$

where \hat{p} is a momentum operator in 2D, $\frac{1}{m(x)} = \frac{1}{m^*}\Theta(-x) + \frac{1}{m}\Theta(x)$ is the effective

mass of the system (m^* in 2DEG and m in the superconductor). $\psi(x, z)$ is a four-

component wave function $\psi(x, z) = \begin{pmatrix} \psi_{e\uparrow} \\ \psi_{e\downarrow} \\ \psi_{h\uparrow} \\ \psi_{h\downarrow} \end{pmatrix}$.

In the superconductor, or the $x > 0$ region, the eigenenergies of excitations are

$$E_k = \sqrt{\xi_k^2 + \Delta^2} \quad (3.2)$$

where $\xi_k = \frac{\hbar^2 k^2}{2m} - E_{F,S}$. The excitation energy dispersion is depicted in Fig. 3.2

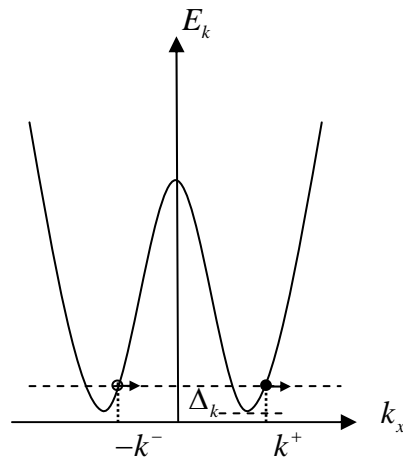


Figure 3.2 The sketch of the excitation energy of the quasiparticles in the superconductor

The wave function of quasiparticle in the superconducting side is a linear combination of the four transmitted excitations:

$$\psi_s(x > 0, z) = \left[c_1 e^{ik_x^+ x} \begin{pmatrix} u_{k^+} \\ 0 \\ 0 \\ -v_{k^+} \end{pmatrix} + c_2 e^{ik_x^+ x} \begin{pmatrix} 0 \\ u_{k^+} \\ v_{k^+} \\ 0 \end{pmatrix} + d_1 e^{-ik_x^- x} \begin{pmatrix} u_{-k^-} \\ 0 \\ 0 \\ -v_{-k^-} \end{pmatrix} + d_2 e^{-ik_x^- x} \begin{pmatrix} 0 \\ u_{-k^-} \\ v_{-k^-} \\ 0 \end{pmatrix} \right] e^{ik_z z}, \quad (3.3)$$

where c_1 , c_2 , d_1 and d_2 are the amplitudes of the four transmissions, and

$$k^+ = \sqrt{\frac{2m}{\hbar^2} (E_F + \sqrt{E^2 - \Delta^2})},$$

$$k^- = \sqrt{\frac{2m}{\hbar^2} (E_F - \sqrt{E^2 - \Delta^2})}.$$

u_k and v_k are the electron-like and hole-like quasiparticle amplitudes; and are defined as

$$u_k = \frac{E + \xi_k}{\sqrt{|E + \xi_k|^2 + |\Delta_k|^2}}, \quad (3.4)$$

$$v_k = \frac{\Delta_k}{\sqrt{|E + \xi_k|^2 + |\Delta_k|^2}}, \quad (3.5)$$

so that $|u_k|^2 + |v_k|^2 = 1$.

In the 2DEG or the $x < 0$ region, the excitation energy dispersion relation is

$$E^\pm = \frac{\hbar^2}{2m^*} (q \pm q_0)^2 - \frac{\hbar^2 q_0^2}{2m^*} - E_{F,2DEG} \quad \text{for electrons}$$

and

$$E^\pm = E_{F,2DEG} - \frac{\hbar^2}{2m^*} (q \pm q_0)^2 + \frac{\hbar^2 q_0^2}{2m^*} \quad \text{for holes.}$$

The energy dispersion on 2DEG is depicted in Fig. 3.3(a).

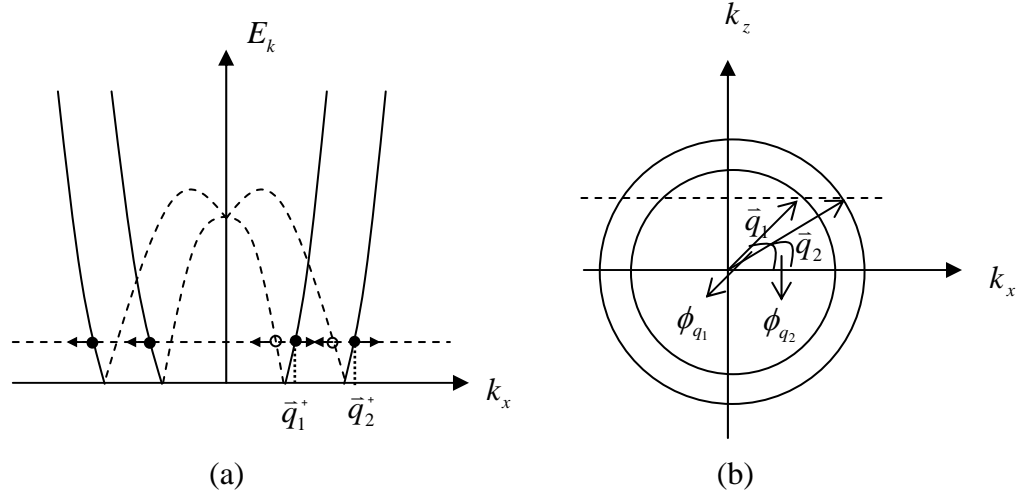


Figure 3.3 (a) The sketch of energy dispersion of 2DEG with RSOC. (b) The energy contours of the electrons in 2DEG. (q_1^+ and q_2^+ are the x -component of wave vector \bar{q}_1 (plus branch) and \bar{q}_2 (minus branch))

Unlike in 2DEG/M junction, the two-component eigenstates of the electron in 2DEG here the eigenstates of the 2DEG here are now four-component:

$$|\bar{q}_1\rangle = \begin{pmatrix} \cos \frac{\phi_1}{2} \\ -\sin \frac{\phi_1}{2} \\ 0 \\ 0 \end{pmatrix} e^{i\bar{q}_1 \cdot \bar{r}} \quad \text{and} \quad |\bar{q}_2\rangle = \begin{pmatrix} \sin \frac{\phi_2}{2} \\ \cos \frac{\phi_2}{2} \\ 0 \\ 0 \end{pmatrix} e^{i\bar{q}_2 \cdot \bar{r}}, \quad \text{for electron} \quad (3.6)$$

$$|\bar{q}_1\rangle = \begin{pmatrix} 0 \\ 0 \\ -\sin\frac{\phi_1}{2} \\ -\cos\frac{\phi_1}{2} \end{pmatrix} e^{i\bar{q}_1\bar{r}} \quad \text{and} \quad |\bar{q}_2\rangle = \begin{pmatrix} 0 \\ 0 \\ \cos\frac{\phi_1}{2} \\ -\sin\frac{\phi_1}{2} \end{pmatrix} e^{i\bar{q}_2\bar{r}}, \quad \text{for hole} \quad (3.7)$$

where $\phi_{1(2)}$ are the angle between wave vector $\bar{q}_{1(2)}$ and wave vector \bar{k}_x as in Fig. 3.3(b).

Most 2DEG systems are semiconductors and one can adjust the Fermi energy by adjusting the density of the carriers. In this chapter, the effect of the different Fermi levels in the 2DEG will be considered.

Case 1: where E_F is located above the crossing of the branches.

Case 2: where E_F is located at the crossing of the branches.

Case 3: where E_F is located below the crossing of the branches.

In all cases, the Rashba energy is assumed to be more than the superconducting gap

($\frac{\hbar^2 q_0^2}{2m^*} > \Delta$) and the gap is set to be $0.01E_F$. The wave function of the excitation in the

2DEG is different for each case.

3.1.1 Case 1: E_F is located above the crossing of the two branches

In this case, the excitation energies of the 2DEG and the superconductor are as depicted in Fig. 3.4. The Fermi energy of the 2DEG is set to be equal to that of the superconductor, i. e. $E_{F,2DEG} = E_{F,S} = E_F$.

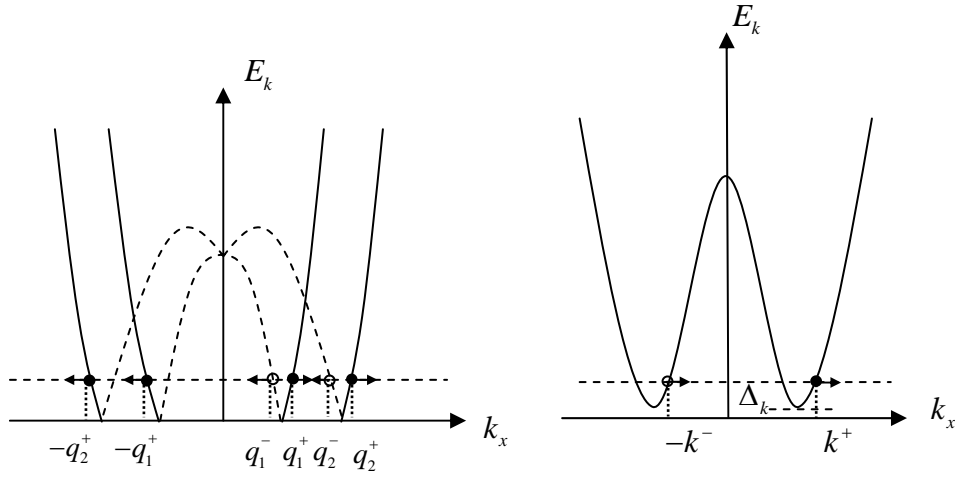


Figure 3.4 The sketch of excitation energy of 2DEG/S junction

There are two possibilities for an incident state.

- 1) From the plus branch with wave vector \bar{q}_1 , where

$$q_1 = -q_0 + \sqrt{q_0^2 + \frac{2m^*}{\hbar^2}(E + E_F)}.$$

In this case, the wave function of the excitation in 2DEG can be written as

$$\begin{aligned} \psi_{2DEG}(x < 0, z) = & \left[e^{iq_1^+ x} \begin{pmatrix} \cos \varphi_1^+ \\ -\sin \varphi_1^+ \\ 0 \\ 0 \end{pmatrix} + a_1 e^{iq_1^- x} \begin{pmatrix} 0 \\ 0 \\ -\sin \varphi_1^- \\ -\cos \varphi_1^- \end{pmatrix} + a_2 e^{iq_2^- x} \begin{pmatrix} 0 \\ 0 \\ \cos \varphi_2^- \\ -\sin \varphi_2^- \end{pmatrix} \right. \\ & \left. + b_1 e^{-iq_1^+ x} \begin{pmatrix} \sin \varphi_1^+ \\ -\cos \varphi_1^+ \\ 0 \\ 0 \end{pmatrix} + b_2 e^{-iq_2^+ x} \begin{pmatrix} \cos \varphi_2^+ \\ \sin \varphi_2^+ \\ 0 \\ 0 \end{pmatrix} \right] e^{ik_z z}, \quad (3.8) \end{aligned}$$

where $\varphi = \frac{\phi}{2}$, a_1 and a_2 are the Andreev reflection amplitudes of the states from the

plus and minus branch respectively, and b_1 and b_2 are the normal reflection

amplitudes of the states from the plus and minus branch respectively. The x -components of the momenta q_1^{+-} and q_2^{+-} are defined as follows.

$$q_1^+ = \sqrt{(-q_0 + \sqrt{q_0^2 + \frac{2m^*}{\hbar^2}(E + E_F)})^2 - k_z^2},$$

$$q_2^+ = \sqrt{(q_0 + \sqrt{q_0^2 + \frac{2m^*}{\hbar^2}(E + E_F)})^2 - k_z^2},$$

$$q_1^- = \sqrt{(-q_0 + \sqrt{q_0^2 + \frac{2m^*}{\hbar^2}(-E + E_F)})^2 - k_z^2},$$

$$q_2^- = \sqrt{(q_0 + \sqrt{q_0^2 + \frac{2m^*}{\hbar^2}(-E + E_F)})^2 - k_z^2},$$

2) From the minus branch with wave vector \bar{q}_2 , where

$$q_2 = q_0 + \sqrt{q_0^2 + \frac{2m^*}{\hbar^2}(E + E_F)}.$$

The wave function of the excitation in this case is

$$\begin{aligned} \psi_{2DEG}(x < 0, z) = & \left[e^{iq_2^+ x} \begin{pmatrix} \sin \varphi_2^+ \\ \cos \varphi_2^+ \\ 0 \\ 0 \end{pmatrix} + a_1' e^{iq_1^- x} \begin{pmatrix} 0 \\ 0 \\ -\sin \varphi_1^- \\ -\cos \varphi_1^- \end{pmatrix} + a_2' e^{iq_2^- x} \begin{pmatrix} 0 \\ 0 \\ \cos \varphi_2^- \\ -\sin \varphi_2^- \end{pmatrix} + \right. \\ & \left. b_1' e^{-iq_1^+ x} \begin{pmatrix} \sin \varphi_1^+ \\ -\cos \varphi_1^+ \\ 0 \\ 0 \end{pmatrix} + b_2' e^{-iq_2^+ x} \begin{pmatrix} \cos \varphi_2^+ \\ \sin \varphi_2^+ \\ 0 \\ 0 \end{pmatrix} \right] e^{ik_z z}, \end{aligned}$$

(3.9)

a_1' and a_2' are the Andreev reflection amplitudes of the states from the plus and minus branch respectively and b_1' and b_2' are the normal reflection amplitudes of the states from the plus and minus branch respectively.

3.1.2 Case 2: E_F is located at the crossing of the two branches

The excitation energy dispersion of the 2DEG in this case is shown in Fig. 3.5

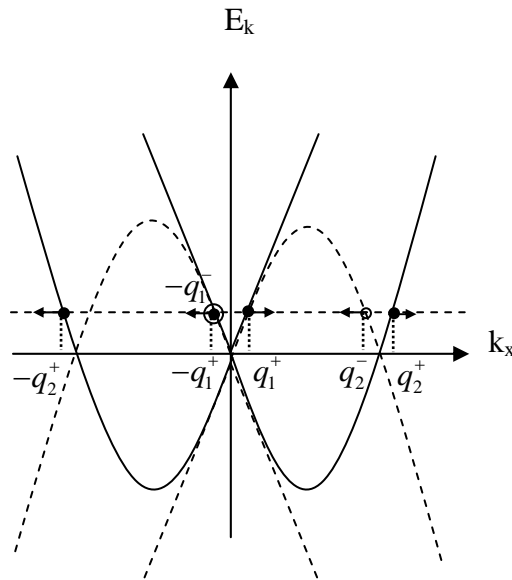


Figure 3.5 The sketch of excitation energy on 2DEG side

In this case the incident electrons are from only minus branch. The two possibilities of the electron wave function of the 2DEG are:

- 1) (The incident is the state with the momentum \bar{q}_1 , $q_1 = -q_0 + \sqrt{q_0^2 + \frac{2m^*E}{\hbar^2}}$)

$$\begin{aligned}
\psi_{2DEG}(x < 0, z) = & \left[e^{iq_1^+ x} \begin{pmatrix} \cos \varphi_1^+ \\ -\sin \varphi_1^+ \\ 0 \\ 0 \end{pmatrix} + a_1 e^{-iq_1^- x} \begin{pmatrix} 0 \\ 0 \\ -\cos \varphi_1^- \\ -\sin \varphi_1^- \end{pmatrix} + a_2 e^{iq_2^- x} \begin{pmatrix} 0 \\ 0 \\ \cos \varphi_2^- \\ -\sin \varphi_2^- \end{pmatrix} \right. \\
& \left. + b_1 e^{-iq_1^+ x} \begin{pmatrix} \sin \varphi_1^+ \\ -\cos \varphi_1^+ \\ 0 \\ 0 \end{pmatrix} + b_2 e^{-iq_2^+ x} \begin{pmatrix} \cos \varphi_2^+ \\ \sin \varphi_2^+ \\ 0 \\ 0 \end{pmatrix} \right] e^{ik_z z},
\end{aligned} \tag{3.10}$$

2) (The incident state is the state with the momentum \bar{q}_2 , $q_2 = q_0 + \sqrt{q_0^2 + \frac{2m^*E}{\hbar^2}}$)

$$\begin{aligned}
\psi_{2DEG}(x < 0, z) = & \left[e^{iq_2^+ x} \begin{pmatrix} \sin \varphi_2^+ \\ \cos \varphi_2^+ \\ 0 \\ 0 \end{pmatrix} + a_1 e^{-iq_1^- x} \begin{pmatrix} 0 \\ 0 \\ -\cos \varphi_1^- \\ -\sin \varphi_1^- \end{pmatrix} + a_2 e^{iq_2^- x} \begin{pmatrix} 0 \\ 0 \\ \cos \varphi_2^- \\ -\sin \varphi_2^- \end{pmatrix} \right. \\
& \left. + b_1 e^{-iq_1^+ x} \begin{pmatrix} \sin \varphi_1^+ \\ -\cos \varphi_1^+ \\ 0 \\ 0 \end{pmatrix} + b_2 e^{-iq_2^+ x} \begin{pmatrix} \cos \varphi_2^+ \\ \sin \varphi_2^+ \\ 0 \\ 0 \end{pmatrix} \right] e^{ik_z z},
\end{aligned} \tag{3.11}$$

The x -components of the momenta $q_1^{+,-}$ and $q_2^{+,-}$ in this case are as follows.

$$q_1^+ = \sqrt{(-q_0 + \sqrt{q_0^2 + \frac{2m^*E}{\hbar^2}})^2 - k_z^2}$$

$$q_2^+ = \sqrt{(q_0 + \sqrt{q_0^2 + \frac{2m^*E}{\hbar^2}})^2 - k_z^2}$$

$$q_1^- = \sqrt{(-q_0 + \sqrt{q_0^2 - \frac{2m^* E}{\hbar^2}})^2 - k_z^2}$$

$$q_2^- = \sqrt{(q_0 + \sqrt{q_0^2 - \frac{2m^* E}{\hbar^2}})^2 - k_z^2}$$

3.1.3 Case 3: E_F is located below the crossing of the two branches

The excitation energy dispersion of the 2DEG in this case is shown in Fig. 3.6.

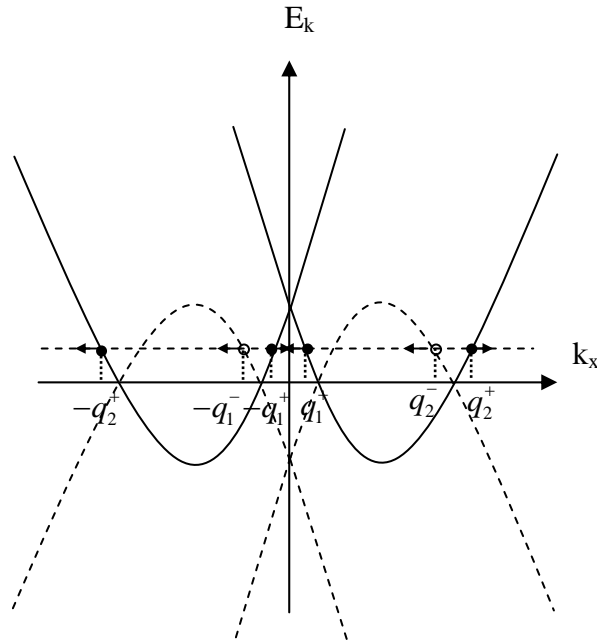


Figure 3.6 The sketch of excitation energy on 2DEG side when voltage V is applied

Similar to the previous case, in this case the incident electrons are also from only minus branch. However, the AR with wave vector \bar{q}_1 comes from different energy branch for the energy above and below the crossing. The two possibilities of the electron wave function of the 2DEG are:

- 1) (The incident state is the state with momentum $-\bar{q}_1$, $q_1 = q_0 - \sqrt{q_0^2 + \frac{2m^*(E-E_c)}{\hbar^2}}$,

E_c is the energy at the crossing)

$$\begin{aligned} \psi_{2DEG}(x < 0, z) = & \left[e^{-iq_1^+ x} \begin{pmatrix} \cos \varphi_1^+ \\ \sin \varphi_1^+ \\ 0 \\ 0 \end{pmatrix} + a_1 e^{-iq_1^- x} \begin{pmatrix} 0 \\ 0 \\ -\cos \varphi_1^- \\ -\sin \varphi_1^- \end{pmatrix} + a_2 e^{iq_2^- x} \begin{pmatrix} 0 \\ 0 \\ \cos \varphi_2^- \\ -\sin \varphi_2^- \end{pmatrix} \right. \\ & \left. + b_1 e^{iq_1^+ x} \begin{pmatrix} \sin \varphi_1^+ \\ \cos \varphi_1^+ \\ 0 \\ 0 \end{pmatrix} + b_2 e^{-iq_2^+ x} \begin{pmatrix} \cos \varphi_2^+ \\ \sin \varphi_2^+ \\ 0 \\ 0 \end{pmatrix} \right] e^{ik_z z} \quad (3.12), \end{aligned}$$

- 2) (The incident state is the state with momentum \bar{q}_2 , $q_2 = q_0 + \sqrt{q_0^2 + \frac{2m^*(E-E_c)}{\hbar^2}}$)

$$\begin{aligned} \psi_{2DEG}(x < 0, z) = & \left[e^{iq_2^+ x} \begin{pmatrix} \sin \varphi_2^+ \\ \cos \varphi_2^+ \\ 0 \\ 0 \end{pmatrix} + a_1' e^{-iq_1^- x} \begin{pmatrix} 0 \\ 0 \\ -\cos \varphi_1^- \\ -\sin \varphi_1^- \end{pmatrix} + a_2' e^{iq_2^- x} \begin{pmatrix} 0 \\ 0 \\ \cos \varphi_2^- \\ -\sin \varphi_2^- \end{pmatrix} \right. \\ & \left. + b_1' e^{iq_1^+ x} \begin{pmatrix} \sin \varphi_1^+ \\ \cos \varphi_1^+ \\ 0 \\ 0 \end{pmatrix} + b_2' e^{-iq_2^+ x} \begin{pmatrix} \cos \varphi_2^+ \\ \sin \varphi_2^+ \\ 0 \\ 0 \end{pmatrix} \right] e^{ik_z z}, \quad (3.13) \end{aligned}$$

Note that equations (3.12) and (3.13) are satisfied the energy higher than the crossing, while below the crossing, only the AR term with momentum \bar{q}_1 in equations (3.12)

and (3.13) is modified to be $a_1 e^{iq_1^- x} \begin{pmatrix} 0 \\ 0 \\ \cos \varphi_1^- \\ -\sin \varphi_1^- \end{pmatrix}$.

The x -components of the momenta $q_1^{+,-}$ and $q_2^{+,-}$ in this case are as follows.

$$q_1^+ = \sqrt{(q_0 - \sqrt{q_0^2 + \frac{2m^*(E-E_c)}{\hbar^2}})^2 - k_z^2} \quad \text{for all E's,}$$

$$q_2^+ = \sqrt{(q_0 + \sqrt{q_0^2 + \frac{2m^*(E-E_c)}{\hbar^2}})^2 - k_z^2} \quad \text{for all E's,}$$

$$q_1^- = \sqrt{(-q_0 + \sqrt{q_0^2 - \frac{2m^*(E+E_c)}{\hbar^2}})^2 - k_z^2} \quad \text{for } E > E_c$$

$$q_1^- = \sqrt{(q_0 - \sqrt{q_0^2 - \frac{2m^*(E+E_c)}{\hbar^2}})^2 - k_z^2} \quad \text{for } E < E_c ,$$

$$q_2^- = \sqrt{(q_0 + \sqrt{q_0^2 - \frac{2m^*(E+E_c)}{\hbar^2}})^2 - k_z^2} \quad \text{for all E's.}$$

The appropriate boundary conditions at the interface are:

(i) Continuity of the wave function at the interface

$$\psi_S(x=0) = \psi_{2DEG}(x=0) = \psi(0) , \quad (3.14)$$

(ii) The discontinuity of the slope of the wave function at the interface are

$$\frac{\partial \psi_{s,e}}{\partial x} \Big|_{x=0^+} - \frac{m}{m^*} \frac{\partial \psi_{2DEG,e}}{\partial x} \Big|_{x=0^-} = (2k_F z + i\sigma_z \frac{m}{m^*} q_0) \psi_e(0) , \quad (3.15)$$

$$\frac{\partial \psi_{s,h}}{\partial x} \Big|_{x=0^+} - \frac{m}{m^*} \frac{\partial \psi_{2DEG,h}}{\partial x} \Big|_{x=0^-} = (2k_F z - i\sigma_z \frac{m}{m^*} q_0) \psi_h(0) , \quad (3.16)$$

where $\psi = \begin{pmatrix} \psi_e \\ \psi_h \end{pmatrix} = \begin{pmatrix} \psi_{e\uparrow} \\ \psi_{e\downarrow} \\ \psi_{h\uparrow} \\ \psi_{h\downarrow} \end{pmatrix}$, $\psi_e = \begin{pmatrix} \psi_{e\uparrow} \\ \psi_{e\downarrow} \end{pmatrix}$, $\psi_h = \begin{pmatrix} \psi_{h\uparrow} \\ \psi_{h\downarrow} \end{pmatrix}$, $z = \frac{mH_s}{\hbar^2 k_{F,S}}$ is the unitless

parameter that characterizes the strength of the barrier potential, k_F is the Fermi wave vector of the superconductor.

As in Chapter II, substitution of the wave functions of each case, now the 8×8 equations (see appendix A) are obtained.

These 8×8 equation are used to obtain all the transmission and reflection amplitudes. The Andreev and normal reflection probabilities are defined as

$$A_{1(2)}(E, kz) = \left| a_{1(2)}(E, kz) \right|^2 \frac{|v_r^{h_{1(2)}}|}{|v_{in}|}, \quad (3.17)$$

$$B_{1(2)}(E, kz) = \left| b_{1(2)}(E, kz) \right|^2 \frac{|v_r^{e_{1(2)}}|}{|v_{in}|}, \quad (3.18)$$

Similarly, the transmission probabilities are equal to

$$C_{1(2)}(E, kz) = \left| c_{1(2)}(E, kz) \right|^2 \frac{|v_t^{h_{1(2)}}|}{|v_{in}|}, \quad (3.19)$$

$$D_{1(2)}(E, kz) = \left| d_{1(2)}(E, kz) \right|^2 \frac{|v_t^{e_{1(2)}}|}{|v_{in}|}, \quad (3.20)$$

where $v_{in}^{1(2)} = \frac{1}{\hbar} \frac{\partial E^{+(-)}}{\partial q_x} \Big|_{q_x=q_{1(2)}^+}$ is the group velocity of injection electron,

$v_r^{h_{1(2)}} = -\frac{1}{\hbar} \frac{\partial E^{+(-)}}{\partial q_x} \Big|_{q_x=q_{1(2)}^-}$ is the group velocity of reflected hole,

$$v_r^{e1,(2)} = \frac{1}{\hbar} \left. \frac{\partial E^{\pm,(-)}}{\partial q_x} \right|_{q_x = -q_1^{\pm(2)}} \quad \text{is the group velocity of reflected electron,}$$

$$v_t^{lh} = \frac{1}{\hbar} \left. \frac{\partial E}{\partial k_x} \right|_{k_x = -k^-} \quad \text{is the group velocity of transmitted hole-like excitation, and}$$

$$v_t^{le} = \frac{1}{\hbar} \left. \frac{\partial E}{\partial k_x} \right|_{k_x = k^+} \quad \text{is the group velocity of transmitted electron-like excitation.}$$

The superscript 1(2) indicates the state with wave vector \bar{q}_1 (\bar{q}_2). The magnitude of these group velocities are different for each case as follows.

1) Case1:

$$v_{in}^1 = \frac{\hbar}{m^*} (q_1^+ + q_0 \cos 2\varphi_1^+) = v_r^{e,1},$$

$$v_{in}^2 = \frac{\hbar}{m^*} (q_2^+ - q_0 \cos 2\varphi_1^+) = v_r^{e,2},$$

$$v_r^{h,1} = \frac{\hbar}{m^*} (-q_1^- - q_0 \cos 2\varphi_1^-),$$

$$v_r^{h,2} = \frac{\hbar}{m^*} (-q_2^- + q_0 \cos 2\varphi_2^-),$$

$$v_t^{lh} = \frac{\hbar k^- \xi_{k^-}}{mE}, \quad v_t^{le} = \frac{\hbar k^+ \xi_{k^+}}{mE}.$$

2) Case2:

$$v_{in}^1 = \frac{\hbar}{m^*} (q_1^+ + q_0 \cos 2\varphi_1^+) = v_r^{e,1},$$

$$v_{in}^2 = \frac{\hbar}{m^*} (q_2^+ - q_0 \cos 2\varphi_1^-) = v_r^{e,2},$$

$$v_r^{h,1} = \frac{\hbar}{m^*} (q_1^- - q_0 \cos 2\varphi_1^-),$$

$$v_r^{h,2} = \frac{\hbar}{m^*} (-q_2^- + q_0 \cos 2\varphi_2^-),$$

$$v_t^{lh} = \frac{\hbar k^- \xi_{k^-}}{mE}, \quad v_t^{le} = \frac{\hbar k^+ \xi_{k^+}}{mE}$$

3) Case3:

$$v_{in}^{e,1} = \frac{\hbar}{m^*} (-q_1^+ + q_0 \cos 2\varphi_1^+) = v_r^{e,1},$$

$$v_{in}^{e,2} = \frac{\hbar}{m^*} (-q_2^+ + q_0 \cos 2\varphi_2^+) = v_r^{e,2},$$

$$v_r^{h,1} = \frac{\hbar}{m^*} (q_1^- - q_0 \cos 2\varphi_1^-),$$

$$v_r^{h,2} = \frac{\hbar}{m^*} (-q_2^- + q_0 \cos 2\varphi_2^-),$$

$$v_t^{lh} = \frac{\hbar k^- \xi_{k^-}}{mE}, \quad v_t^{le} = \frac{\hbar k^+ \xi_{k^+}}{mE}$$

The conservation of probability requires $A_1(E, k_z) + A_2(E, k_z) + B_1(E, k_z) + B_2(E, k_z) + C_1(E, k_z) + C_2(E, k_z) + D_1(E, k_z) + D_2(E, k_z) = 1$.

In the 2D system, the general relation for current density in x -direction across the junction is given by

$$J = \sum_{k_x, k_z} n_k v_k e \quad , \quad (3.21)$$

where v_k is the group velocities a long the x -direction, e is the electron charge and the electron concentration, $n_k = (1 + A_1(E) + A_2(E) - B_1(E) - B_2(E))f(E)$, $f(E)$ is the

Fermi Dirac distribution function. The current flowing across junction from 2DEG to superconductor with applied voltage V is therefore

$$I_{2DEG \rightarrow S} = \frac{L^2 e}{4\pi^2} \iint dk_x dk_z v_k (1 + A_1(E, k_z) + A_2(E, k_z) - B_1(E, k_z) - B_2(E, k_z)) f(E - eV). \quad (3.22)$$

And similarly the current flowing across junction from superconductor to 2DEG is

$$I_{S \rightarrow 2DEG} = \frac{L^2 e}{4\pi^2} \iint dk_x dk_z v_k (1 + A_1(E, k_z) + A_2(E, k_z) - B_1(E, k_z) - B_2(E, k_z)) f(E),$$

(3.23) Thus, the net current crossing the junction is

$$\begin{aligned} I(eV) &= I_{2DEG \rightarrow S} - I_{S \rightarrow 2DEG} \\ &= \frac{L^2 e}{4\pi^2} \iint dk_x dk_z v_k (1 + A_1(E, k_z) + A_2(E, k_z) - \\ &\quad B_1(E, k_z) - B_2(E, k_z)) [f(E - eV) - f(E)] \\ &= \frac{L^2 e}{4\pi^2 \hbar} \iint dk_z dE v_k (1 + A_1(E, k_z) + A_2(E, k_z) - \\ &\quad B_1(E, k_z) - B_2(E, k_z)) [f(E - eV) - f(E)] \end{aligned} \quad (3.24).$$

The tunneling conductance of the 2DEG/S junction is the derivative of the current flows across junction with respect to the applied voltage

$$G_{2DEG/S}(eV) = \frac{dI_{2DEG/S}(eV)}{dV}, \quad (3.25)$$

At zero temperature, the tunneling conductance becomes

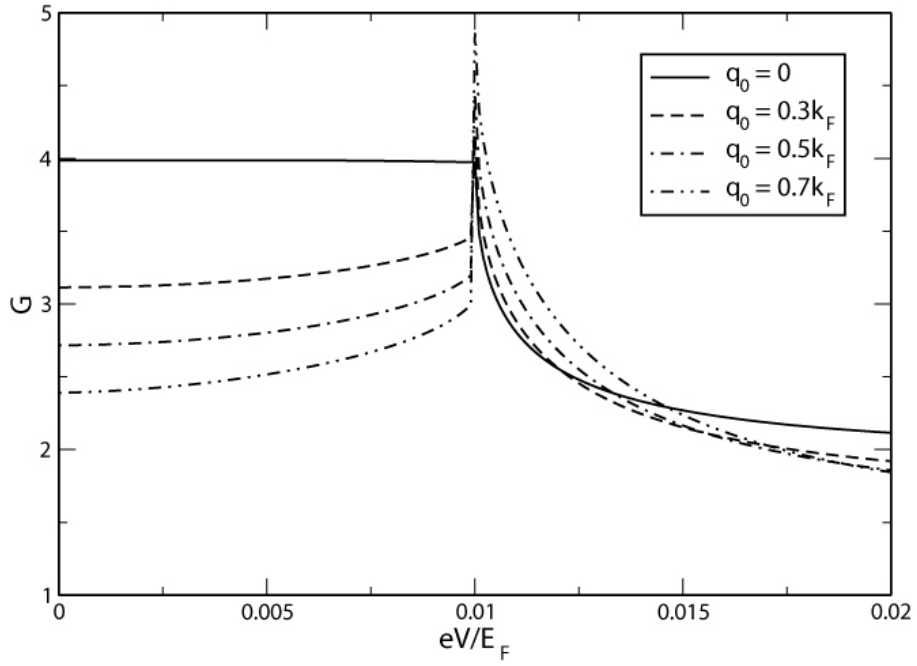
$$G(eV) = \frac{L^2 e^2}{4\pi^2 \hbar} \int dk_z (1 + A_1(eV, k_z) + A_2(eV, k_z) - B_1(eV, k_z) - B_2(eV, k_z)), \quad (3.26)$$

3.2 Results and Discussion

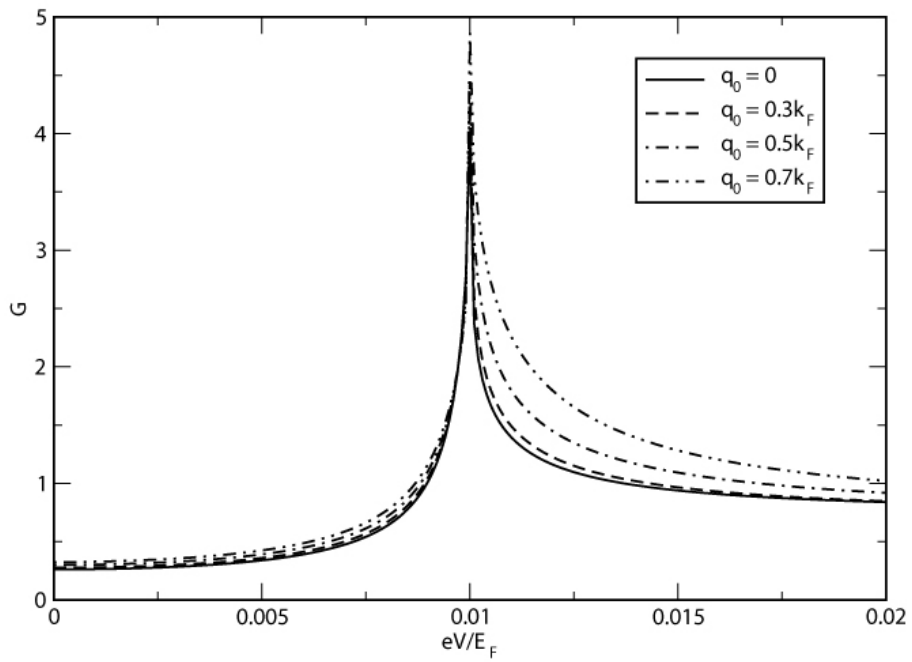
3.2.1 Case 1: E_F lies above the crossing of the two energy branches

Figs. 3.7 ($r_m = 1$) and 3.8 ($r_m = 10$), the plots of the tunneling conductance spectra for different values of RSOC strength (q_0) are shown in the different limit. In the Andreev limit (low z) (Figs. 3.7, 3.8 (a)), all the spectra for finite q_0 contain peaks at the applied voltage equal to the superconducting gap and these peaks are enhanced with the increase in q_0 . The conductance below the energy gap, which is mostly influenced by the Andreev reflection process, is suppressed as q_0 is increased. In tunneling limit (high z) (Figs. 3.7, 3.8 (b)), the conductance below the energy gap are enhanced as q_0 is increased up to a critical value and one q_0 is higher than this value, the increase in q_0 suppresses the conductance. Moreover, there occurs a feature at the voltage less than the energy gap for mismatch effective mass is big (Fig. 3.8), it is obviously in Fig. 3.9 (b) when the potential barrier get bigger. The position of this feature depends on the magnitude of the RSOC. In fact, it slowly moves towards the peak at the energy gap as the strength of RSOC is increased.

The potential barrier does not affect the peak at the energy gap. This peak is completely independent on potential as shown in Fig. 3.9.

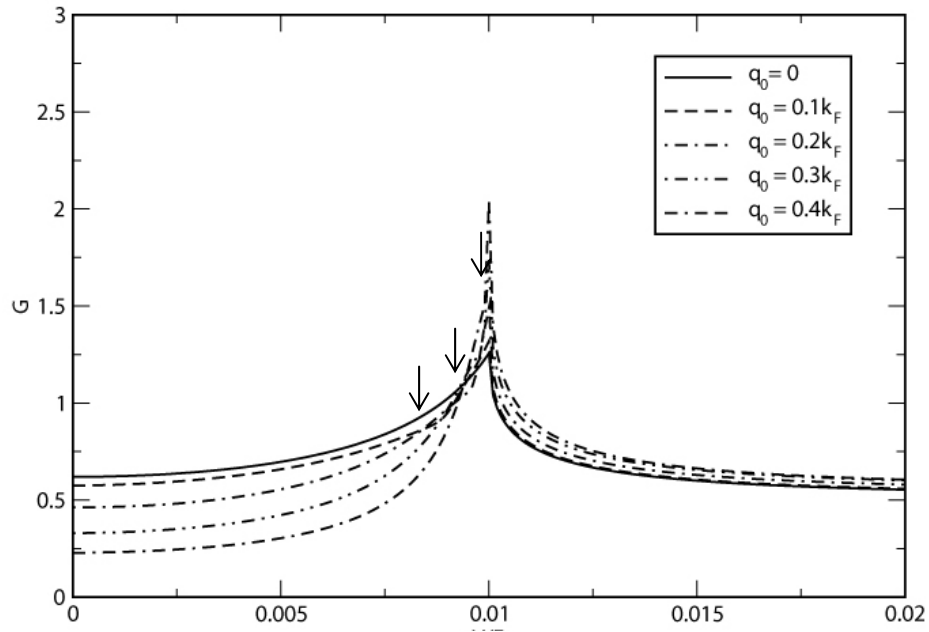


(a)

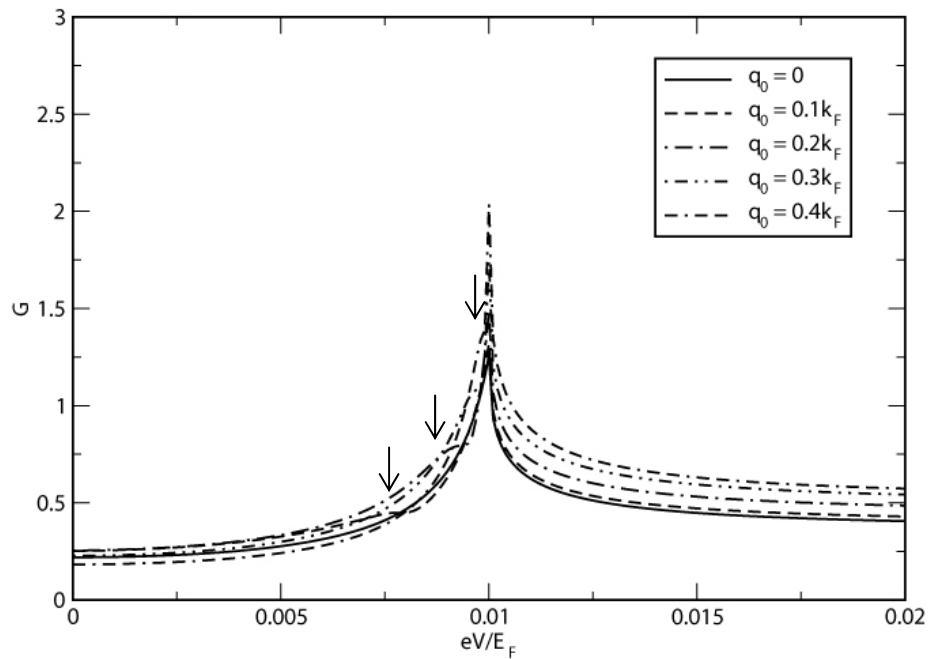


(b)

Figure 3.7 The conductance spectra (normalized by $e^2 L^2 / 2\pi\hbar$) as a function of bias voltage for different $q_0 = 0, 0.3k_F, 0.5k_F$ and $0.7k_F$ where $r_m = 1$ (a) $z = 0$, (b) $z = 1$.

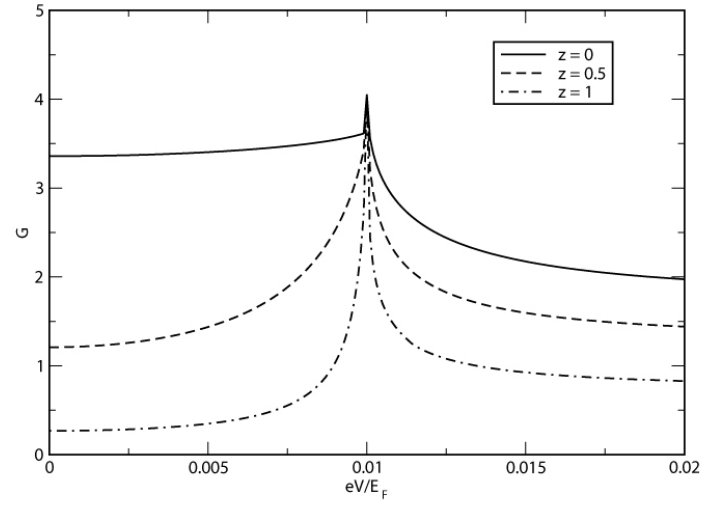


(a)

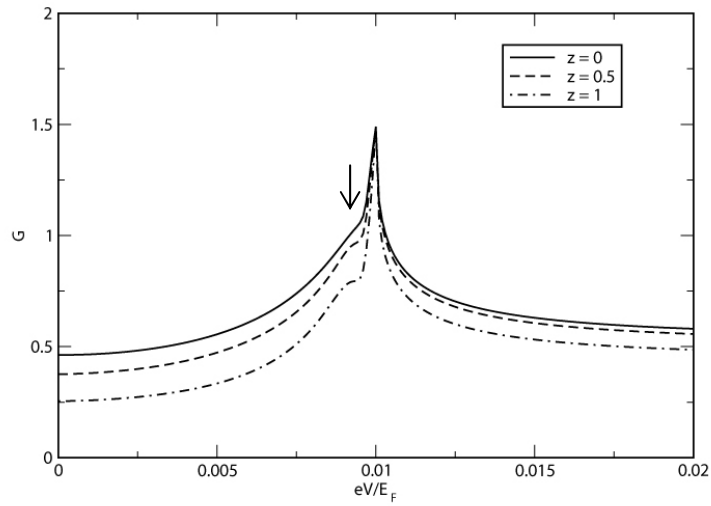


(b)

Figure 3.8 The conductance spectra (normalized by $e^2 L^2 / 2\pi h$) of 2DEG/S junction: $r_m = 10$, (a) $z = 0$, (b) $z = 1$. The arrows indicate the feature at the voltage below the superconducting gap.



(a)



(b)

Figure 3.9 The conductance spectra (normalized by $e^2 L^2 / 2\pi\hbar$) of 2DEG/S junction for different value of z , $q_0 = 0.2k_F$: (a) $r_m = 1$ (b) $r_m = 10$. The arrows indicate the feature at the voltage below the superconducting gap.

In order to understand the line shapes of the conductance, one considers the angle averaged of normal and Andreev reflection probabilities as a function of voltage (see Appendix B) It is found that the conductance spectra at the voltage less than the

gap are influenced mostly by the AR probabilities, which involves the states with the same wave number as the injected electron as mentioned in the previous work of T. Yokoyama and coworker's work (Yokoyama, Tanaka and Inoue, 2006)

To clarify the effect of q_0 on the conductance, consider the conductance as a function of q_0 for different values of z and r_m at $eV = 0$ (Fig. 3.10) and $eV = \Delta$ (Fig. 3.11). It is found that the conductance at $eV = 0$ is affected by both barrier potential and the mismatch of effective mass. As seen in Fig. 3.10 (a), when the insulating barrier potential is low, the conductance at $eV = 0$ is decreased with q_0 , but when the barrier potential is high, the conductance is increased with q_0 . When there is a mismatch in effective mass, the conductance at $eV = 0$ can be increased with q_0 up to a critical value and is decreased as q_0 gets bigger (see Fig. 3.10 (c)).

The conductance at $eV = \Delta$ is increased with q_0 . This behavior makes it possible for this feature to be used to measure the RSOC strength.

The effect of the mismatch in the effective mass and the potential barrier on the conductance spectra seems similar. That is, both suppress the conductance at most of the energies except at the energy gap, where only the mismatch suppress the conductance but the barrier potential has no effect on. In order to further investigate the effect of both factors, the conductance at zero bias voltage and at the energy gap as a function of barrier strength and the mismatch are shown in Figs. 3.12 and 3.13 for a fixed value of q_0 . The ratio of the effective mass affects the conductance at both voltages in the same way, whereas the barrier potential only affects on the conductance a zero voltage but does not affect the conductance at the energy gap at all.

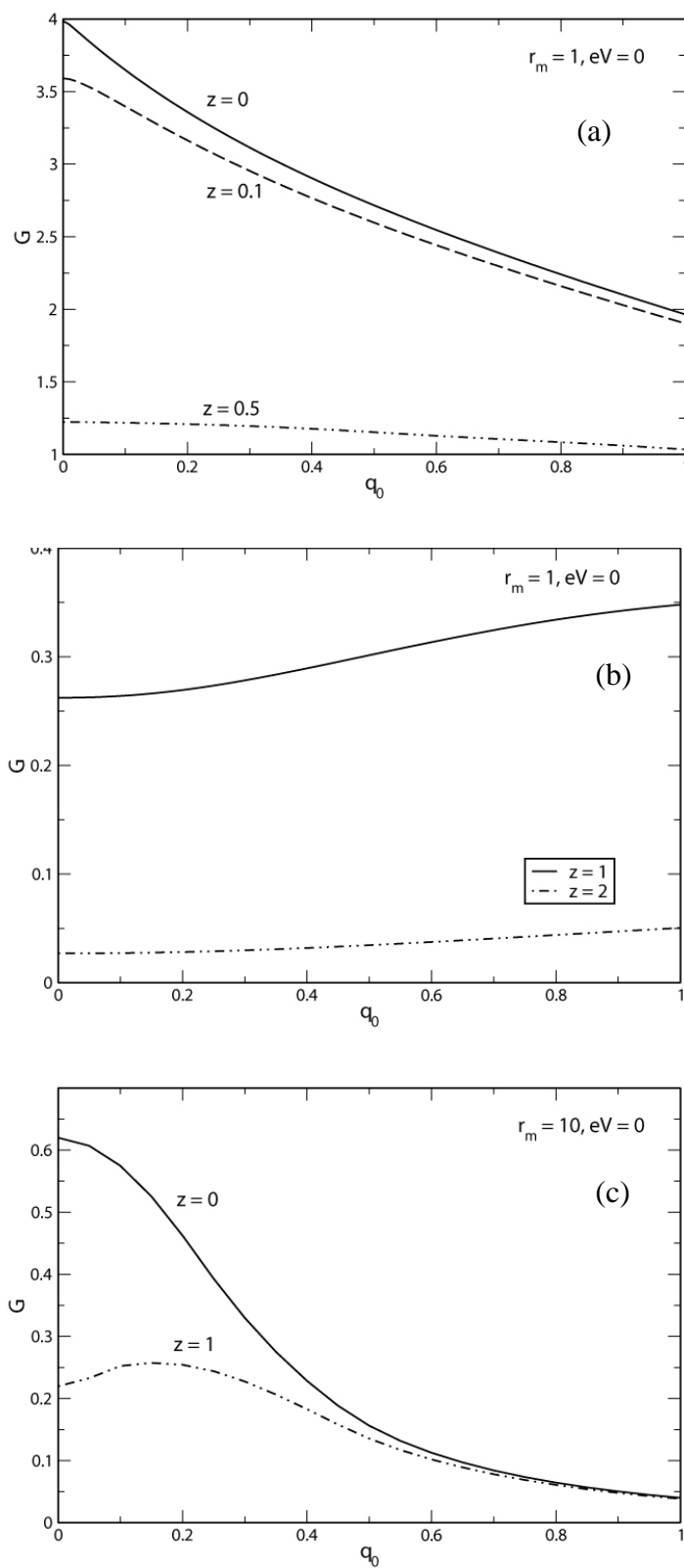


Figure 3.10 The q_0 dependence conductance (normalized by $e^2 L^2 / 2\pi\hbar$) at $eV = 0$ where $r_m = 1$ (a) $z = 0, 0.1$ and 0.5 (b) $z = 1$ and 2 (c) $r_m = 10, z = 0$ and 1 .

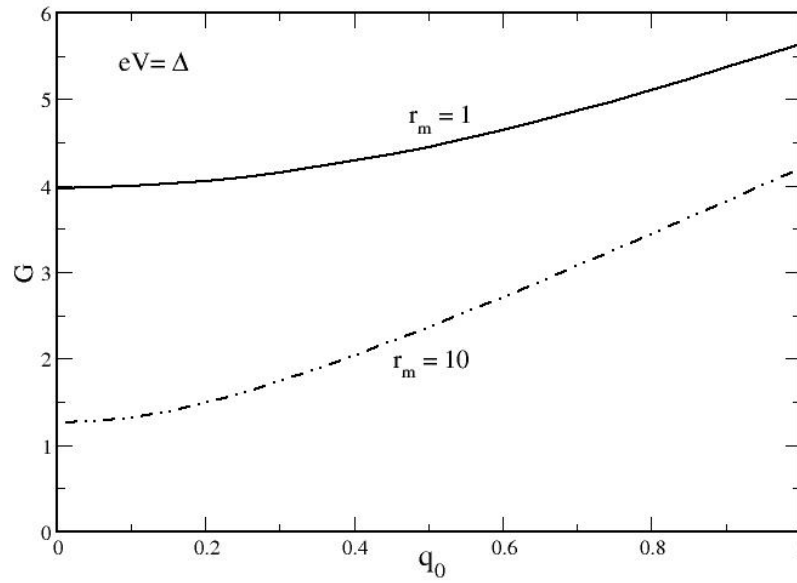


Figure 3.11 The q_0 dependence conductance (normalized by $e^2 L^2 / 2\pi\hbar$) at $eV = \Delta$ where $r_m = 1$ and 10.

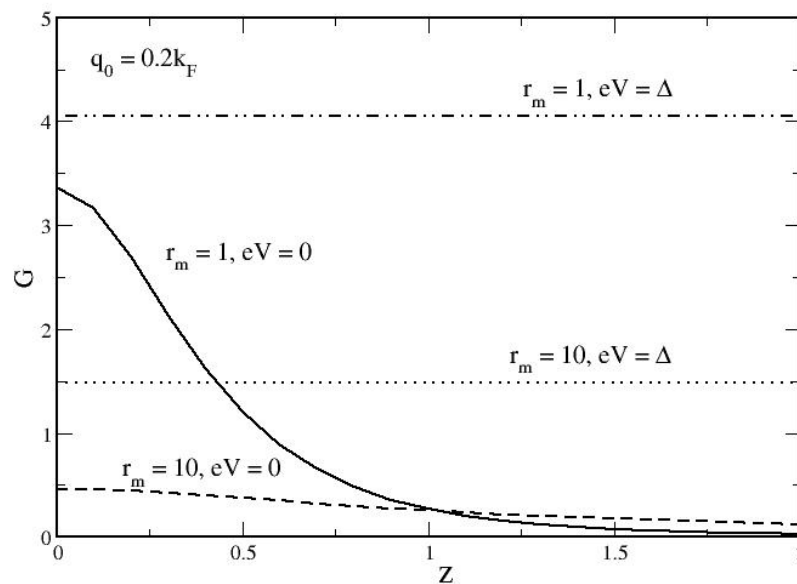


Figure 3.12 The z dependence conductance (normalized by $e^2 L^2 / 2\pi\hbar$) for $q_0 = 0.2k_F$, $r_m = 1$ and 10 at $eV = 0$ and Δ .

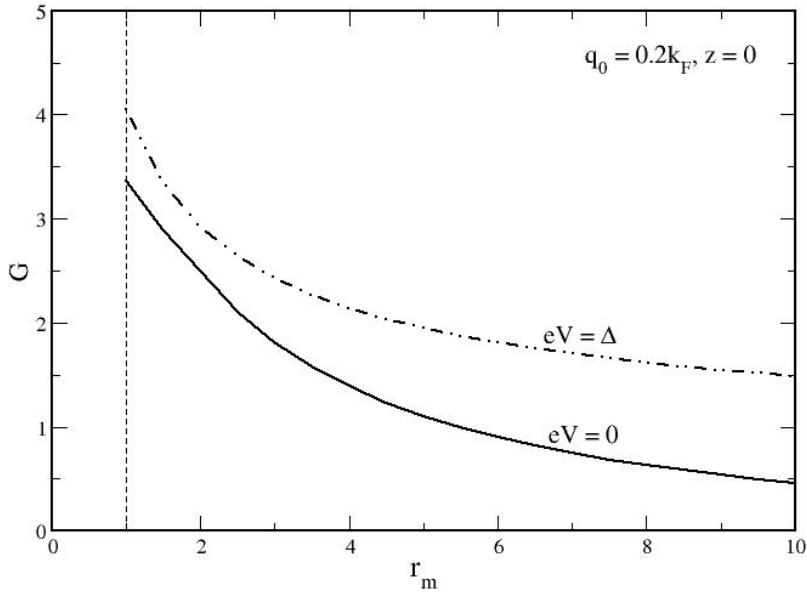
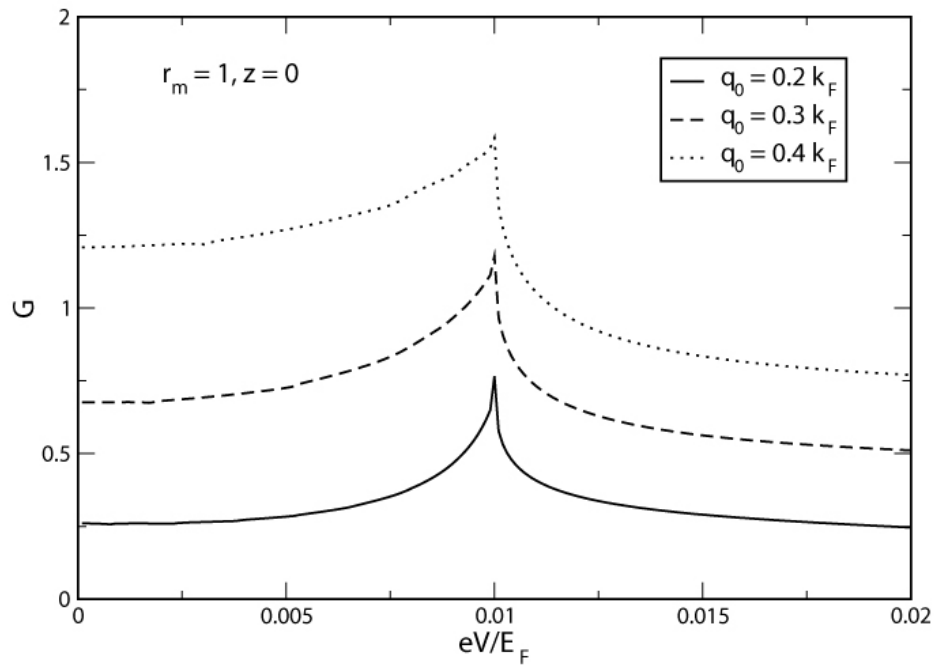


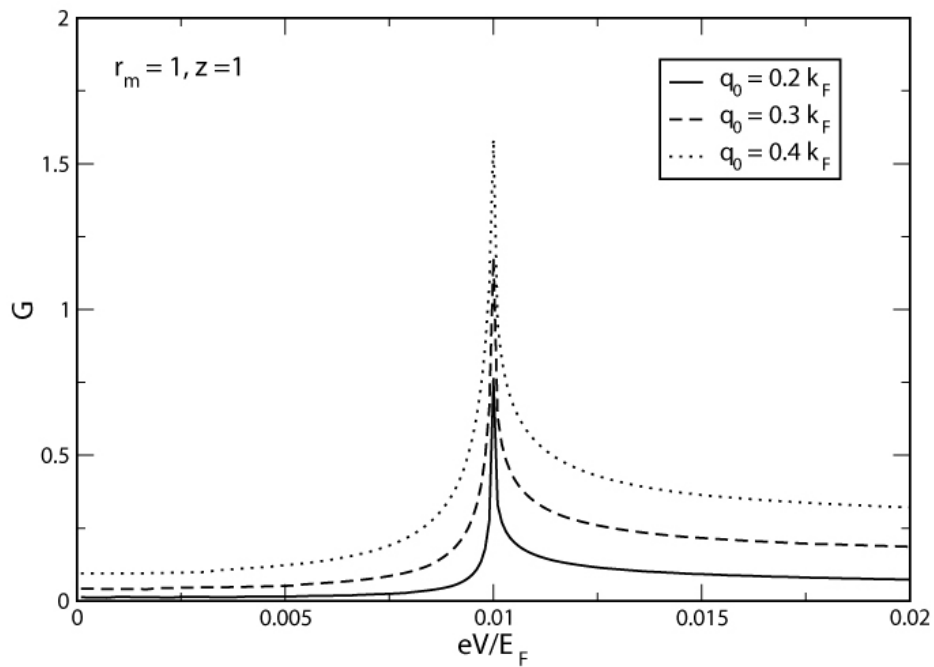
Figure 3.13 The r_m dependence conductance (normalized by $e^2 L^2 / 2\pi\hbar$) for $q_0 = 0.2k_F$, $z = 0$, at $eV = 0$ and Δ .

3.2.2 Case 2: E_F lies at the crossing of the two energy branches

When E_F is located at the crossing of the two energy branches of the 2DEG on 2DEG, the effect of q_0 differs from when E_F lies above the crossing. When the effective masses are the same on both sides, the increase in q_0 enhances the conductance spectrum at all energy (see Fig. 3.14). When there is a mismatch in the effective mass, the conductance at the $eV = \Delta$ is increased with q_0 in both Andreev and tunneling limit (see Fig. 3.15). However, the conductance at $eV = 0$ is suppressed with q_0 in case of Andreev limit (see Fig. 3.15(a)), while in the tunneling limit, conductance at $eV = 0$ is enhanced up to a critical value and then is suppressed with q_0 (see Fig. 3.15(b)).

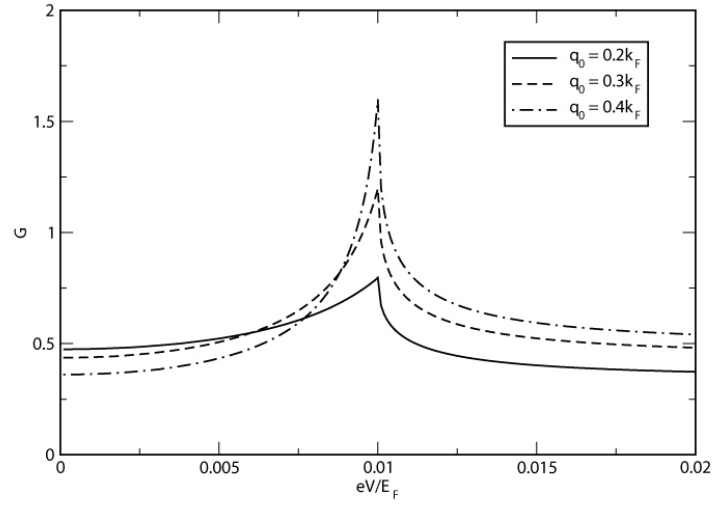


(a)

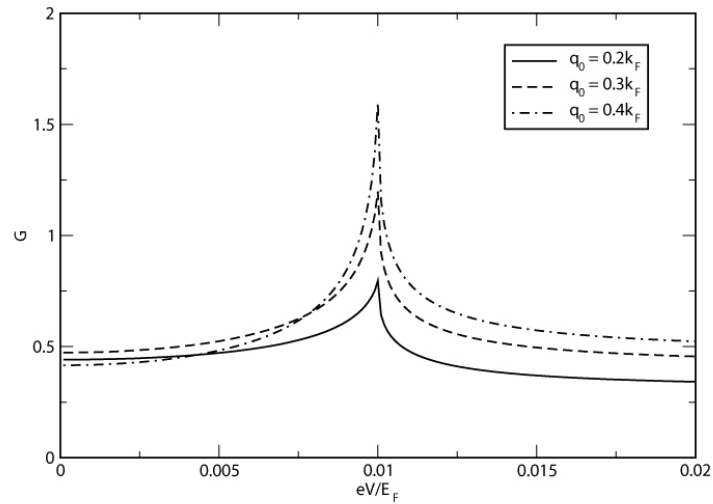


(b)

Figure 3.14 The conductance spectra (normalized by $e^2 L^2 / 2\pi\hbar$) of 2DEG/S junction for different value of q_0 , $r_m = 1$ (a) $z = 0$ (b) $z = 1$.



(a)



(b)

Figure 3.15 The conductance spectra (normalized by $e^2 L^2 / 2\pi\hbar$) of 2DEG/S junction for $r_m = 10$ and different value of q_0 (a) $z = 0$ (b) $z = 1$

To clarify more the effect of q_0 on the conductance at $eV = 0$, consider the conductance as a function of q_0 for different values of z for $r_m = 1$ (see Fig. 3.16) and $r_m = 10$ (see Fig. 3.17). It is found that in both $r_m = 1$ and 10, the conductance at $eV = 0$ is enhanced with q_0 up to a critical value of each z . When q_0 is higher than that

value, the conductance at $eV = 0$ is depressed with q_0 . For $r_m = 1$ this critical value of q_0 is very different for different value of z . For $r_m = 10$, this critical value lies around $q_0 = 0.2k_F - 0.3k_F$.

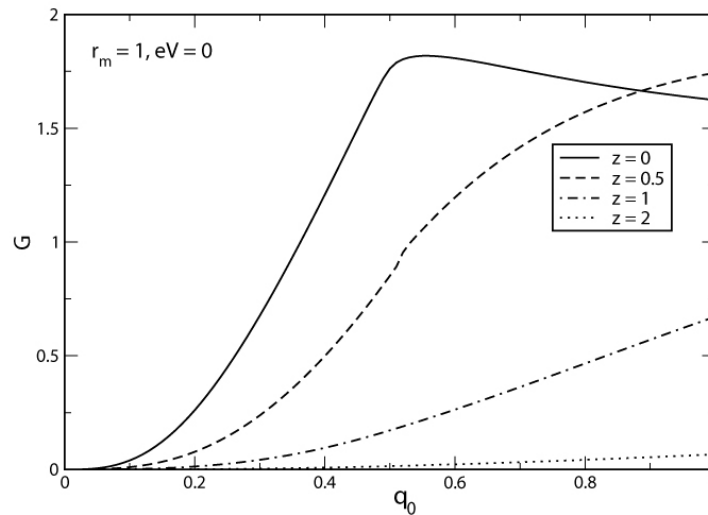


Figure 3.16 The conductance (normalized by $e^2 L^2 / 2\pi\hbar$) as a function of q_0 for different $z = 0, 0.5, 1$ and 2 at $eV = 0$ for $r_m = 1$.

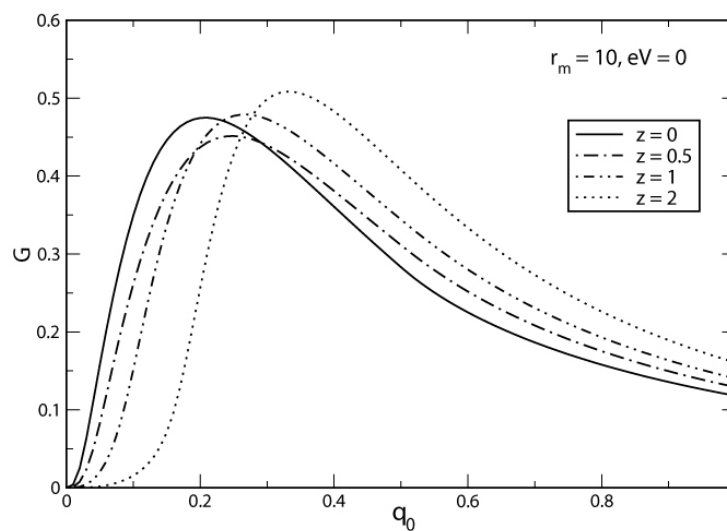
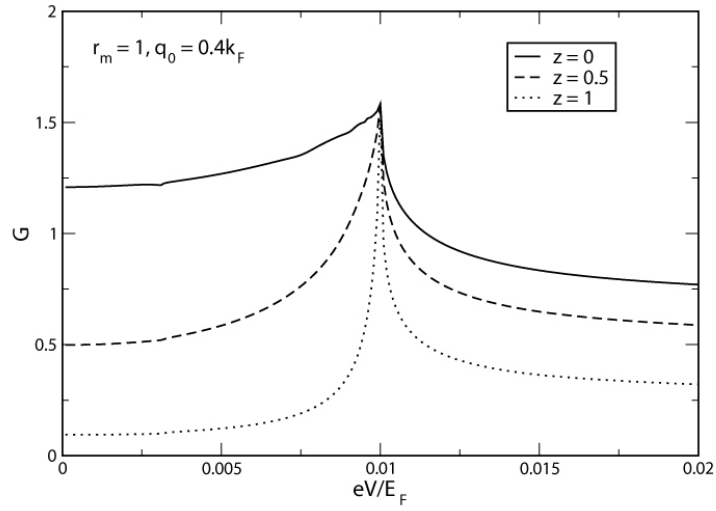
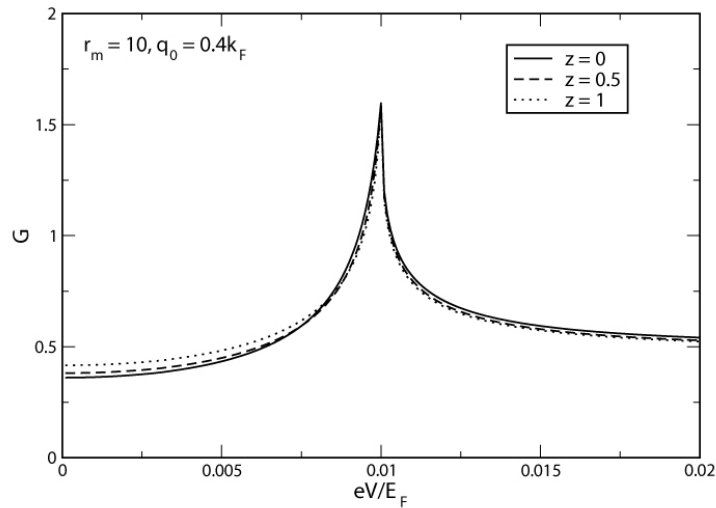


Figure 3.17 The conductance (normalized by $e^2 L^2 / 2\pi\hbar$) as a function of q_0 for different $z = 0, 0.5, 1$ and 2 at $eV = 0$ for $r_m = 10$



(a)



(b)

Figure 3.18 The conductance spectra (normalized by $e^2 L^2 / 2\pi\hbar$) of 2DEG/S junction for different value of z , where $q_0 = 0.4k_F$ (a) $r_m = 1$ (b) $r_m = 10$

The conductance at the energy gap in this case is independent of the barrier potential (see Fig. 3.18). Also, it is almost independent of the ratio of the effective mass as shown in Fig. 3.19. Comparing Fig. 3.19 and Fig. 3.11, one can see that the

conductances at the energy gap as a function of q_0 in both cases are different. In this case the dependence of the conductance at the gap on q_0 is linear over a large range of q_0 . Therefore, the conductance at the energy gap can be used to measure the strength of RSOC more accurately in this case

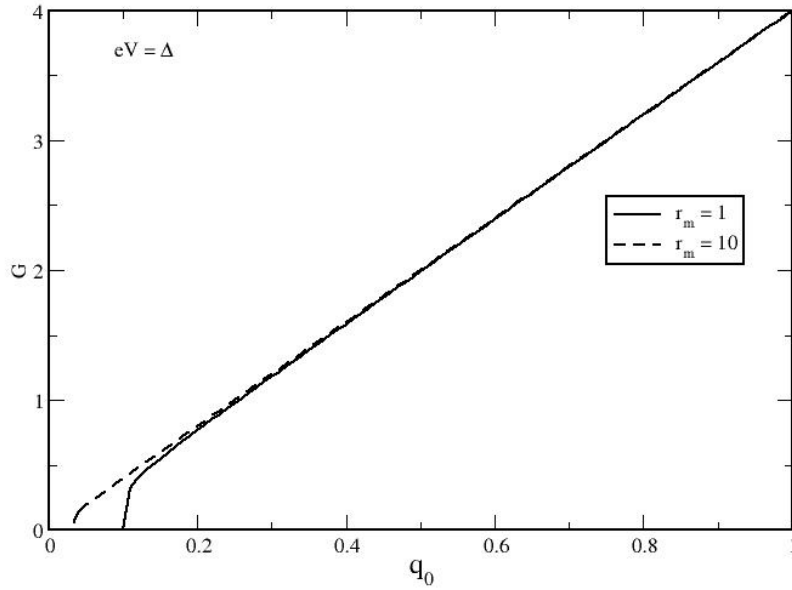


Figure 3.19 The conductance (normalized by $e^2 L^2 / 2\pi\hbar$) as a function of q_0 at $eV = \Delta$ and different $z = 0, 0.5, 1$, $r_m = 1$ and 10 .

Fig. 3.20 contain the plots of conductances at $eV = 0$ and $eV = \Delta$ as a function of barrier potential with different ratios of the effective mass for a fixed value of q_0 . The effect of potential barrier on the conductance at $eV = \Delta$ is nil, the same as in case 1. The conductance at zero bias voltage is decreased with the barrier potential.

In Fig. 3.21, the plots of conductance at $eV = 0$ and $eV = \Delta$ as a function of the ratio of the effective mass for a fixed q_0 in the Andreev limit are shown. The increase in the ratio of the effective mass does not affect the conductance at the energy gap, but at zero bias voltage, the increase in the ratio of the effective mass

enhance and then suppress the conductance. When comparing this case and the previous case, one can see that the ratio of the effective mass affects the conductance at $eV = 0$ in a different way.

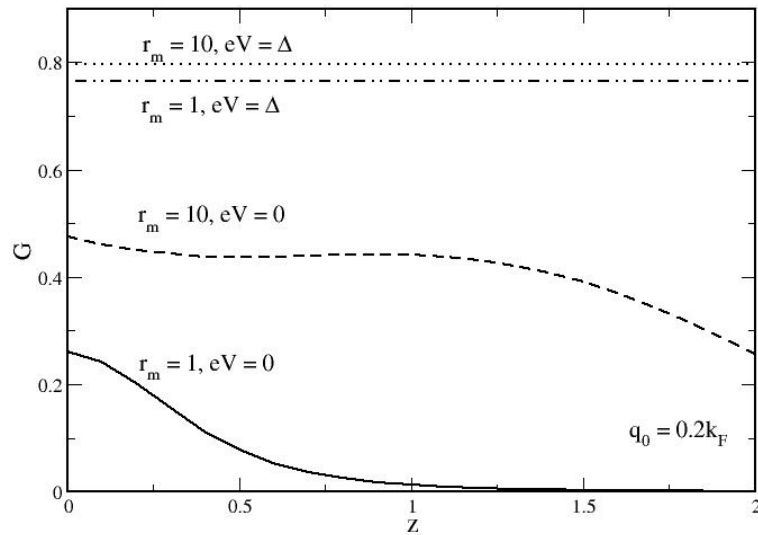


Figure 3.20 The conductance (normalized by $e^2 L^2 / 2\pi\hbar$) as a function of z , $q_0 = 0.2$, $r_m = 1$ and 10 , at $eV = 0$ and Δ .

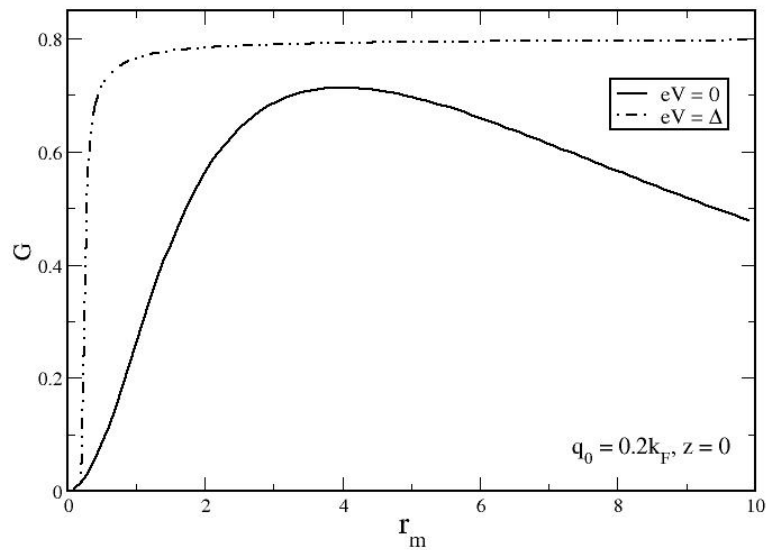


Figure 3.21 The conductance (normalized by $e^2 L^2 / 2\pi\hbar$) as a function of r_m where $z = 0$ and $q_0 = 0.2$ at $eV = 0$ and Δ .

3.2.3 Case 3: E_F lie below the crossing of the two energy branches

The tunneling conductance spectrum in this case is similar to when E_F lies at the crossing. That is the effect of the ratio of the effective mass and the potential barrier on the conductance spectrum is the same as in the previous case. However, the conductance spectrum at voltages below the crossing has a feature at the crossing (see Figs. 3.22 and 3.23).

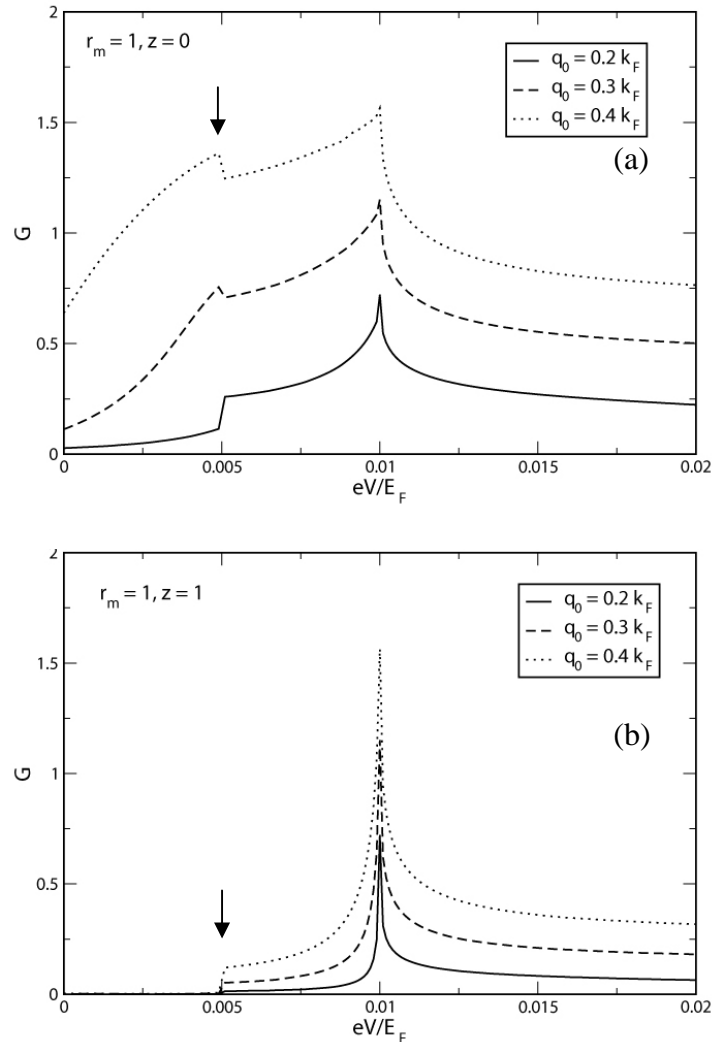


Figure 3.22 The conductance spectra (normalized by $e^2 L^2 / 2\pi\hbar$) of 2DEG/S junction : for different $q_0 = 0.2k_F, 0.3k_F$ and $0.4k_F$ (a) $z = 0$ and (b) $z = 1$. The arrows indicate the feature at the crossing of the two energy branches.

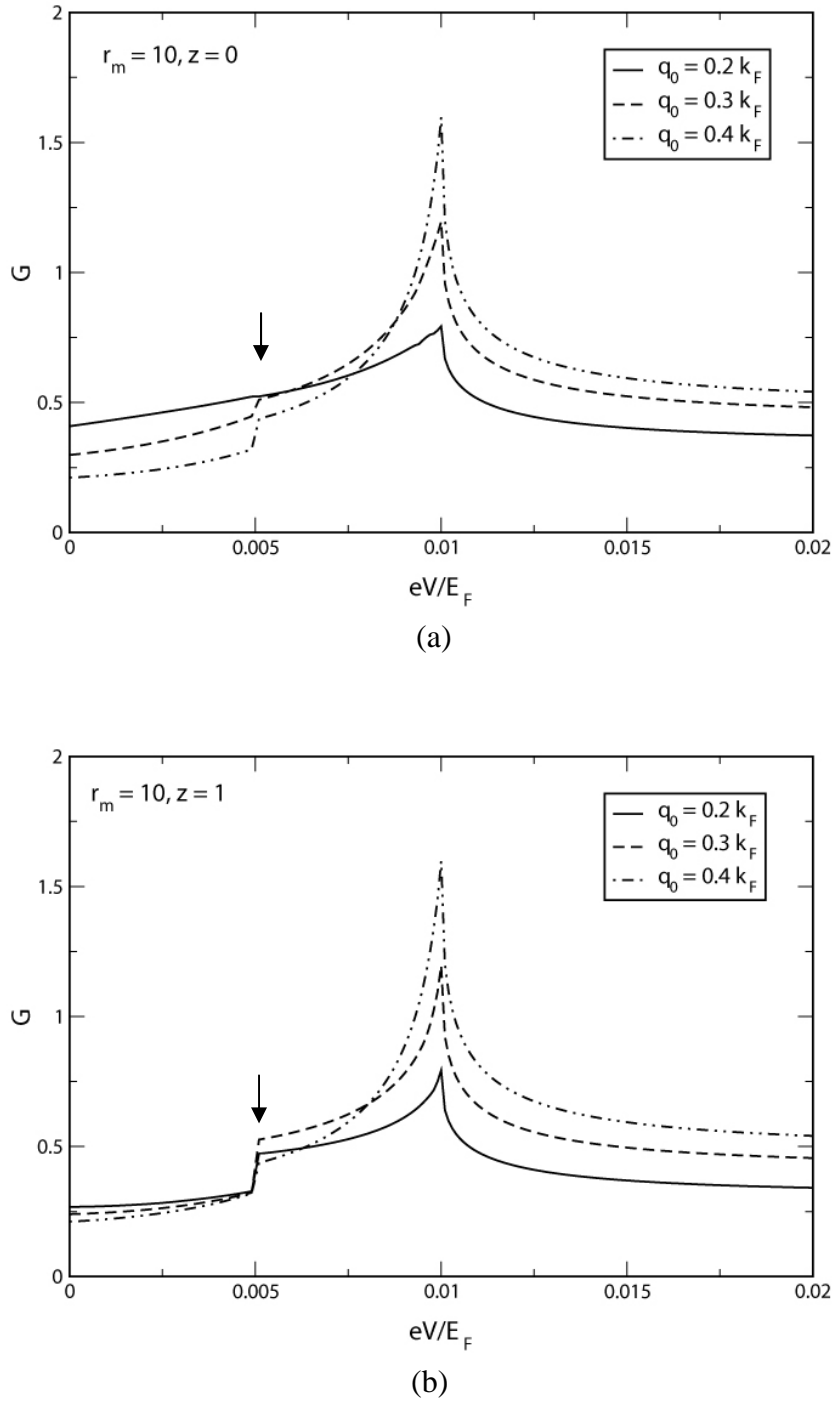


Figure 3.23 The conductance spectra (normalized by $e^2 L^2 / 2\pi\hbar$) of 2DEG/S junction : $r_m = 10$, $q_0 = 0.2, 0.3, 0.4$ (a) $z = 0$, (b) $z = 1$. The arrows indicate the feature at the crossing of the two energy branches.

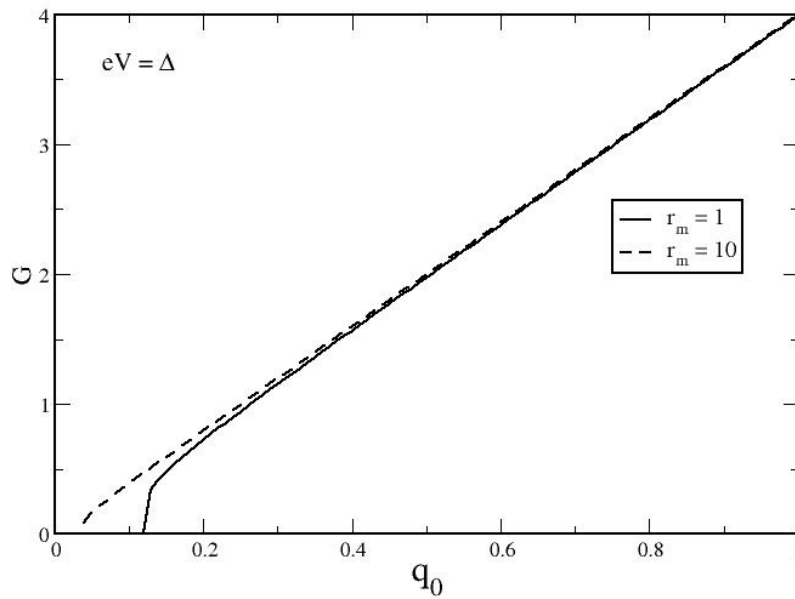


Figure 3.24 The conductance (normalized by $e^2 L^2 / 2\pi\hbar$) as a function of q_0 at $eV = \Delta$, $r_m = 1$ and 10.

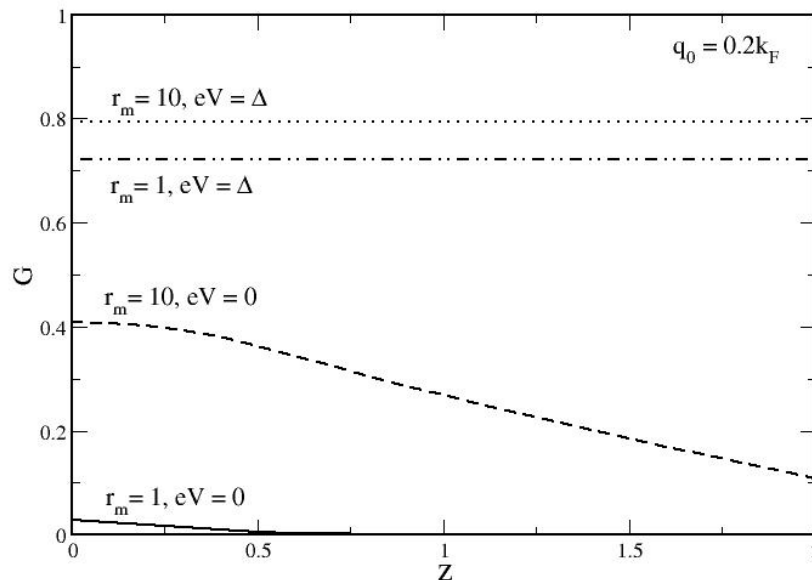


Figure 3.25 The conductance (normalized by $e^2 L^2 / 2\pi\hbar$) as a function of z for fixed $q_0 = 0.2k_F$, $r_m = 1$ and 10, at $eV = 0$ and Δ .

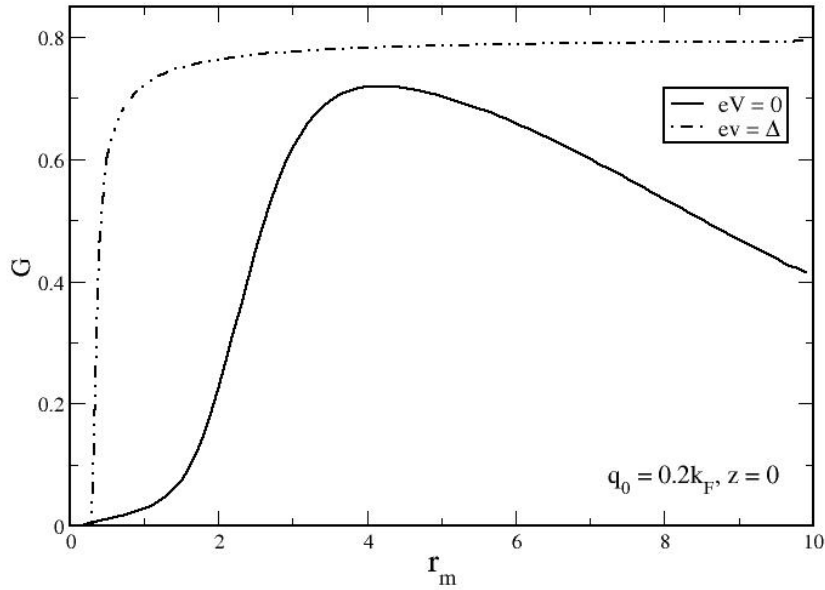


Figure 3.26 The conductance (normalized by $e^2 L^2 / 2\pi\hbar$) as a function of r_m where $z = 0$ and $q_0 = 0.2$ at $eV = 0$ and Δ .

3.3 Conclusions

In this chapter, the tunneling conductance spectroscopy of 2DEG/S junction is investigated. The effects of RSOC strength, potential barrier, the ratio of the effective masses of the two sides and the different Fermi level of the 2DEG are studied. It is found that the effects of RSOC strength, potential barrier, and the ratio of the effective masses of the two sides on the tunneling conductance are different for different Fermi levels of the 2DEG.

When the Fermi level lies above the crossing of the two branches, the conductance over the range of the applied voltage less than the superconducting gap is decreased with the RSOC. The conductance over this range can be increased with the RSOC when a mismatch in effective mass exists and in the tunneling limit. The

conductance peak at the energy gap is increased with the RSOC but independent on the potential barrier.

In the case where the Fermi level of the 2DEG lies at the crossing, the conductance spectrum below the energy gap is increased with the RSOC up to a critical value and then is decreased with the RSOC. The effect of potential barrier is similar to case 1. The effect of the ratio of the effective mass on the conductance at zero voltage in this case is similar to that of RSOC, but the effect on the conductance at the energy gap is similar to that of potential barrier.

For the Fermi level of the 2DEG is below the crossing, the effect of RSOC, barrier strength and mismatch effective mass are similar to that in case where the Fermi level is at the crossing. The only difference is that in this case the conductance spectrum below the crossing and there exists a feature at the crossing.

In all cases of Fermi levels, the conductance peak at the energy gap is increased with the strength of RSOC and independent on potential barrier. One can use the height of this peak to measure the strength of RSOC. Also, it is shown that the effects of the mismatch effective mass and the barrier potential are not equivalent as it was believed (Yokoyama, Tanaka and Inoue, 2006).

CHAPTER IV

2DEG/D JUNCTION

In the previous chapter, the tunneling spectroscopy of the junction between 2DEG and s-wave superconductor was considered. The s-wave superconducting gap is independent of direction. In this chapter, 2DEG/d-wave superconductor junctions will be considered. The d-wave superconducting gap has four-fold symmetry, dependent on the direction of the momentum.

The crystal structures of most high temperature superconductors are tetragonal and their physical properties are quasi-two-dimensional. These superconductors have a $d_{a^2-b^2}$ -wave paring symmetry (Tsuei and Kirtley, 2000). The energy gap of such a paring state, $\Delta_0 \cos 2\theta$ (θ is the angle between wave vector \vec{k} and the interface normal vector, Δ_0 is the gap maximum) depend strongly on wave vector and has a sign change at $\theta = \frac{\pi}{4}$ and $\theta = 3\frac{\pi}{4}$. Due to this sign change, the existence of the midgap surface states, were predicted (Hu, 1994). These midgap states cause the presence of a peak at zero-bias voltage in the conductance spectrum of a metal/d-wave superconductor junction (Walsh, Moreland, Ono and Kalkur, 1991; Cucolo and Di Leo, 1993; Kashiwaya, Tanaka, Koyanagi, Takashima and Kajimura, 1995; Alff, Takashima, Kashiwaya, Terada, Ihara, Tanaka, Koyanagi and Kajimura, 1997; Wei1, Yeh, Garrigus and Strasik, 1998; Wei, Tsuei, van Bentum, Xiong and Chu and Wu,

1998; Iguchi1, Wang, Yamazaki, Tanaka and Kashiwaya, 2000; Aubin, Greene, Sha Jian and Hinks, 2002).

In this chapter, the a-b plane tunneling spectroscopy of 2DEG/d-wave superconductor junction will be investigated. The effect of RSOC, potential barrier, different Fermi levels of the 2DEG, and the junction orientation will be examined.

4.1 Assumption and Method of Calculation

The 2DEG/d-wave superconductor (2DEG/D) junction is modeled as an infinite 2D system. The geometry of the junction is depicted in Fig. 4.1. The potential barrier of 2DEG/D junction is represented by a delta-function potential of strength H_s . The superconducting gap is assumed to be zero in the 2DEG and to be spatially constant with a $d_{a^2-b^2}$ -wave symmetry in the superconductor. That is, the superconducting gap depends on wave vector \vec{k} as follows:

$$\Delta(\theta_k) = \Delta_0 \cos[2(\theta_k - \alpha)],$$

where θ_k is the angle between wave vector \vec{k} and the interface normal vector, and α is the angle between the a -axis of the $d_{a^2-b^2}$ -wave superconductor and the interface normal vector. This angle specifies the orientation of the junction, for example, {100} junction is equivalent to $\alpha = 0$. The sketch of the $d_{a^2-b^2}$ gap function of the superconductor of {100} junction is displayed in Fig. 4.2.

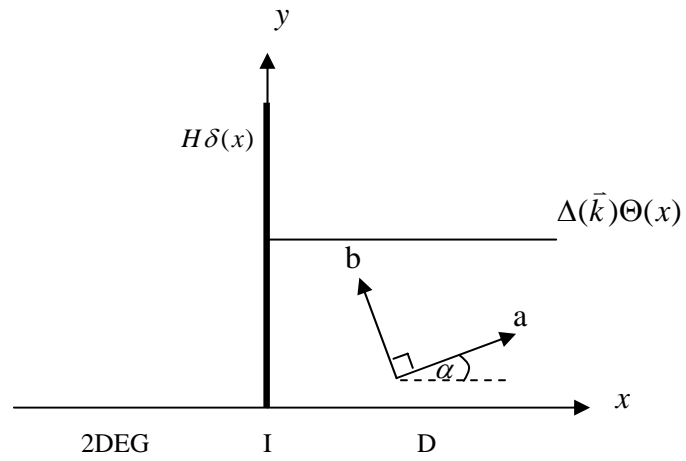


Figure 4.1 The sketch of the 2DEG/D junction

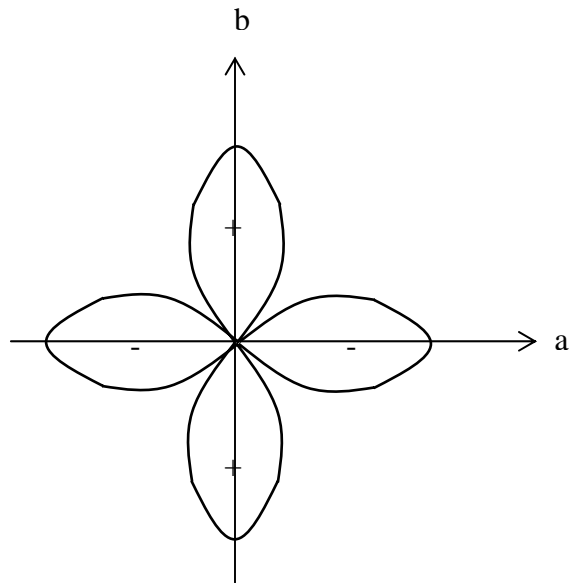


Figure 4.2 The sketch of $d_{x^2-y^2}$ - wave superconducting gap function. Plus and minus sign represent the phase of the gap

Similar to 2DEG/S junction, the Hamiltonian of 2DEG/D junction is

$$\begin{pmatrix} \hat{H}_0 + \hat{H}_{R\uparrow} + H\delta(x) & 0 & \Delta\Theta(x) & 0 \\ 0 & \hat{H}_0 + \hat{H}_{R\downarrow} + H\delta(x) & 0 & \Delta\Theta(x) \\ \Delta\Theta(x) & 0 & -\hat{H}_0 + \hat{H}_{R\uparrow} - H\delta(x) & 0 \\ 0 & \Delta\Theta(x) & 0 & -\hat{H}_0 + \hat{H}_{R\downarrow} - H\delta(x) \end{pmatrix} \psi(x, z) = E\psi(x, z), \quad (4.1)$$

where \hat{H}_0 and $\hat{H}_{R\uparrow,\downarrow}$ are the Hamiltonian of the free electron and Rashba Hamiltonian of electron and/or hole with spin up and spin down respectively. That is,

$$\hat{H}_0 = \hat{p} \frac{1}{2m(x)} \hat{p} - E_{F,S} \Theta(x) - E_{F,2DEG} \Theta(-x),$$

$$\hat{H}_{R\uparrow} = \frac{\lambda}{2} (\Theta(-x)(\sigma_{z(11)} \hat{p}_x - \sigma_{x(12)} \hat{p}_z) + (\sigma_{z(11)} \hat{p}_x - \sigma_{x(12)} \hat{p}_z) \Theta(-x)),$$

$$\hat{H}_{R\downarrow} = \frac{\lambda}{2} (\Theta(-x)(\sigma_{z(22)} \hat{p}_x - \sigma_{x(12)} \hat{p}_z) + (\sigma_{z(22)} \hat{p}_x - \sigma_{x(12)} \hat{p}_z) \Theta(-x)),$$

where \hat{p} is a momentum operator in 2D, $\frac{1}{m(x)} = \frac{1}{m^*} \Theta(-x) + \frac{1}{m} \Theta(x)$ is the effective mass of the system (m^* in 2DEG and m in the superconductor). $\psi(x, z)$ is a four-

component wave function $\psi(x, z) = \begin{pmatrix} \psi_{e\uparrow} \\ \psi_{e\downarrow} \\ \psi_{h\uparrow} \\ \psi_{h\downarrow} \end{pmatrix}$.

The wave function of the superconducting side is the combination of the four transmitted excitations. That is,

$$\psi_S(x > 0, z) = \left[c_1 e^{ik_x^+ x} \begin{pmatrix} u_{k^+} \\ 0 \\ 0 \\ -v_{k^+} \end{pmatrix} + c_2 e^{ik_x^+ x} \begin{pmatrix} 0 \\ u_{k^+} \\ v_{k^+} \\ 0 \end{pmatrix} + d_1 e^{-ik_x^- x} \begin{pmatrix} u_{-k^-} \\ 0 \\ 0 \\ -v_{-k^-} \end{pmatrix} + d_2 e^{-ik_x^- x} \begin{pmatrix} 0 \\ u_{-k^-} \\ v_{-k^-} \\ 0 \end{pmatrix} \right] e^{ik_z z}, \quad (4.2)$$

where c_1 , c_2 , d_1 and d_2 are the amplitudes of the four transmissions. u_k and v_k are the electron-like and hole-like quasiparticle amplitudes and are defined as

$$u_k = \frac{E + \xi_k}{\sqrt{|E + \xi_k|^2 + |\Delta_k|^2}}, \quad (4.3)$$

$$v_k = \frac{\Delta_k}{\sqrt{|E + \xi_k|^2 + |\Delta_k|^2}}, \quad (4.4)$$

so that $|u_k|^2 + |v_k|^2 = 1$. E is the quasiparticle energy and ξ_k is the electron energy of state \bar{k} in normal state. The relation between E , ξ_k and $\Delta_k(\theta)$ is

$$E_k = \sqrt{\xi_k^2 + \Delta_k^2(\theta)} \quad (4.5)$$

Since the energy range of interest is in order of meV, which is the order of the maximum superconducting gap and is usually smaller than the Fermi energy of the superconductor, so the approximation $k^+ = k^- = k_F \cos \theta$ is used. Also, $\theta_{-k^-} = \pi - \theta_{k^+}$.

In the previous chapter, 2DEG/S junction was considered in 3 cases of different Fermi levels of the 2DEG, i.e., the Fermi level is (1) above the crossing of the two branches, (2) at the crossing, and (3) below the crossing. It was found that the last two cases lead to the similar results. Therefore, in this chapter only the first two cases will

be examined. Also, the effect of the ratio of the effective mass on the conductance spectrum will not be considered. The ratio will be set to 10 throughout this chapter.

4.2 Results and Discussion

The conductance spectrum of 2DEG/D junction is dependent on the orientation of the junction as that of metal/D junction (Tanaka and Kashiwaya, 1995; Pairor and Walker, 2002). In all the following plots the conductance spectra is normalized by the conductance at $eV = 0.02E_F$. This section is divided into 2 parts according to the Fermi levels of the 2DEG.

4.2.1 Case 1: E_F is located above the crossing

Fig. 4.3 shows the tunneling conductance spectra of $\{100\}$ junction ($\alpha = 0$). Unlike 2DEG/S and metal/D junction, there occurs a feature at the voltage less than the maximum gap of the d-wave superconductor. The position of this feature depends on the magnitude of the RSOC. In fact, it moves towards the peak at the maximum gap as the strength of RSOC is increased. This feature is not robust against the potential barrier, i.e., it gets smeared out as the potential barrier is larger. This feature also exists in the conductance spectrum of the junction small with non-zero α (see Figs. 4.4(b) and 4.5). Its position moves toward zero energy as α is increased (see Fig.4.5). The shape of this feature is different from that of 2DEG/S junction due to the dependence on wave vector of the d-wave superconducting gap which different from that of s-wave superconductor.

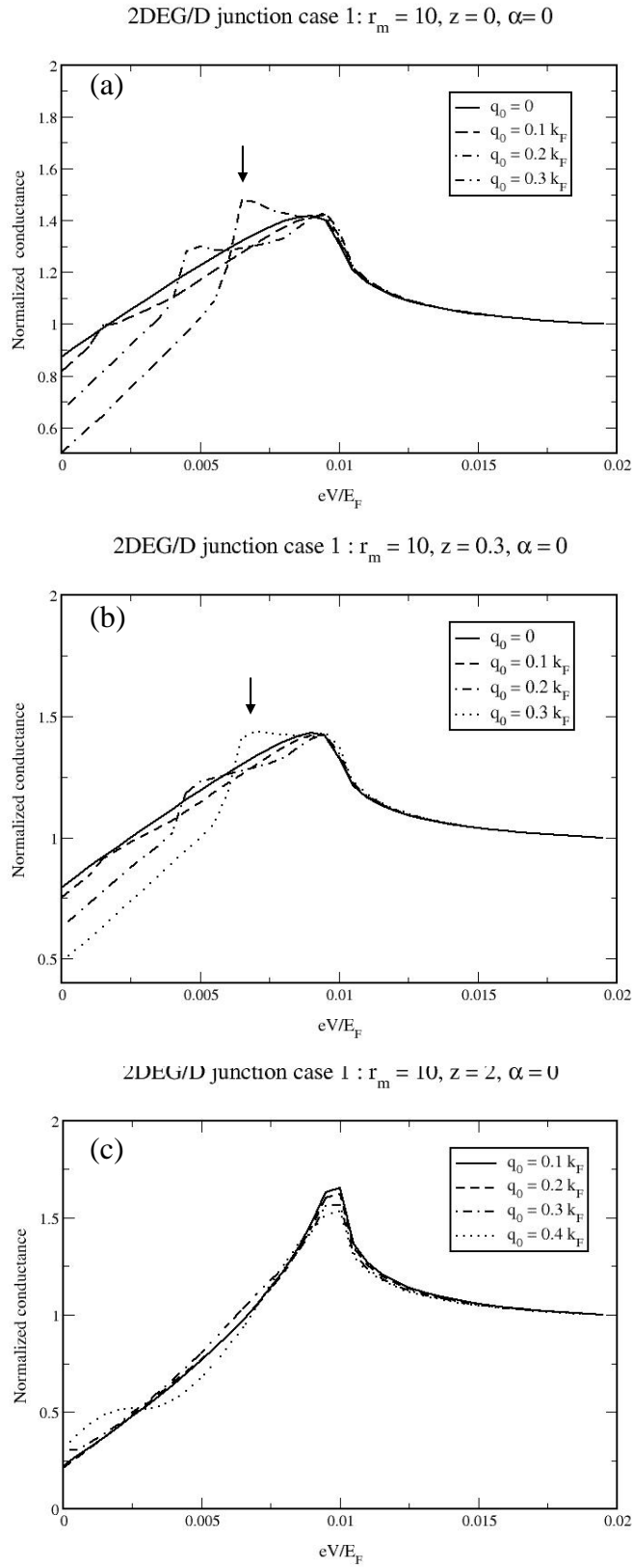


Figure 4.3 The conductance spectra of 2DEG/D junction with various q_0 where $\alpha = 0, r_m = 10$ (a). $z = 0$, (b) $z = 0.3$ (c) $z = 2$. The arrows indicate the feature at $eV < \Delta$

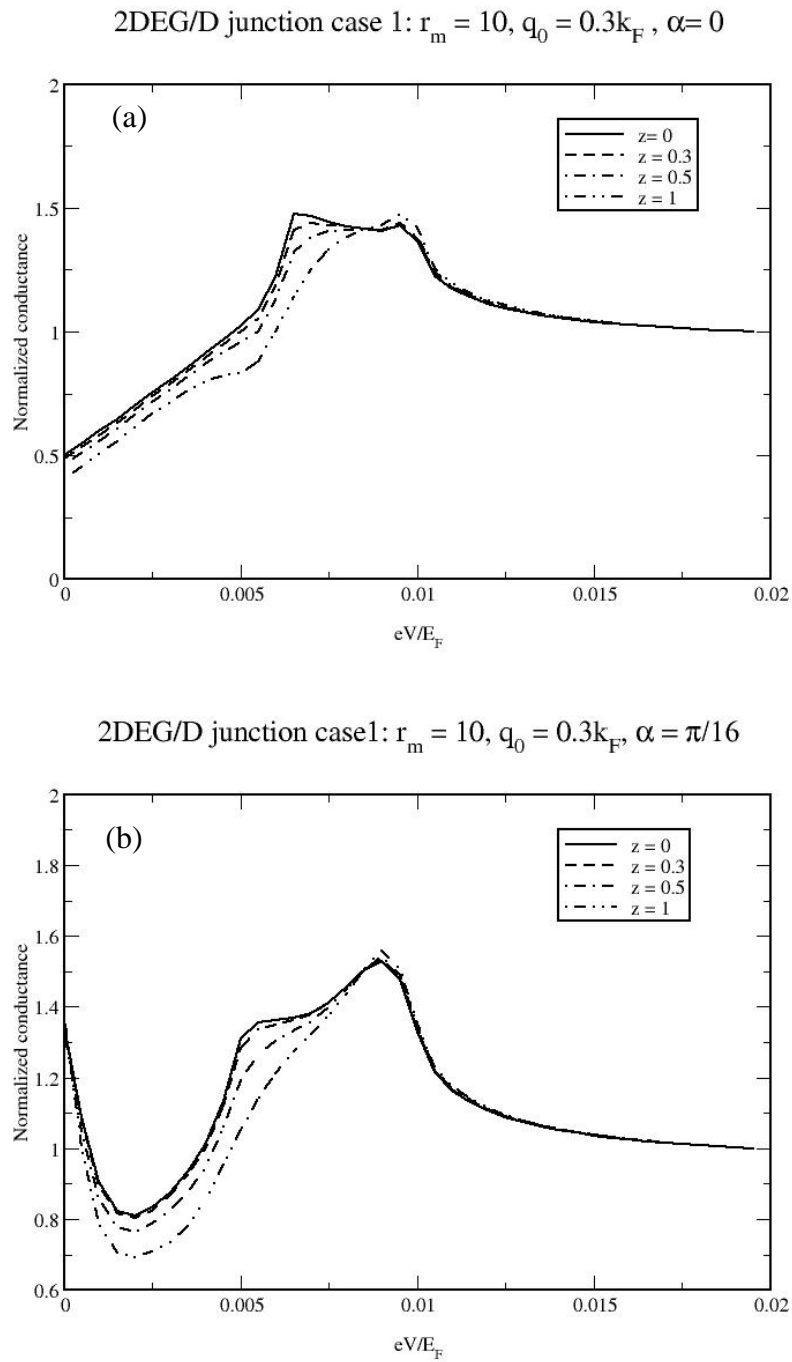


Figure 4.4 The conductance spectra of 2DEG/D junction with various z , $r_m = 10$

(a). $\alpha = 0$ (b) $\alpha = \frac{\pi}{16}$.

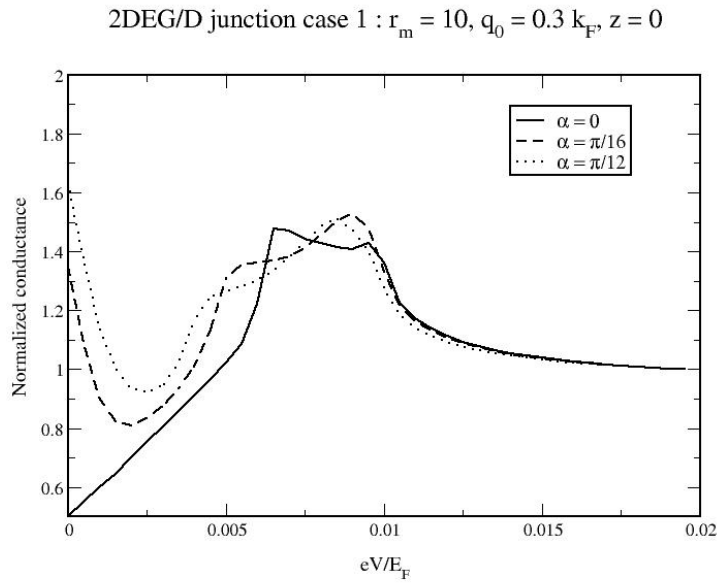


Figure 4.5 The conductance spectra of 2DEG/D junction with various α , $z = 0$, $r_m = 10$ and $q_0 = 0.3k_F$

As shown in Fig. 4.6, the potential barrier decreases the normalized conductance at the bias voltage below the maximum gap similar to that in the spectrum of M/D junction (Tanaka and Kashiwaya, 1995).

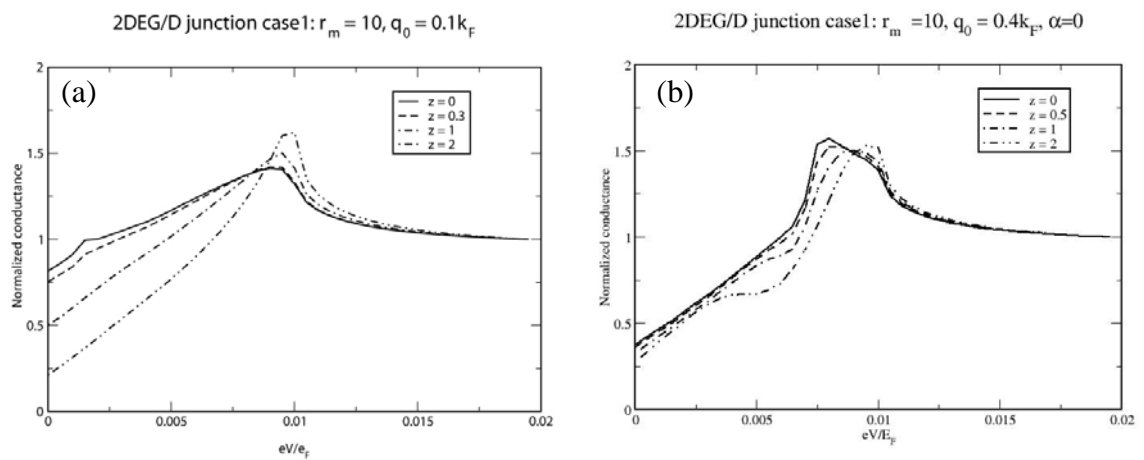


Figure 4.6 The conductance spectra of 2DEG/D junction with various $z = 0, 0.3, 1$ and 2 , $\alpha = 0$, $r_m = 10$ (a) $q_0 = 0.1k_F$. (b) $q_0 = 0.4k_F$.

In the spectrum of junctions with α away from zero, there occurs a zero-bias conductance peak (ZBCP), which is the signature of the surface bound states of the d-wave superconductor (Hu, 1994). Fig. 4.7 shows the plots of normalized conductance vs bias voltage of the $\{110\}$ ($\alpha = \frac{\pi}{4}$) junction with various values of RSOC strength (q_0). It is found that in the Andreev limit q_0 enhances the height but decreases the width of ZBCP (Fig. 4.7(a)). In the tunneling limit, q_0 reduces the height of the peak but does not affect its width (Fig. 4.7(b)). Fig. 4.8 contains the plot of normalized conductance for different value of potential barrier. It is found that the height of ZBCP is increased with z , whereas its width is decreased for small q_0 . When q_0 is big, the potential barrier does not affect the width of ZBCP.

The effect of the RSOC and the potential barrier on ZBCP in the conductance spectrum of junction with $\alpha = \frac{\pi}{8}$ is the same as in that of $\{110\}$ junction (see Figs. 4.9 and 4.10). There is a peak occurring at $eV = \Delta_0 \cos 2\alpha$, where $\alpha = \frac{\pi}{8}$ as also seen in M/D junction (Tanaka and Kashiwaya, 1995; Pairor and Walker, 2002).

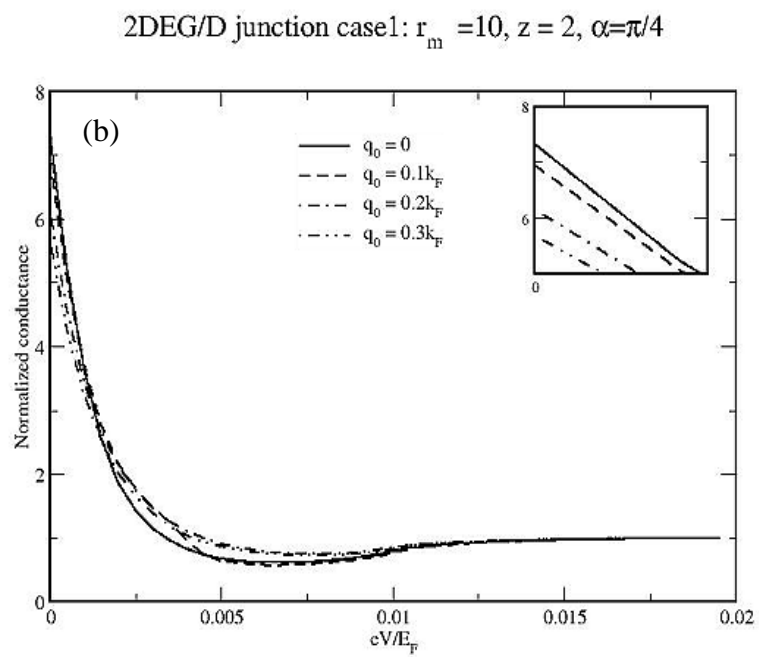
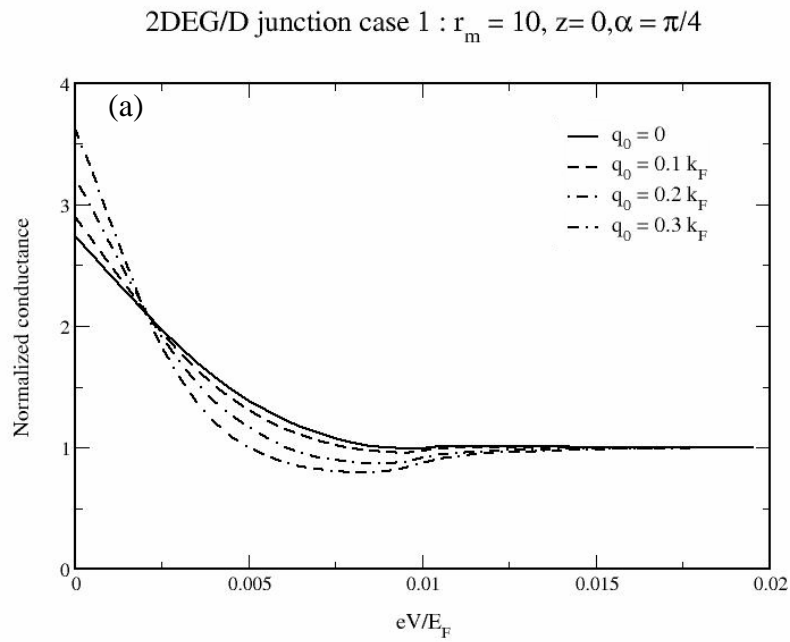
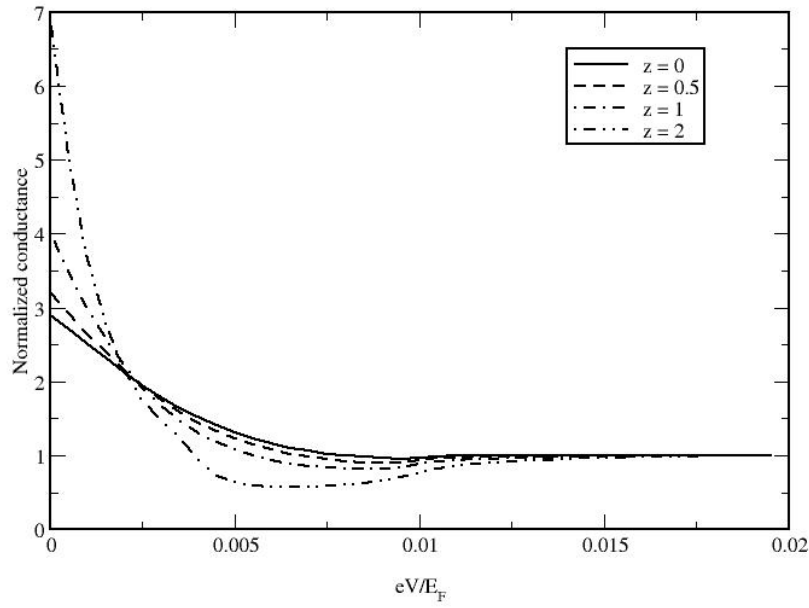


Figure 4.7 The conductance spectra with various RSOC, $\alpha = \frac{\pi}{4}$, (a) $z = 0$ (b). $z = 2$.

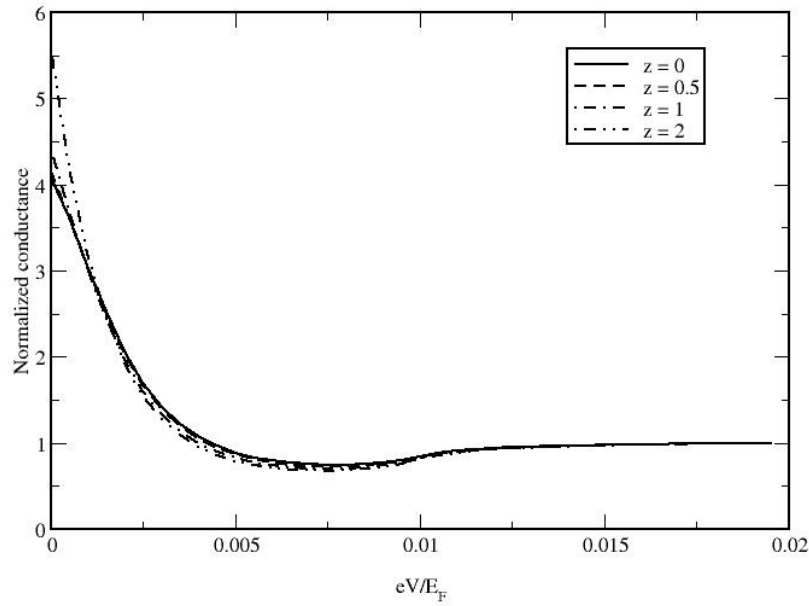
The inset is the close up plot of the conductance spectra near $eV = 0$

2DEG/D junction case1: $r_m = 10$, $q_0 = 0.1k_F$, $\alpha = \pi/4$



(a)

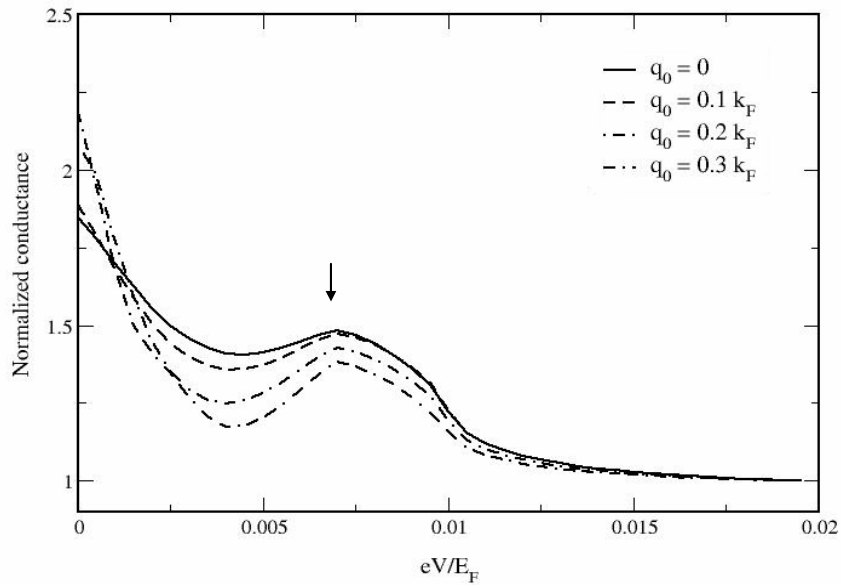
2DEG/D junction case1: $r_m = 10$, $q_0 = 0.4k_F$, $\alpha = \pi/4$



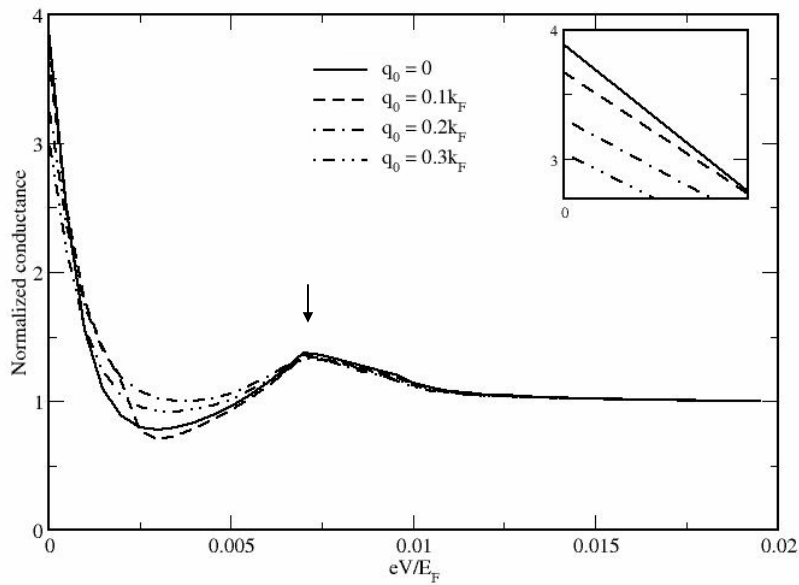
(b)

Figure 4.8 The conductance spectra of 2DEG/D junction with various $z = 0, 0.5, 1$ and

2 , $\alpha = \frac{\pi}{4}$, $r_m = 10$ (a) $q_0 = 0.1k_F$. (b) $q_0 = 0.4k_F$.

2DEG/D junction case 1 : $r_m = 10$, $z = 0$, $\alpha = \pi/8$ 

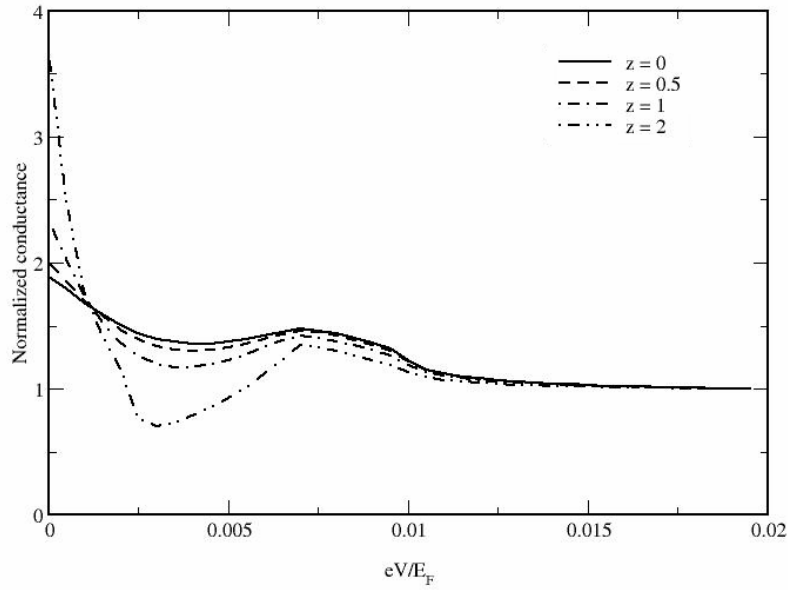
(a)

2DEG/D junction case 1: $r_m = 10$, $z = 2$, $\alpha = \pi/8$ 

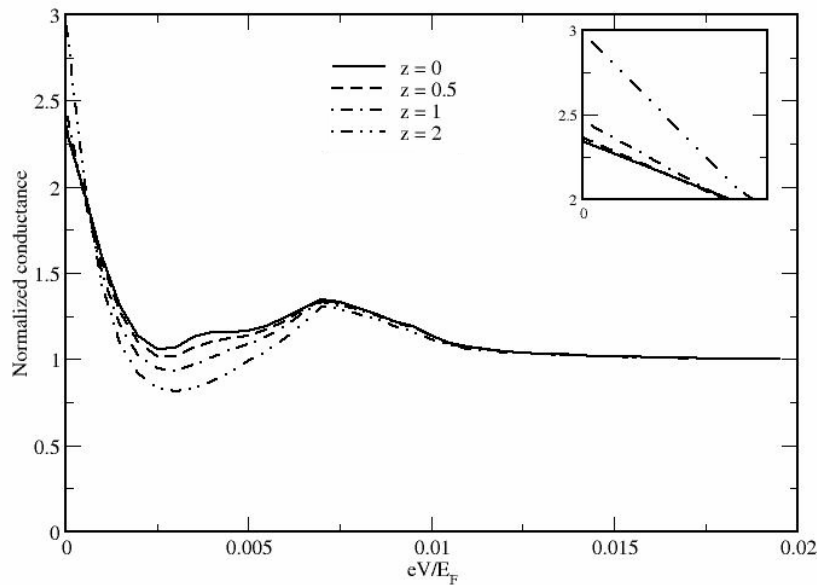
(b)

Figure 4.9 The conductance spectra with various RSOC, $\alpha = \frac{\pi}{8}$, (a) $z = 0$ (b). $z = 2$.

The arrows indicate the feature at $eV = \Delta_0 \cos 2\alpha$. The inset is the close up plot of the conductance spectra near $eV = 0$

2DEG/D junction case1: $r_m = 10$, $q_0 = 0.1k_F$, $\alpha = \pi/8$ 

(a)

2DEG/D junction case1: $r_m = 10$, $q_0 = 0.4k_F$, $\alpha = \pi/8$ 

(b)

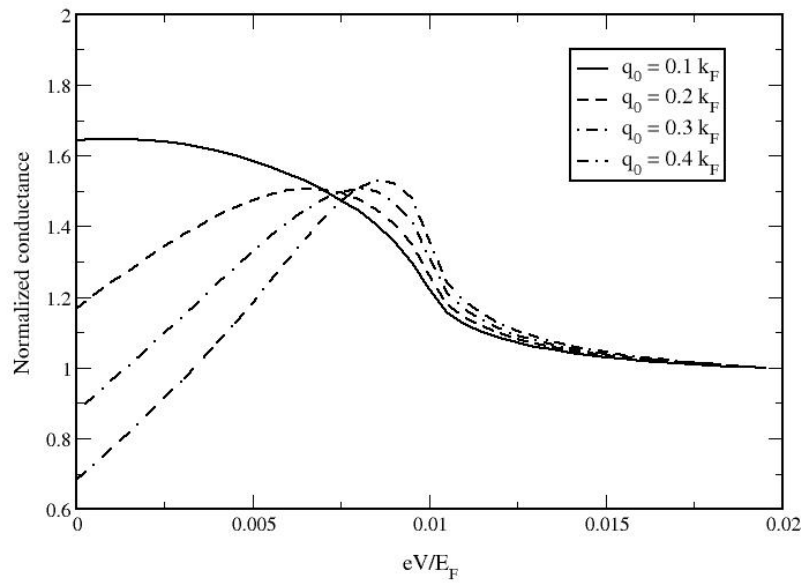
Figure 4.10 The conductance spectra of 2DEG/D junction with various $z = 0, 0.5, 1$ and 2 , $\alpha = \frac{\pi}{8}$, $r_m = 10$ (a) $q_0 = 0.1k_F$. (b) $q_0 = 0.4k_F$. The inset is the close up plot of the conductance spectra near $eV = 0$

4.2.2 Case 2: E_F is located at the crossing

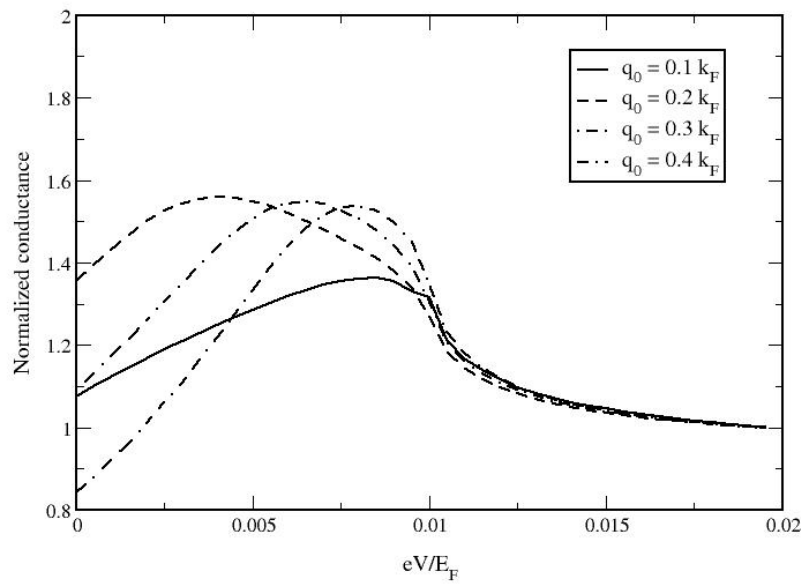
For the $\{100\}$ junction, in the Andreev limit the normalized conductance at zero bias voltage is decreased with q_0 (see Fig. 4.11(a)). In the tunneling limit, the conductance at zero voltage is increased with q_0 and then later is decreased with q_0 (see Fig. 4.11(b)). Fig. 4.12 contains the plots of normalized conductance for different values of potential barrier for a fixed q_0 . It is found that for small q_0 , potential barrier suppresses the conductance at zero voltage, while for big q_0 , the potential barrier can enhance it.

The conductance spectra for different values of q_0 of junctions with $\alpha = \frac{\pi}{4}$ and $\alpha = \frac{\pi}{8}$ are shown in Figs. 4.13 and 4.14. In the Andreev limit, the effect of q_0 on ZBCP is the same as in the previous case where E_F is located above the crossing, that is, it enhances the height of ZBCP. However, in the tunneling limit, the increase in q_0 can cause the height of ZBCP to decrease and after a critical value of q_0 the height start to increase.

Figs. 4.15 and 4.16 contains the plots of conductance spectra of the junction with $\alpha = \frac{\pi}{4}$ and $\alpha = \frac{\pi}{8}$ for different values of z . It is found in junction with both orientations that as the potential barrier is increased, the height of ZBCP is increased for small q_0 , while for big q_0 the height of ZBCP is almost unchanged.

2DEG/D junction case 2 : $r_m = 10$, $z = 0$, $\alpha = 0$ 

(a)

2DEG/D junction case 2 : $r_m = 10$, $z = 1$, $\alpha = 0$ 

(b)

Figure 4.11 The conductance spectra with various RSOC, $\alpha = 0$, (a) $z = 0$ (b). $z = 1$

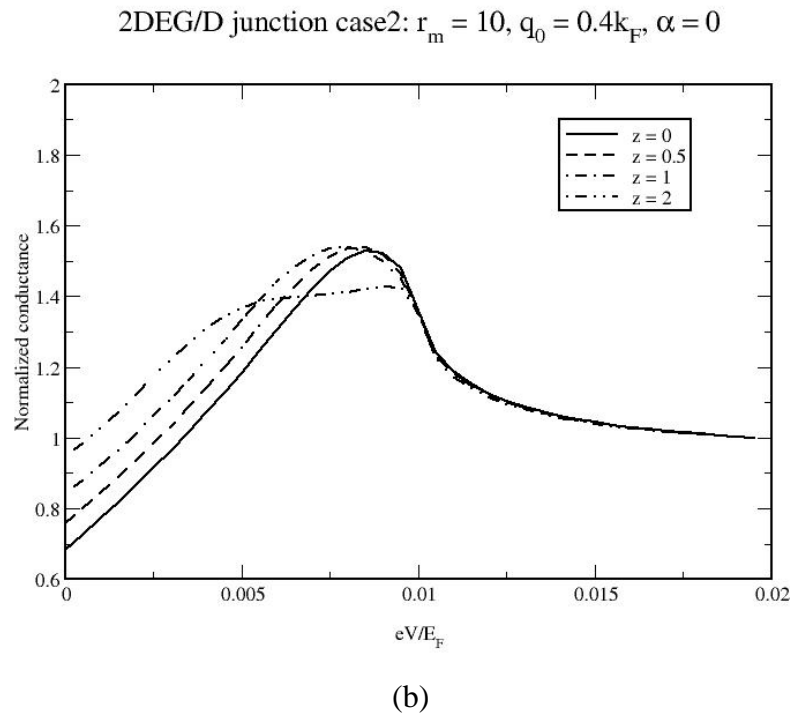
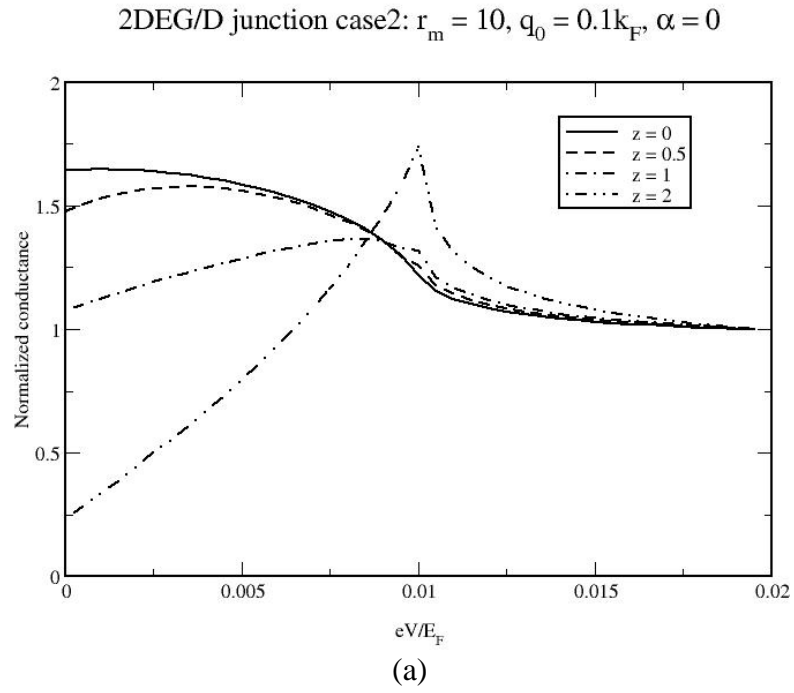


Figure 4.12 The conductance spectra of 2DEG/D junction with various $z = 0, 0.5, 1$ and 2 , $\alpha = 0$, $r_m = 10$ (a) $q_0 = 0.1k_F$. (b) $q_0 = 0.4k_F$

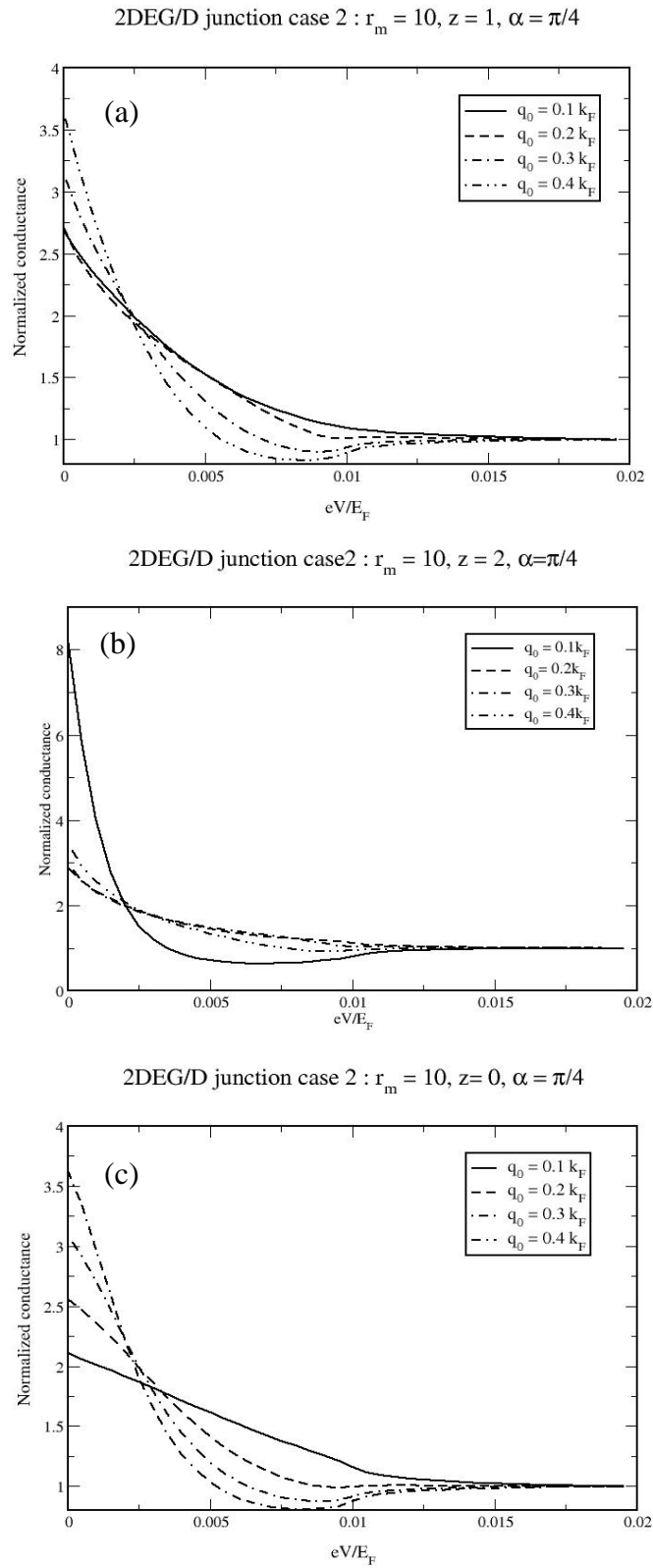


Figure 4.13 The conductance spectra with various RSOC, $\alpha = \frac{\pi}{4}$, (a) $z = 0$ (b) $z = 1$

(c) $z = 2$

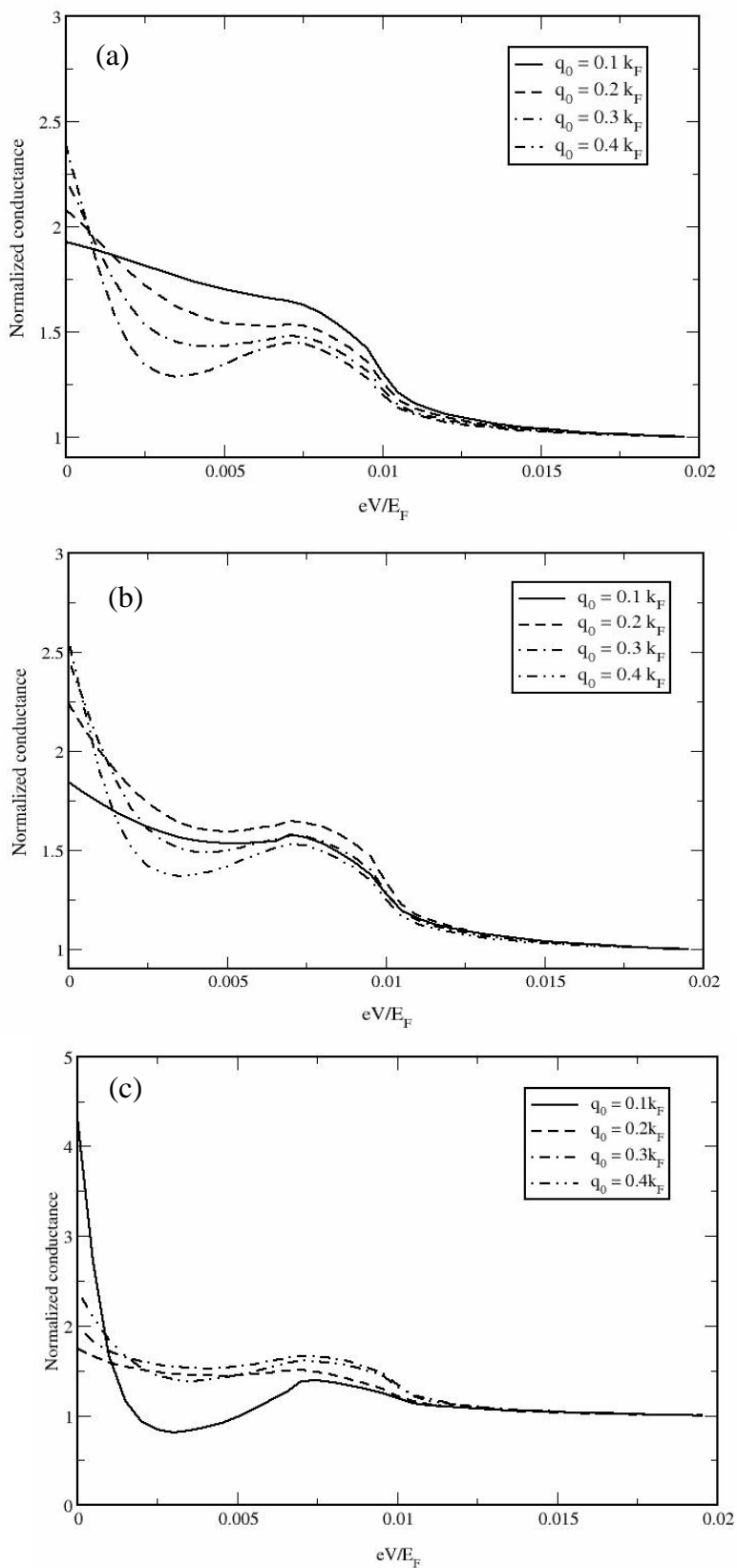
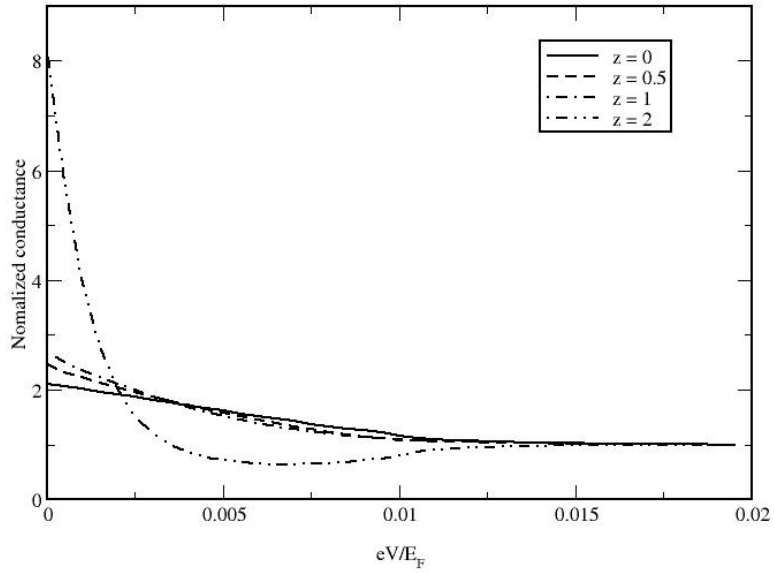


Figure 4.14 The conductance spectra with various RSOC, $\alpha = \frac{\pi}{8}$, (a) $z = 0$ (b) $z = 1$

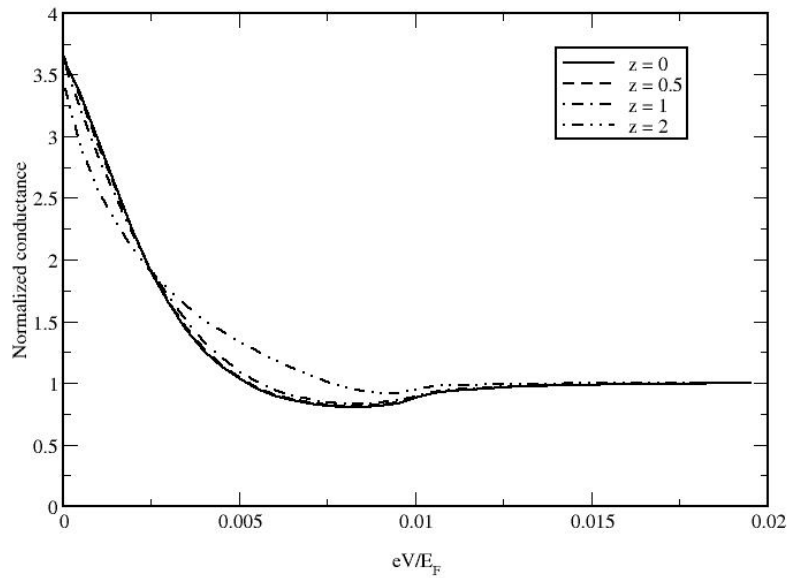
(c) $z = 2$

2DEG/D junction case 2 : $r_m = 10$, $q_0 = 0.1k_F$, $\alpha = \pi/4$



(a)

2DEG/D junction case2 : $r_m = 10$, $q_0 = 0.4k_F$, $\alpha = \pi/4$

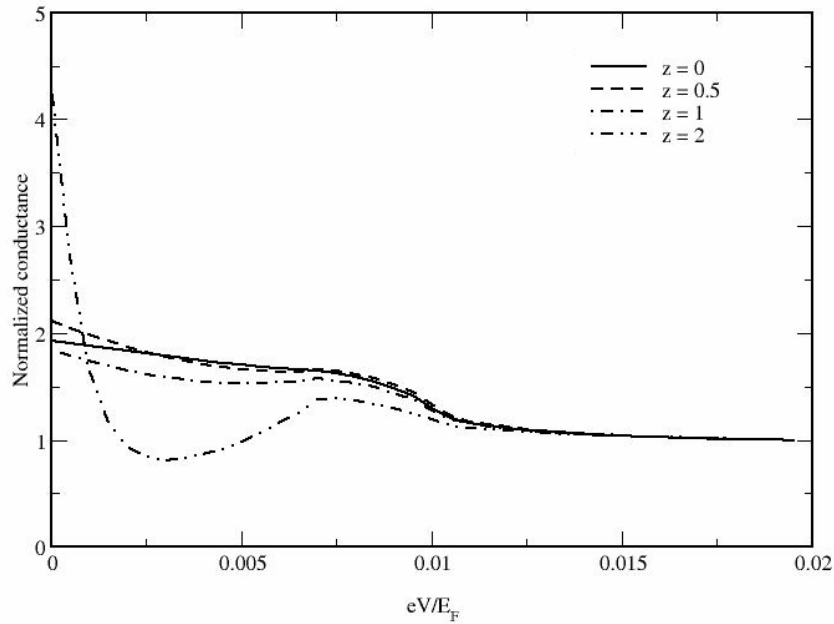


(b)

Figure 4.15 The conductance spectra of 2DEG/D junction with various $z = 0, 0.5, 1$

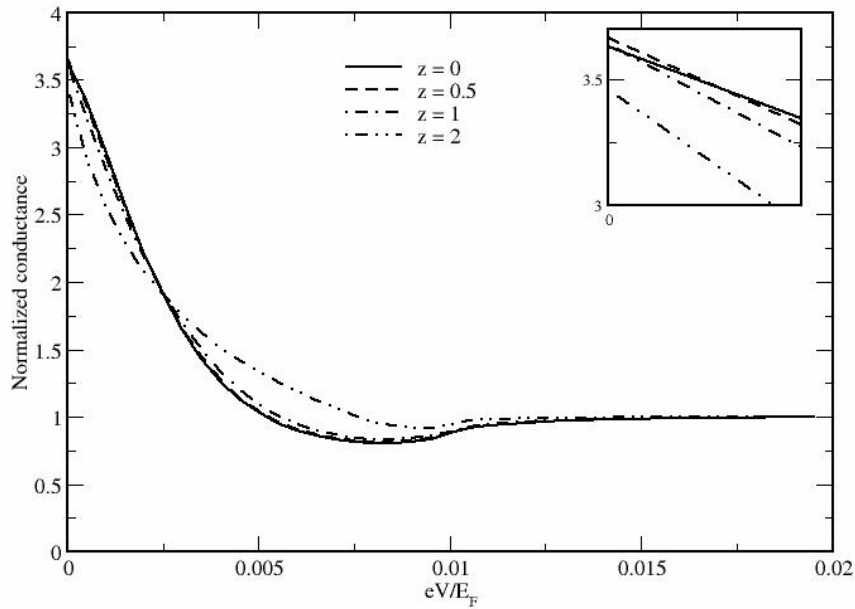
and 2, $\alpha = \frac{\pi}{4}$, $r_m = 10$ (a) $q_0 = 0.1k_F$ (b) $q_0 = 0.4k_F$

2DEG/D junction case2: $r_m = 10$, $q_0 = 0.1k_F$, $\alpha = \pi/8$



(a)

2DEG/D junction case2: $r_m = 10$, $q_0 = 0.4k_F$, $\alpha = \pi/8$



(b)

Figure 4.16 The conductance spectra of 2DEG/D junction with various $z = 0, 0.5, 1$ and 2 , $\alpha = \frac{\pi}{8}$, $r_m = 10$ (a) $q_0 = 0.1k_F$. (b) $q_0 = 0.4k_F$. The inset is the close up plot

of the conductance spectra near $eV = 0$

4.3 Conclusions

The tunneling conductance spectra of 2DEG/D junction show strong dependence on junction orientation. In junction with {100} orientation, a peak near the maximum gap of the d-wave superconductor is present in the conductance spectra. In junction away from {100}, there occurs a ZBCP, which is the signature of the surface bound states of d-wave superconductor (Hu, 1994; Tanaka and Kashiwaya, 1995). Like in 2DEG/S junction, it is found that the effects of RSOC strength and potential barrier on the tunneling conductance are different for different Fermi levels of the 2DEG.

When the Fermi level lies above the crossing of the two branches, there occurs a peak at finite bias voltage but less than the maximum gap in {100} junction. The position of this feature depends on the magnitude of the RSOC. However, this feature is not robust against the barrier potential, i. e. it disappear when the barrier potential is in the tunneling limit. The normalized conductance at the bias voltage below the maximum gap is decreased by the potential barrier. In the junction with $\alpha = \frac{\pi}{4}$ and $\alpha = \frac{\pi}{8}$, RSOC enhance the height but decrease the width of ZBCP in Andreev limit. In the tunneling limit, RSOC reduce the height of the peak but does not affect its width. It is found that the height of ZBCP is increased with the barrier potential, whereas its width is decreased for small RSOC. When RSOC is big, the barrier potential does not affect the width of ZBCP.

In the case where the Fermi level of the 2DEG lies at the crossing, for the {100} junction, the normalized conductance at zero bias voltage is decreased with

RSOC in the Andreev limit. In the tunneling limit, the conductance at zero bias voltage is increased with RSOC and then later is decreased with RSOC. It is found that for small RSOC, potential barrier suppress the conductance at zero bias voltage, while for big RSOC, the potential barrier can enhance it. In the junction with $\alpha = \frac{\pi}{4}$ and $\alpha = \frac{\pi}{8}$, the effect of RSOC on ZBCP in Andreev limit is the same as in the case where Fermi level lies above the crossing, that is, it enhances the height of ZBCP. However, in the tunneling limit, the increase in RSOC strength can cause the height of ZBCP to decrease and after a critical value of RSOC the height start to increase. It is found in the junction with both $\alpha = \frac{\pi}{4}$ and $\alpha = \frac{\pi}{8}$ orientations that the barrier potential increases the height of ZBCP for small RSOC, while for RSOC is big the height of ZBCP is almost not affected.

CHAPTER V

CONCLUSIONS

In this thesis, the tunneling conductance spectra of 2DEG/M, 2DEG/S and 2DEG/D junctions are theoretically investigated. The effect of RSOC and the potential barrier on the conductance spectrum are examined in detail. For the conductance spectra of 2DEG/S and 2DEG/D junctions, the effect of Fermi level of 2DEG is also considered.

For 2DEG/M junction, it is assumed that the Fermi level of 2DEG is much higher than the Rashba energy. The results for the lower Fermi level can also be obtained by shifting the zero voltage according to the Fermi level. It is found in 2DEG/M junction that the injection from 2DEG can generate the spin polarization in the metal. The spin polarization depends on the applied voltage. It is maximum at the crossing of two energy branches. The increase in the barrier potential decreases the spin polarization and also generally suppresses the conductance. As for the RSOC strength, it enhances the conductance, but does not generally enhance the spin polarization. From the plot of conductance as a function of bias voltage, it suggests that one can use the tunneling spectroscopy to measure the strength of RSOC.

For 2DEG/S junction, the effect of RSOC, the mismatch effective mass, the barrier strength and the Fermi level of the 2DEG on the tunneling conductance is investigated. It is found that the effect of RSOC strength, potential barrier, and the ratio of the effective masses on the tunneling conductance are different for different

Fermi levels. When the Fermi level lies above the crossing of the two branches, the conductance over the range of the applied voltage less than the superconducting gap is decreased with the RSOC. The conductance over this range can be increased with the RSOC when the mismatch in effective mass exists and the potential barrier is in the tunneling limit. The conductance peak at the energy gap is increased with the RSOC but independent on the potential barrier.

In the case where the Fermi level of the 2DEG lies at the crossing, the conductance spectrum below the energy gap is increased with the RSOC up to a critical value and then is decreased with the RSOC. The effect of the potential barrier is similar to that in the previous case. The effect of the ratio of the effective mass on the conductance at zero voltage in this case is similar to that of the RSOC, but the effect of the ratio on the conductance at the energy gap is similar to that of the potential barrier.

For the Fermi level of the 2DEG is below the crossing, the effect of RSOC, barrier strength and mismatch effective mass are similar to that in case where the Fermi level is at the crossing. The only difference is that in this case there exists a feature in the conductance spectra at the crossing.

In all cases of Fermi levels, the conductance peak at the energy gap is increased with the strength of RSOC and independent on barrier potential. One can use the height of this peak to measure the strength of RSOC.

The tunneling conductance spectra of 2DEG/D junction show strong dependence on junction orientation, which is characterized by the angle α between the a-axis of the superconductor and the direction normal to the interface. In junction

with $\{100\}$ orientation ($\alpha = 0$), a peak near the maximum gap of the d-wave superconductor is present in the conductance spectrum. In junction away from $\{100\}$, there occurs a ZBCP, which is the signature of the surface bound states of d-wave superconductor (Hu, 1994; Tanaka and Kashiwaya, 1995). Like in 2DEG/S junctions, it is found that the effect of RSOC strength and potential barrier on the tunneling conductance are different for different Fermi levels of the 2DEG.

When the Fermi level lies above the crossing of the two branches, there occurs a peak at finite bias voltage but less than the maximum gap in $\{100\}$ junction. The position of this feature depends on the magnitude of the RSOC. However, this feature is not robust against the barrier potential, i.e. it disappears when the potential barrier is in the tunneling limit. The normalized conductance at the bias voltage below the maximum gap is decreased by the potential barrier. In the $\{110\}$ junction, RSOC enhance the height but decrease the width of ZBCP in the Andreev limit. In the tunneling limit, RSOC reduces the height of the peak but does not affect its width. It is found that the height of ZBCP is increased with the potential barrier, whereas its width is decreased for small RSOC. When RSOC is big, the potential barrier does not affect the width of ZBCP.

In the case where the Fermi level of the 2DEG lies at the crossing, for the $\{100\}$ junction, the normalized conductance at zero bias voltage is decreased with RSOC in the Andreev limit. In the tunneling limit, the conductance at zero bias voltage is first increased with RSOC and then later decreased with RSOC. It is found that for small RSOC, barrier strength suppresses the conductance at zero bias voltage, while for big RSOC, the barrier strength can enhance it. In the $\{110\}$ junction, the effect of RSOC on ZBCP in Andreev limit is the same as in the case where Fermi

level lies above the crossing; that is, it enhances the height of ZBCP. However, in the tunneling limit, the increase in RSOC strength can cause the height of ZBCP to decrease and after a critical value of RSOC the height start to increase. It is found in the {110} junction that the barrier strength increases the height of ZBCP for small RSOC, while for RSOC is big the height of ZBCP is almost not affected.

REFERENCES

REFERENCES

- Alff, L., Takashima, H., Kashiwaya, S., Terada, N., Ihara, H., Tanaka, Y., Koyanagi, M. and Kajimura, K. (1997). Spatially continuous zero-bias conductance peak on (110) $\text{YBa}_2\text{Cu}_3\text{O}_{7-\delta}$ Surfaces. **Phys. Rev. B** 55(22): R14757 - R14760.
- Andreev, A. F. (1964). The thermal conductivity of the intermediate state in superconductors. **Sov. Phys. JEPT.** 19: 1228.
- Aronov, A. G. Lyanda-Geller, and Y. B. (1993). Spin-orbit Berry phase in conducting rings. **Phys. Rev. Lett.** 70(3): 343 - 346.
- Aubin, H., Greene, L. H., Sha Jian and Hinks, D. G. (2002). Andreev Bound States at the Onset of Phase Coherence in $\text{Bi}_2\text{Sr}_2\text{CaCu}_2\text{O}_8$. **Phys. Rev. Lett.** 89(17): 177001 - 1 - 177001 - 4.
- Blonder, G. E., Tinkham, M., and Klapwijk, T. M. (1982). Transition from metallic to tunneling regimes in superconducting microconstrictions: Excess current, charge imbalance and supercurrent conversion. **Phys. Rev. B** 25 (7): 4515 - 4532.
- Bychkov, Yu. A. and Rashba, E. I. (1984). Oscillatory effects and the magnetic susceptibility of carrier in inversion layers. **J. Phys. C** 17(33): 6039 - 6045.
- Chen, G. L., Han, J., Huang, T. T., Datta, S. and Janes, D. B. (1993). Observation of the interfacial-field-induced weak antilocalization in InAs quantum structures. **Phys. Rev. B** 47(7): 4084 - 4087.
- Cucolo, A. M. and Di Leo, R. (1993). Zero-bias anomalies in high- T_c -superconductor tunnel junctions. **Phys. Rev. B** 47(5): 2916 - 2919.

- Cummings, A. W., Akis, R. and Ferry, D. K. (2006). Electron spin filter based on Rashba spin-orbit coupling. **Appl. Phys. Lett.** 89: 172115 - 172117.
- Das, B., Miller, D. C., Datta, S., Reifenberger, R., Hong, W. P., Bhattacharya, P. K., Singh, J. and Jaffe, M. (1989). Evidence for spin splitting in $\text{In}_x\text{Ga}_{1-x}\text{As}/\text{In}_{0.52}\text{Al}_{0.48}\text{As}$ heterostructures as $B \rightarrow 0$. **Phys. Rev. B** 39(2): 1411 - 1414.
- Das, B., Datta, S. and Reifenberger, R. (1990). Zero-field spin splitting in a two-dimensional electron gas. **Phys. Rev. B** 41(12): 8278 - 8287.
- Datta, S., and Das, B., (1990). Electronic analog of the electro-optic modulator. **Appl. Phys. Lett.** 56(7): 665 - 667.
- Griffin, A. and Demers, J. (1971). Tunneling in the normal-metal-insulator-superconductor geometry using Bogoliubov equations of motion. **Phys. Rev. B** 4(7): 2202-2208.
- Hammar, P. R., Bennett, B. R., Yang, M. J. and Johnson, M. (1999). Observation of Spin Injection at a Ferromagnet-Semiconductor Interface. **Phys. Rev. Lett.** 83(1): 203 – 206.
- Hu, C-R. (1994). Midgap surface states as a novel signature for $d_{x^2-y^2}$ -wave superconductivity. **Phys. Rev. Lett.** 72(10): 1526 – 1529.
- Jiang, Y. and Jalil, M. B. A. (2003). Rashba effects in an FM/I/2DEG/I/FM structure. **IEEE Transactions on Magnetics.** 39(5): 2836-2838.
- Kashiwaya, S., Tanaka, Y., Koyanagi, M., Takashima, H. and Kajimura, K. (1995). Origin of zero-bias conductance peaks in high-Tc superconductors. **Phys. Rev. B** 51(2): 1350 - 1353.

- Knap, W., Skierbiszewski, C., Zduniak, A., Litwin-Staszewska, E., Bertho, D., Kobbi, F. and Robert, J. L. (1996). Weak antilocalization and spin precession in quantum wells. **Phys. Rev. B** 53(7): 3912 - 3924.
- Koga, T., Nitta, J., Takayanagi, H., Datta, S. (2002). Spin-Filter Device Based on the Rashba Effect Using a Nonmagnetic Resonant Tunneling Diode. **Phys. Rev. Lett.** 88(12): 126601 - 126604.
- Luo, J., Munekata, H., Fang, F.F. and Stiles, P. J. (1988). Observation of the zero-field spin splitting of the ground electron subband in gasb-inas-gasb quantum wells. **Phys. Rev. B** 38(14): 10142 - 10145.
- Luo, J., Munekata, H., Fang, F. F., and Stiles, P. J. (1990). Effects of inversion asymmetry on electron energy band structures in GaSb/InAs/GaSb quantum wells. **Phys. Rev. B** 41(11): 7685 - 7693.
- Matsuyama, T., Hu, C.-M., Grundler, D., Meier, G. and Merkt, U. (2001). Ballistic spin transport and spin interference in ferromagnet/InAs(2DES)/ferromagnet devices. **Phys. Rev. B** 65(15): 155322 - 1 - 155322 - 12.
- Miller, J. B., Zumbühl, D. M., Marcus, C. M., Lyanda-Geller, Y. B., Goldhaber-Gordon, D., Campman, K. and Gossard, A. C. (2003). Gate-Controlled Spin-Orbit Quantum Interference Effects in Lateral Transport. **Phys. Rev. Lett.** 90(7): 076807 - 076810.
- Nitta, J., Akazaki, T., Takayanagi, H., and Enoki, T. (1997). Gate Control of Spin-Orbit Interaction in an Inverted $\text{In}_{0.53}\text{Ga}_{0.47}\text{As}/\text{In}_{0.52}\text{Al}_{0.48}\text{As}$ Heterostructure. **Phys. Rev. Lett.** 78(7): 1335 - 1338.

- Pairor, P. and Walter, M. B. (2002). Tunneling conductance for *d*-wave superconductor : Dependence on Crystallographic and Fermi Surface. **Phys. Rev. B** 65(6): 64507-1-64507-16.
- Schnittler, Ch. and Kirilov, M. (1993). Hamiltonian and Boundary Conditions for Electrons in Semiconductor Heterostructures. **Phys. Stat. Sol.** 176(b) : 143 - 155.
- Středa, P. and Šeba, P. (2003). Antisymmetric Spin Filtering in One-Dimensional Electron Systems with Uniform Spin-Orbit Coupling. **Phys. Rev. Lett.** 90(25): 256601 - 1 - 256601 - 4.
- Tanaka, Y. and Kashiwaya, S. (1995). Theory of Tunneling Spectroscopy of *d*-Wave Superconductors. **Phys. Rev. Lett.** 74(17): 3451 - 3454.
- Tsuei, C. C. and Kirtley, J. R. (2000). Pairing symmetry in cuprate superconductors. **Rev. Mod. Phys.** 72(4): 969 - 1016.
- Walsh, T., Moreland, J., Ono, R. H. and Kalkur, T. S.(1991). Tunneling measurements of the zero-bias conductance peak and the Bi-Sr-Ca-Cu-O thin-film energy gap. **Phys. Rev. Lett.** 66(4): 516 - 519.
- Wang, W., Yamazaki, M., Tanaka, Y. and Kashiwaya, S. (2000). Angle-resolved Andreev bound states in anisotropic *d*-wave high- T_c YBa₂Cu₃O_{7-y} superconductors. **Phys. Rev. B** 62(10): R6131 - R6134.
- Wei1, J. Y. T., Yeh, N.-C., Garrigus, D. F. and Strasik, M. (1998). Directional Tunneling and Andreev Reflection on YBCO Single Crystals: Predominance of *d*-Wave. **Phys. Rev. Lett.** 81(12): 2542 - 2545.
- Wei, J. Y. T., Tsuei, C. C., van Bentum, P. J. M., Xiong, Q. and Chu, C. W. and Wu, M. K. (1998). Quasiparticle tunneling spectra of the high- T_c mercury

cuprates: Implications of the d-wave two-dimensional van Hove scenario. **Phys. Rev. B** 57(6): 3650 - 3662.

Yokoyama, T., Tanaka, Y. and Inoue, J. (2006). Charge transport in two-dimensional electron gas/insulator/superconductor junctions with Rashba spin-orbit coupling. **Phys. Rev. B** 74: 035318 - 1 - 035318 - 7.

Zulicke, U. and Schroll, C. (2002). Interface Conductance of Ballistic Ferromagnetic-Metal-2DEG Hybrid Systems with Rashba Spin-Orbit Coupling. **Phys. Rev. Lett.** 88(2): 029701.

Žutić, I., Fabian, J. and Das Sarma, S.(2004). Spintronics: Fundamentals and applications. **Rev. Mod. Phys.** 72 (2): 323 - 410.

APPENDICES

APPENDIX A

8 × 8 EQUATIONS OF 2DEG/S JUNCTION

In this appendix, the 8 × 8 equations for the reflection and transmission amplitudes of each case of the 2DEG/S junction are written in details.

1) case1: E_F is located above E_c

$$\begin{aligned} b_1 \sin \varphi_1^+ + b_2 \cos \varphi_2^+ - c_1 u_k - d_1 v_k &= -\cos \varphi_1^+ \\ -b_1 \cos \varphi_1^+ + b_2 \sin \varphi_2^+ - c_2 u_k - d_2 v_k &= \sin \varphi_1^+ \\ -a_1 \sin \varphi_1^- + a_2 \cos \varphi_2^- - c_2 v_k - d_2 u_k &= 0 \\ -a_1 \cos \varphi_1^- - a_2 \sin \varphi_2^- + c_1 v_k + d_1 u_k &= 0 \end{aligned}$$

$$\begin{aligned} q_1^+ r_m b_1 \sin \varphi_1^+ + q_2^+ r_m b_2 \cos \varphi_2^+ + (k^+ + 2ik_F z - q_0 r_m) c_1 u_k - (k^- - 2ik_F z + q_0 r_m) d_1 v_k &= q_1^+ r_m \cos \varphi_1^+ \\ -q_1^+ r_m b_1 \cos \varphi_1^+ + q_2^+ r_m b_2 \sin \varphi_2^+ + (k^+ + 2ik_F z + q_0 r_m) c_2 u_k - (k^- - 2ik_F z - q_0 r_m) d_2 v_k &= -q_1^+ r_m \sin \varphi_1^+ \\ q_1^- r_m a_1 \sin \varphi_1^- - q_2^- r_m a_2 \cos \varphi_2^- + (k^+ + 2ik_F z + q_0 r_m) c_2 v_k - (k^- - 2ik_F z - q_0 r_m) d_2 u_k &= 0 \\ q_1^- r_m a_1 \cos \varphi_1^- + q_2^- r_m a_2 \sin \varphi_2^- - (k^+ + 2ik_F z - q_0 r_m) c_1 v_k + (k^- - 2ik_F z + q_0 r_m) d_1 u_k &= 0 \end{aligned}$$

The above 8 × 8 equations are defined for the incident states from the plus branch. In case of incident states from the minus branch, only inhomogeneous term of the above equations is modified. That is, the right hand side of 8 × 8 equations

become $(-\sin \varphi_2^+, -\cos \varphi_2^+, 0, 0, q_2^+ r_m \sin \varphi_2^+, q_2^+ r_m \cos \varphi_2^+, 0, 0)$.

2) case2 : E_F is located at E_c

$$\begin{aligned} b_1 \sin \varphi_1^+ + b_2 \cos \varphi_2^+ - c_1 u_k - d_1 v_k &= -\cos \varphi_1^+ \\ -b_1 \cos \varphi_1^+ + b_2 \sin \varphi_2^+ - c_2 u_k - d_2 v_k &= \sin \varphi_1^+ \\ -a_1 \cos \varphi_1^- + a_2 \cos \varphi_2^- - c_2 v_k - d_2 u_k &= 0 \\ -a_1 \sin \varphi_1^- - a_2 \sin \varphi_2^- + c_1 v_k + d_1 u_k &= 0 \end{aligned}$$

$$\begin{aligned}
& q_1^+ r_m b_1 \sin \varphi_1^+ + q_2^+ r_m b_2 \cos \varphi_2^+ + (k^+ + 2ik_F z - q_0 r_m) c_1 u_k - (k^- - 2ik_F z + q_0 r_m) d_1 v_k = q_1^+ r_m \cos \varphi_1^+ \\
& -q_1^+ r_m b_1 \cos \varphi_1^+ + q_2^+ r_m b_2 \sin \varphi_2^+ + (k^+ + 2ik_F z + q_0 r_m) c_2 u_k - (k^- - 2ik_F z - q_0 r_m) d_2 v_k = -q_1^+ r_m \sin \varphi_1^+ \\
& -q_1^- r_m a_1 \cos \varphi_1^- - q_2^- r_m a_2 \cos \varphi_2^- + (k^+ + 2ik_F z + q_0 r_m) c_2 v_k - (k^- - 2ik_F z - q_0 r_m) d_2 u_k = 0 \\
& -q_1^- r_m a_1 \sin \varphi_1^- + q_2^- r_m a_2 \sin \varphi_2^- - (k^+ + 2ik_F z - q_0 r_m) c_1 v_k + (k^- - 2ik_F z + q_0 r_m) d_1 u_k = 0
\end{aligned}$$

In the same way, these equations are defined for the incident states from plus branch.

For incident states are from the minus branch, only inhomogeneous terms are modified. That is, the right hand side of 8×8 equations become

$$(-\sin \varphi_2^+, -\cos \varphi_2^+, 0, 0, q_2^+ r_m \sin \varphi_2^+, q_2^+ r_m \cos \varphi_2^+, 0, 0)$$

1) case3: E_F is located below E_c

3.1. For $E < E_c$

$$\begin{aligned}
& b_1 \sin \varphi_1^+ + b_2 \cos \varphi_2^+ - c_1 u_k - d_1 v_k = -\cos \varphi_1^+ \\
& b_1 \cos \varphi_1^+ + b_2 \sin \varphi_2^+ - c_2 u_k - d_2 v_k = -\sin \varphi_1^+ \\
& a_1 \sin \varphi_1^- + a_2 \cos \varphi_2^- - c_2 v_k - d_2 u_k = 0 \\
& -a_1 \cos \varphi_1^- - a_2 \sin \varphi_2^- + c_1 v_k + d_1 u_k = 0
\end{aligned}$$

$$\begin{aligned}
& -q_1^+ r_m b_1 \sin \varphi_1^+ + q_2^+ r_m b_2 \cos \varphi_2^+ + (k^+ + 2ik_F z - q_0 r_m) c_1 u_k - (k^- - 2ik_F z + q_0 r_m) d_1 v_k = -q_1^+ r_m \cos \varphi_1^+ \\
& -q_1^+ r_m b_1 \cos \varphi_1^+ + q_2^+ r_m b_2 \sin \varphi_2^+ + (k^+ + 2ik_F z + q_0 r_m) c_2 u_k - (k^- - 2ik_F z - q_0 r_m) d_2 v_k = -q_1^+ r_m \sin \varphi_1^+ \\
& q_1^- r_m a_1 \sin \varphi_1^- - q_2^- r_m a_2 \cos \varphi_2^- + (k^+ + 2ik_F z + q_0 r_m) c_2 v_k - (k^- - 2ik_F z - q_0 r_m) d_2 u_k = 0 \\
& -q_1^- r_m a_1 \cos \varphi_1^- + q_2^- r_m a_2 \sin \varphi_2^- - (k^+ + 2ik_F z - q_0 r_m) c_1 v_k + (k^- - 2ik_F z + q_0 r_m) d_1 u_k = 0
\end{aligned}$$

The above 8×8 equations are for the incident states with momentum $-\bar{q}_1$. For the incident states with momentum \bar{q}_2 , inhomogeneous term of the above equations is modified. That is the right hand side of 8×8 equations become

$$(-\sin \varphi_2^+, -\cos \varphi_2^+, 0, 0, q_2^+ r_m \sin \varphi_2^+, q_2^+ r_m \cos \varphi_2^+, 0, 0)$$

3.2. For $E > E_c$

$$\begin{aligned}
b_1 \sin \varphi_1^+ + b_2 \cos \varphi_2^+ - c_1 u_k - d_1 v_k &= -\cos \varphi_1^+ \\
-b_1 \cos \varphi_1^+ + b_2 \sin \varphi_2^+ - c_2 u_k - d_2 v_k &= \sin \varphi_1^+ \\
a_1 \sin \varphi_1^- + a_2 \cos \varphi_2^- - c_2 v_k - d_2 u_k &= 0 \\
-a_1 \cos \varphi_1^- - a_2 \sin \varphi_2^- + c_1 v_k + d_1 u_k &= 0
\end{aligned}$$

$$\begin{aligned}
q_1^+ r_m b_1 \sin \varphi_1^+ + q_2^+ r_m b_2 \cos \varphi_2^+ + (k^+ + 2ik_F z - q_0 r_m) c_1 u_k - (k^- - 2ik_F z + q_0 r_m) d_1 v_k &= q_1^+ r_m \cos \varphi_1^+ \\
-q_1^+ r_m b_1 \cos \varphi_1^+ + q_2^+ r_m b_2 \sin \varphi_2^+ + (k^+ + 2ik_F z + q_0 r_m) c_2 u_k - (k^- - 2ik_F z - q_0 r_m) d_2 v_k &= -q_1^+ r_m \sin \varphi_1^+ \\
q_1^- r_m a_1 \sin \varphi_1^- - q_2^- r_m a_2 \cos \varphi_2^- + (k^+ + 2ik_F z + q_0 r_m) c_2 v_k - (k^- - 2ik_F z - q_0 r_m) d_2 u_k &= 0 \\
-q_1^- r_m a_1 \cos \varphi_1^- + q_2^- r_m a_2 \sin \varphi_2^- - (k^+ + 2ik_F z - q_0 r_m) c_1 v_k + (k^- - 2ik_F z + q_0 r_m) d_1 u_k &= 0
\end{aligned}$$

The above 8×8 equations are for the incident states with momentum \bar{q}_1 . For the incident states with momentum \bar{q}_2 , inhomogeneous term of the above equations is modified. That is the right hand side of 8×8 equations become

$$\left(-\sin \varphi_2^+, \quad -\cos \varphi_2^+, \quad 0, \quad 0, \quad q_2^+ r_m \sin \varphi_2^+, \quad q_2^+ r_m \cos \varphi_2^+, \quad 0, \quad 0 \right).$$

APPENDIX B

AVERAGE TUNNELING PROBABILITIES

In this appendix, the plots of the angle average of the Andreev reflection (A_1 , A_1' , A_2 and A_2') and normal reflection (B_1 , B_1' , B_2 and B_2') probabilities of 2DEG/S and 2DEG/D junctions as a function of energy are shown. The left (A_1 , A_2 , B_1 and B_2) and right (A_1' , A_2' , B_1' and B_2') panels are the reflection of an incoming electron from plus and minus branches respectively. Note that the energy is in unit of the Fermi energy of the superconductor. The s-wave energy gap and the energy gap maximum of d-wave superconductor are set to be one hundredth of the Fermi energy.

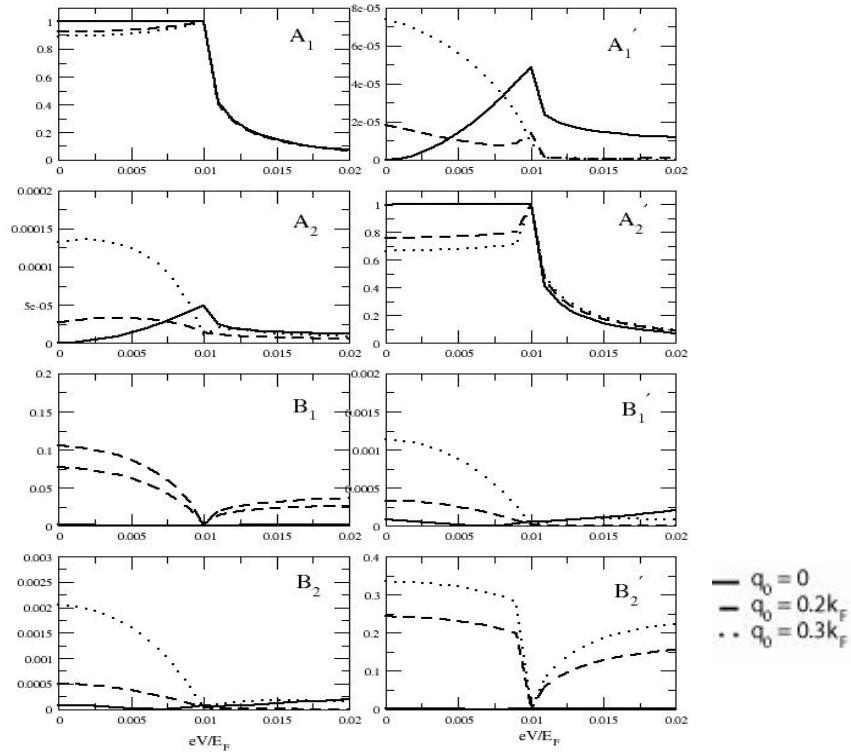


Figure A1 Average tunneling probabilities of 2DEG/S junction (case1) for $r_m = 1$, $z = 0$, $\Delta = 0.01E_F$

Angle Average of Tunneling Probabilities of 2DEG/S Junction: $r_m = 1, z = 1$

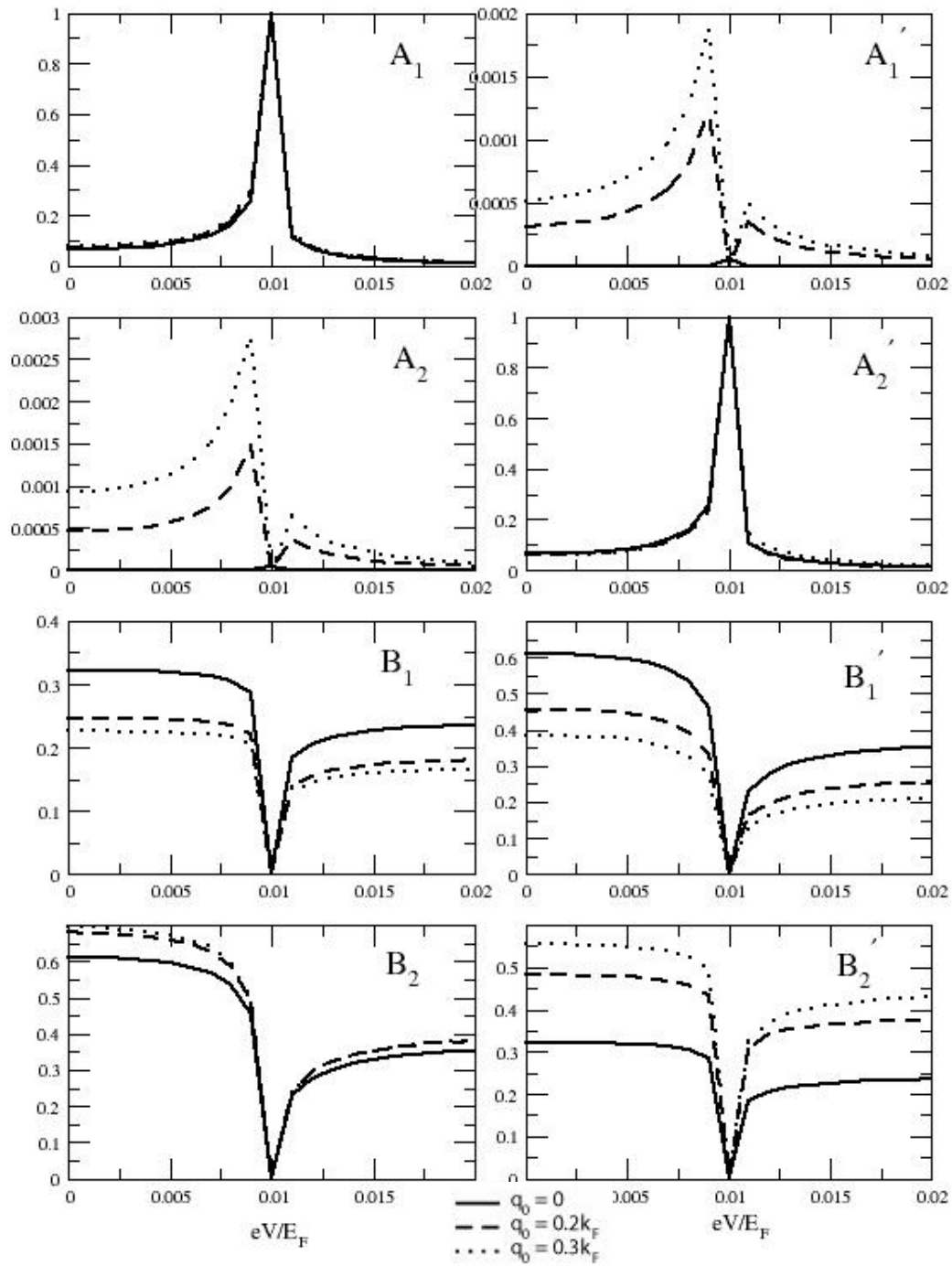


Figure A2 Average tunneling probabilities of 2DEG/S junction(case1) where $r_m = 1$, $z = 1$, $\Delta = 0.01E_F$.

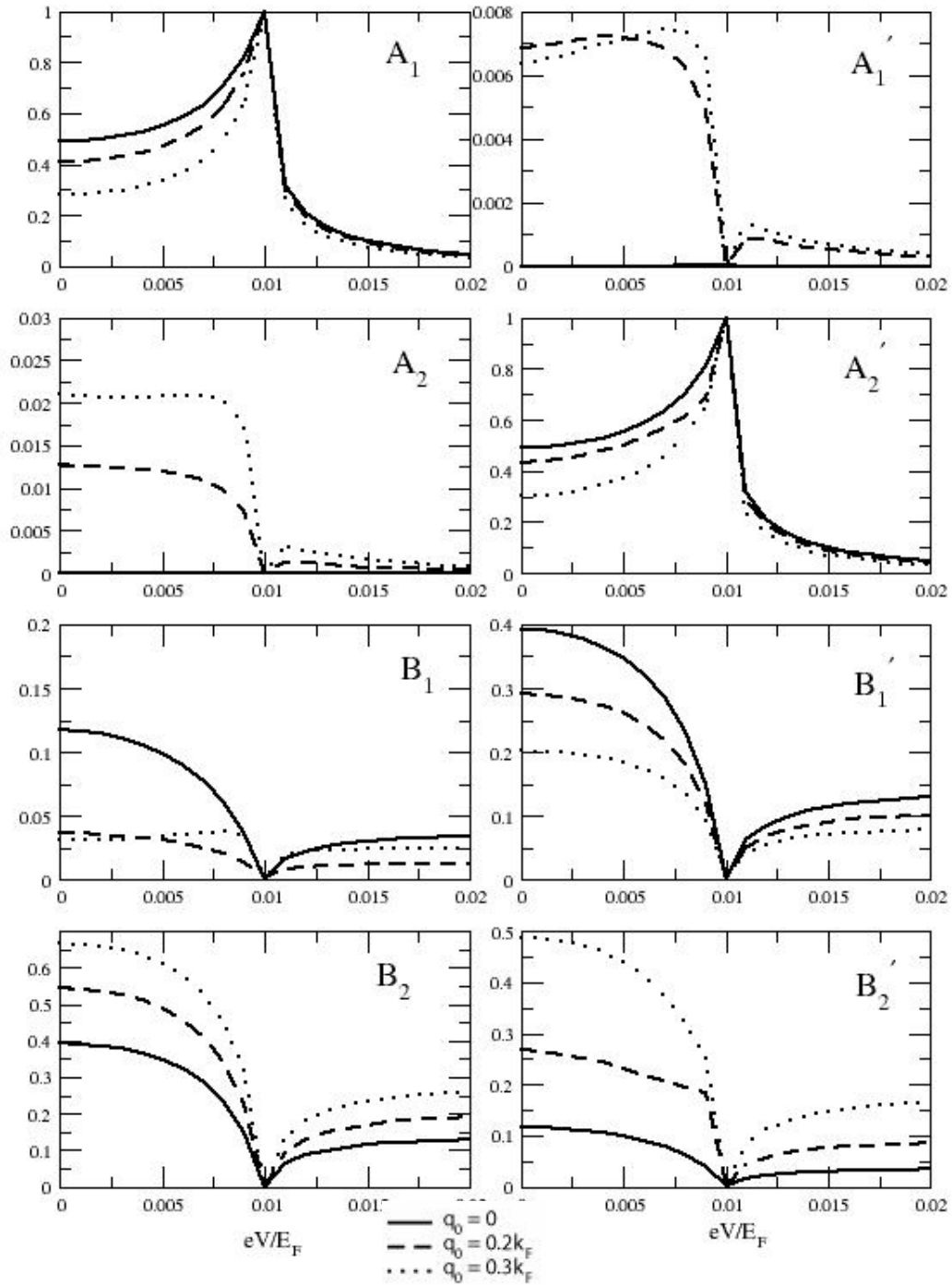
Angle Average of Tunneling Probabilities of 2DEG/S Junction: $r_m = 10, z = 0$ 

Figure A3 Average tunneling probabilities of 2DEG/S junction (case1) where $r_m = 10, z = 0, \Delta = 0.01E_F$.

Angle Average of Tunneling Probabilities of 2DEG/S Junction: $r_m = 10, z = 1$

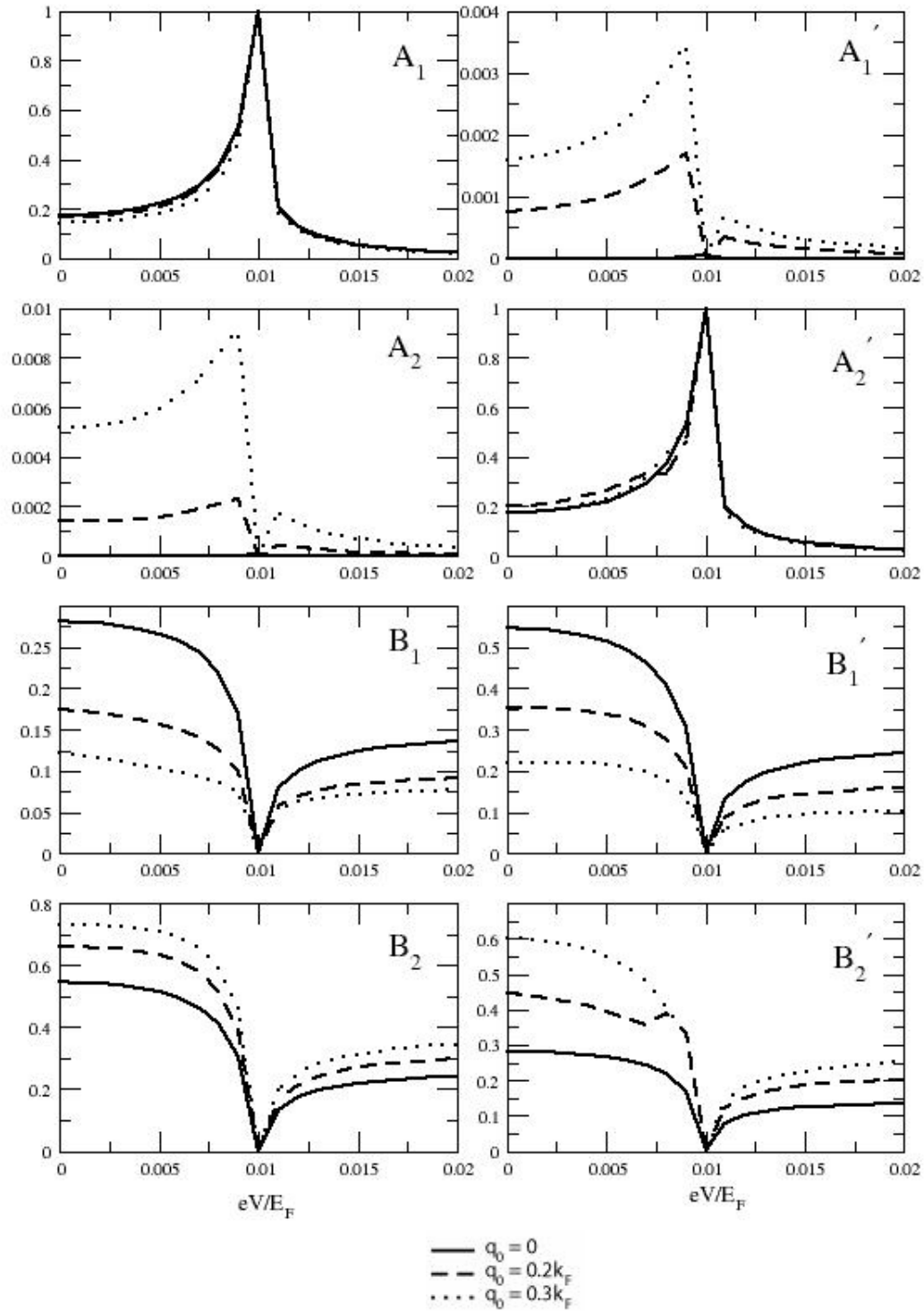


Figure A4 Average tunneling probabilities of 2DEG/S junction (case1) where $r_m = 10, z = 10, \Delta = 0.01E_F$.

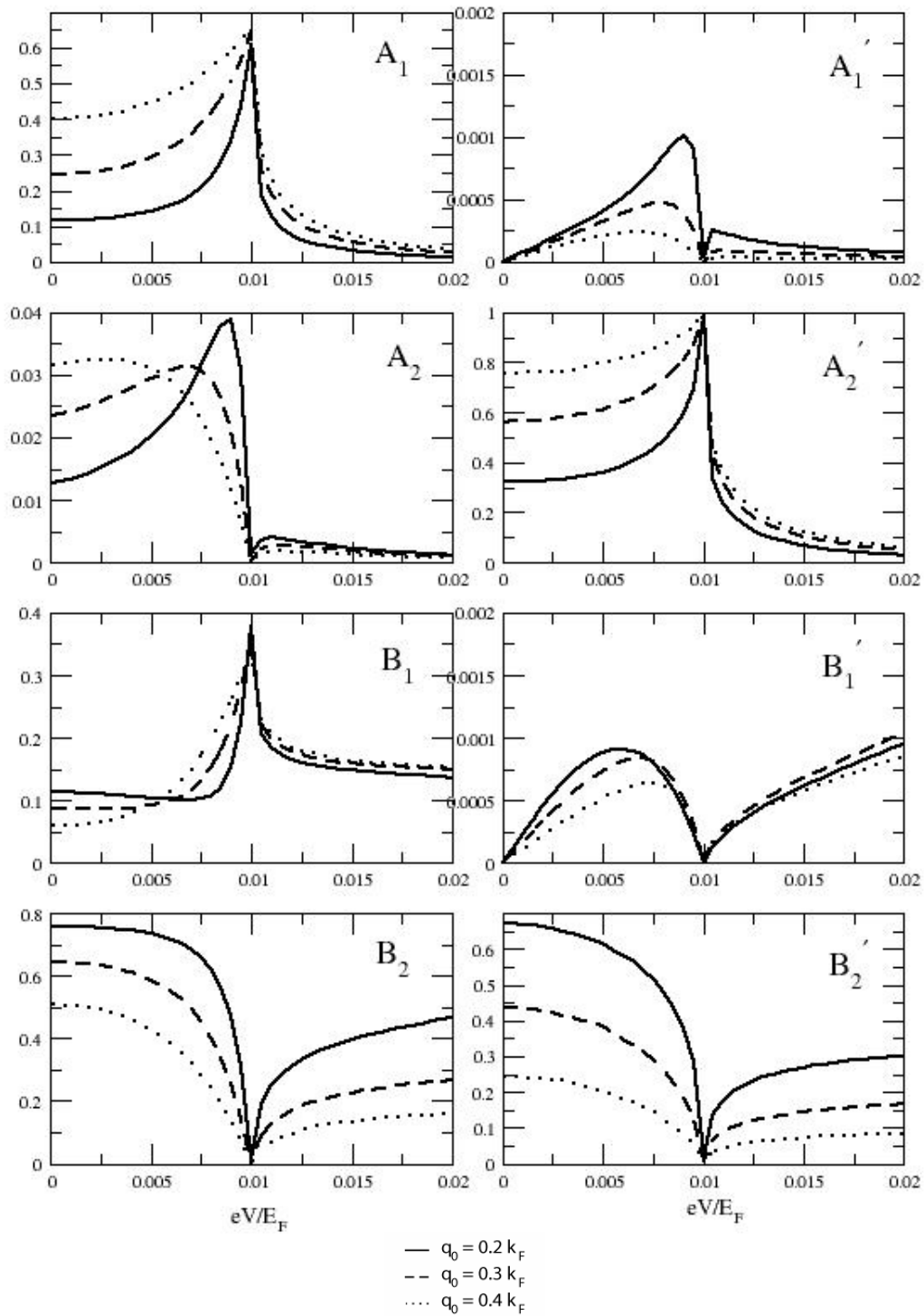
Angle Average of Tunneling Probabilities of 2DEG/S case 2: $r_m = 1, z = 0$ 

Figure A5 Average tunneling probabilities of 2DEG/S junction (case2) where $r_m = 1$, $z = 0$, $\Delta = 0.01E_F$.

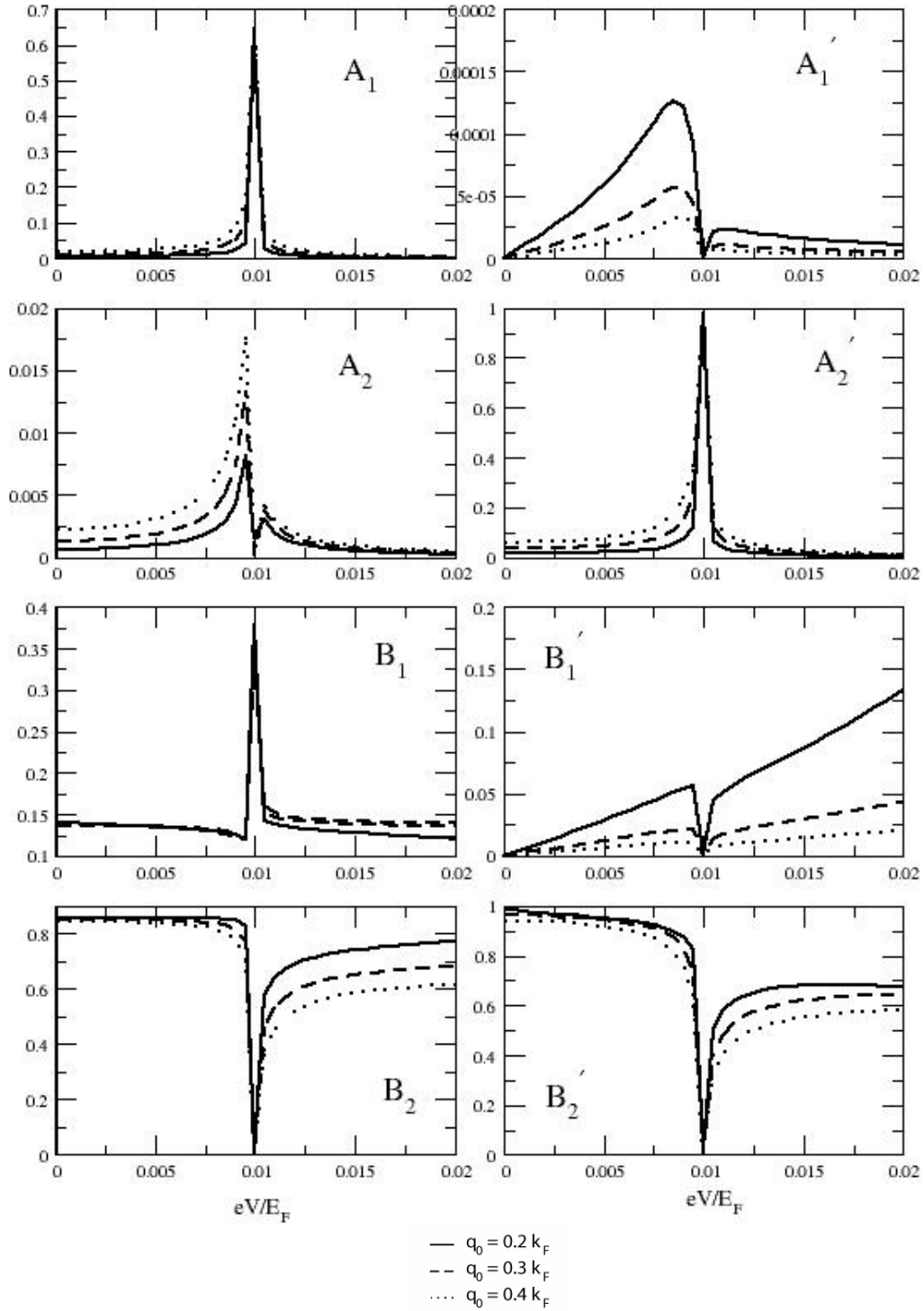
Angle Average of Tunneling Probabilities of case 2DEG/S case 2: $r_m = 1, z = 1$ 

Figure A6 Average tunneling probabilities of 2DEG/S junction (case2) where $r_m = 1$, $z = 1$, $\Delta = 0.01E_F$.

Angle Average of Tunneling Probabilities of 2DEG/S case 3: $r_m = 1, z = 0$

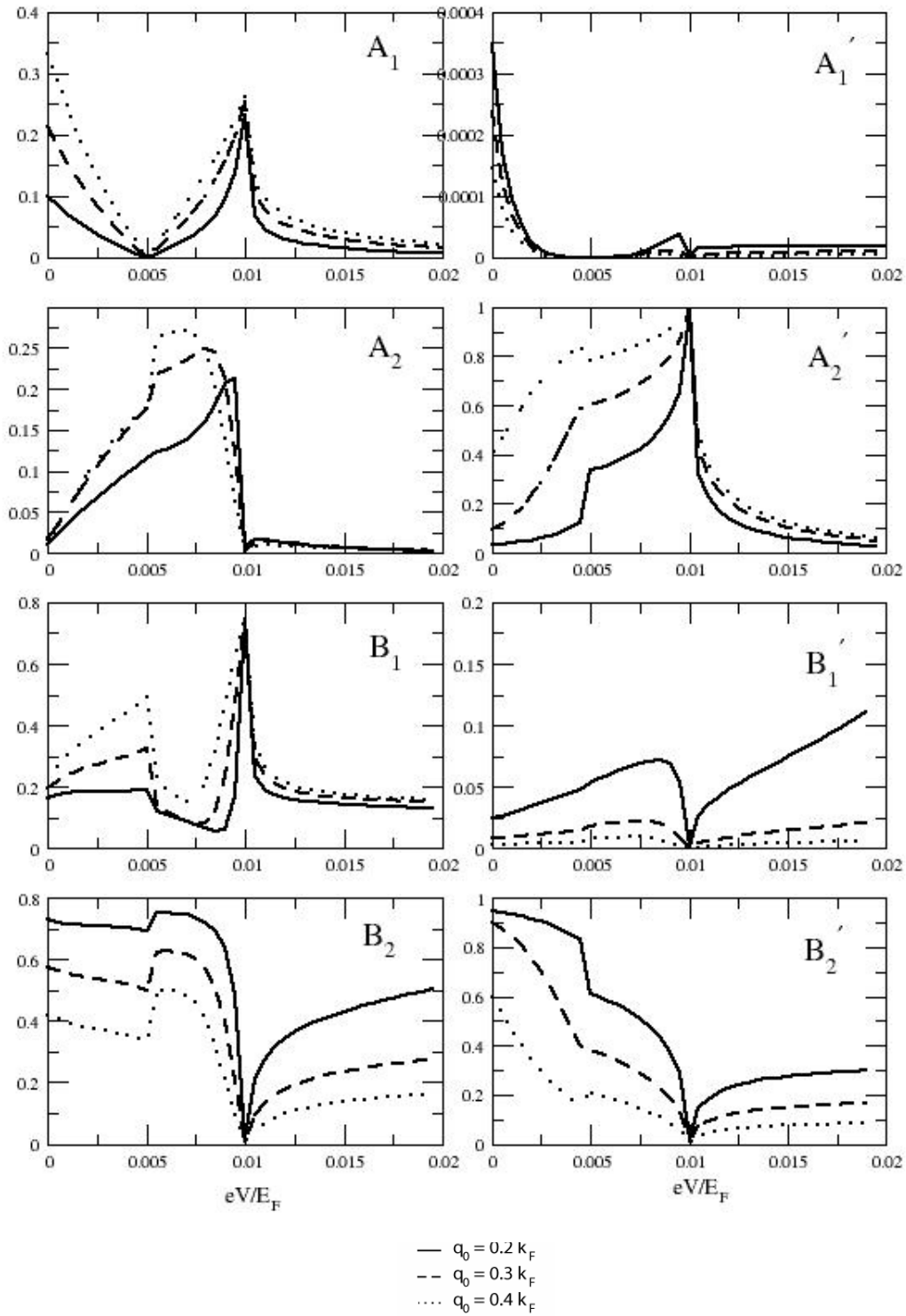


Figure A7 Average tunneling probabilities of 2DEG/S junction (case3) where $r_m = 1$, $z = 0$, $\Delta = 0.01E_F$.

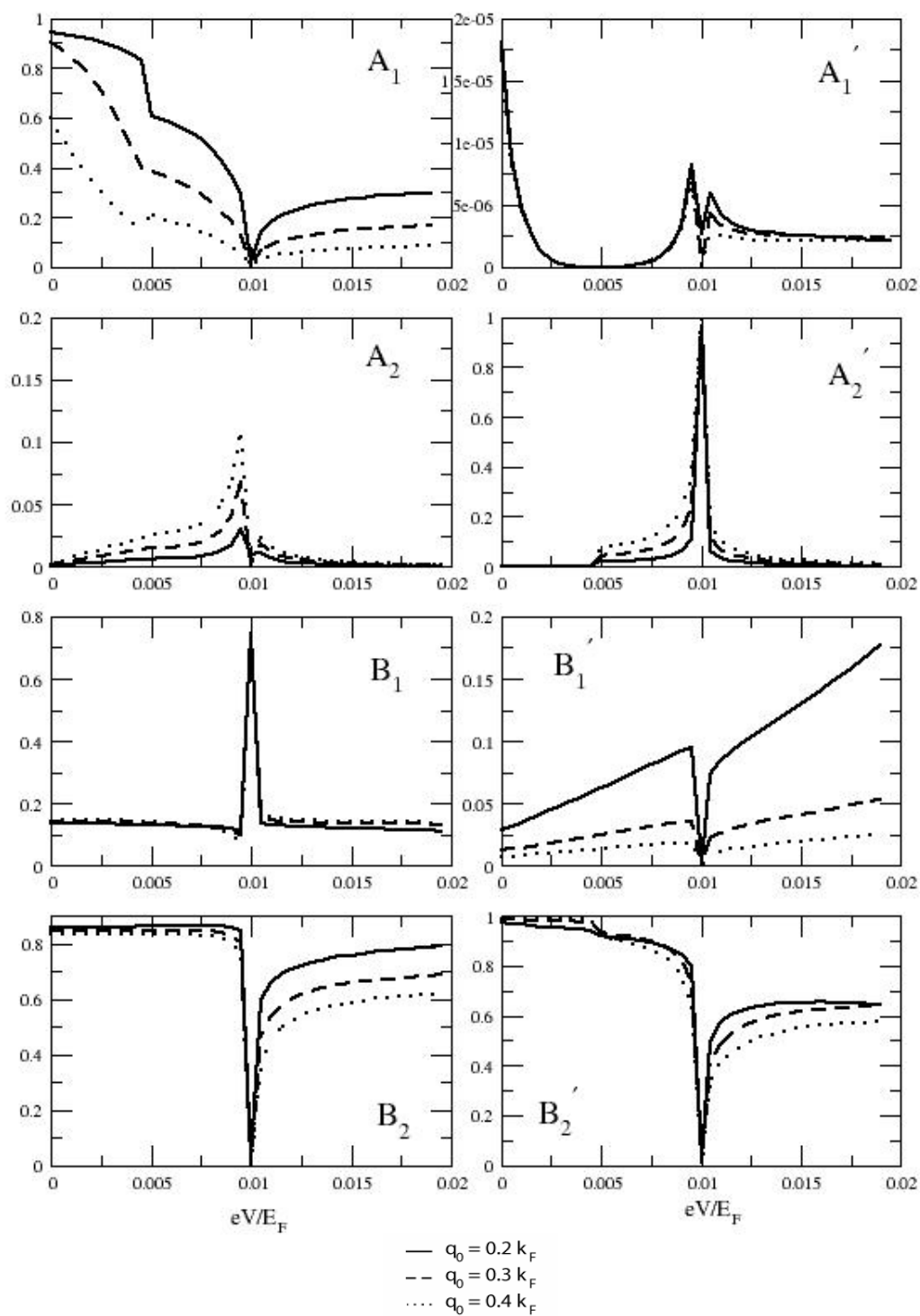
Angle Average of Tunneling Probabilities of 2DEG/S case 3: $r_m = 1, z = 1$ 

Figure A8 Average tunneling probabilities of 2DEG/S junction (case3) where $r_m = 1$, $z = 1$, $\Delta = 0.01E_F$.

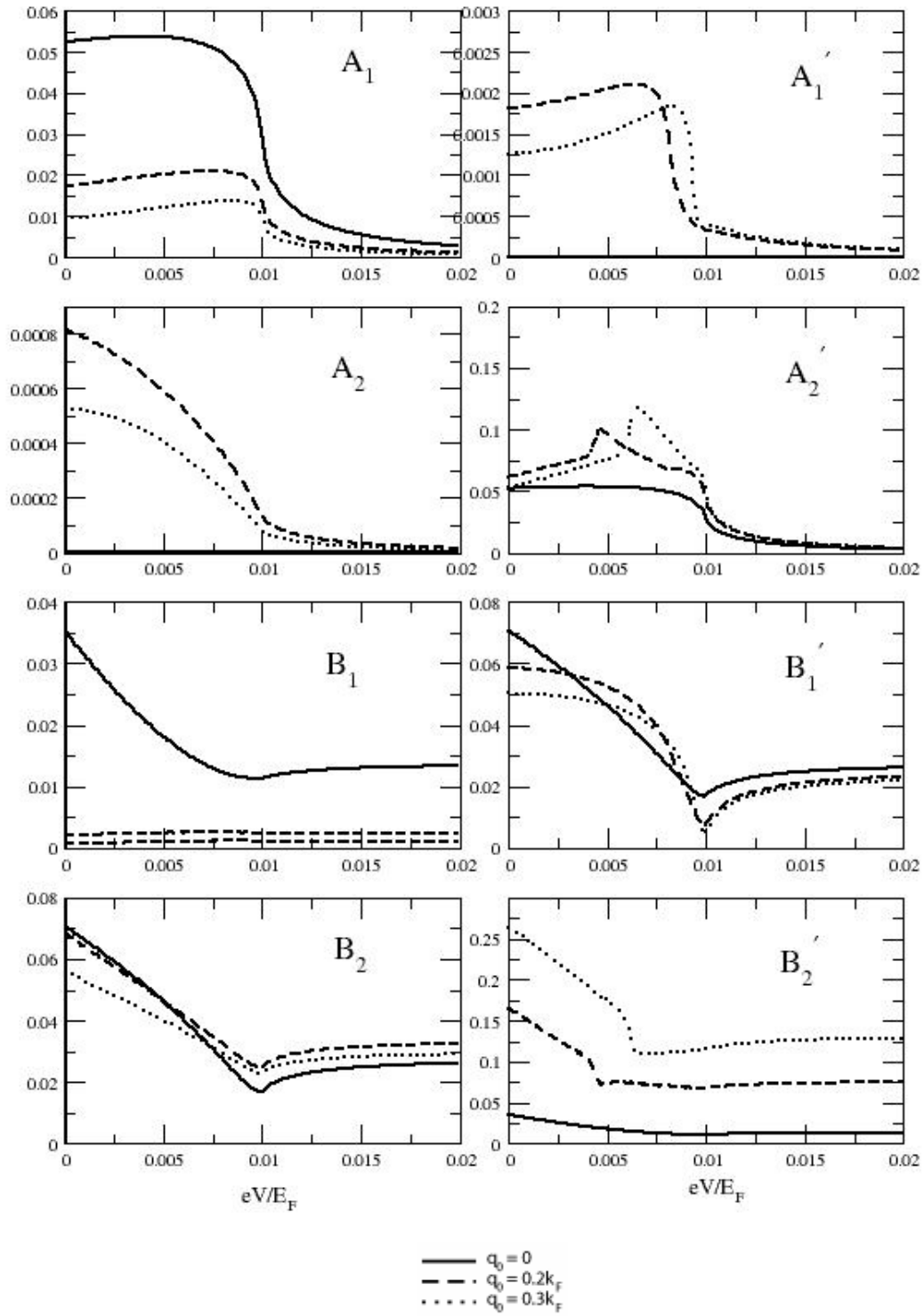
Angle Average of Tunneling Probabilities of case 2DEG/D Junction: $r_m = 10, z = 0$ 

Figure A9 Average tunneling probabilities of 2DEG/D junction (case1) where $r_m = 10, z = 0, \alpha = 0, \Delta = 0.01E_F$.

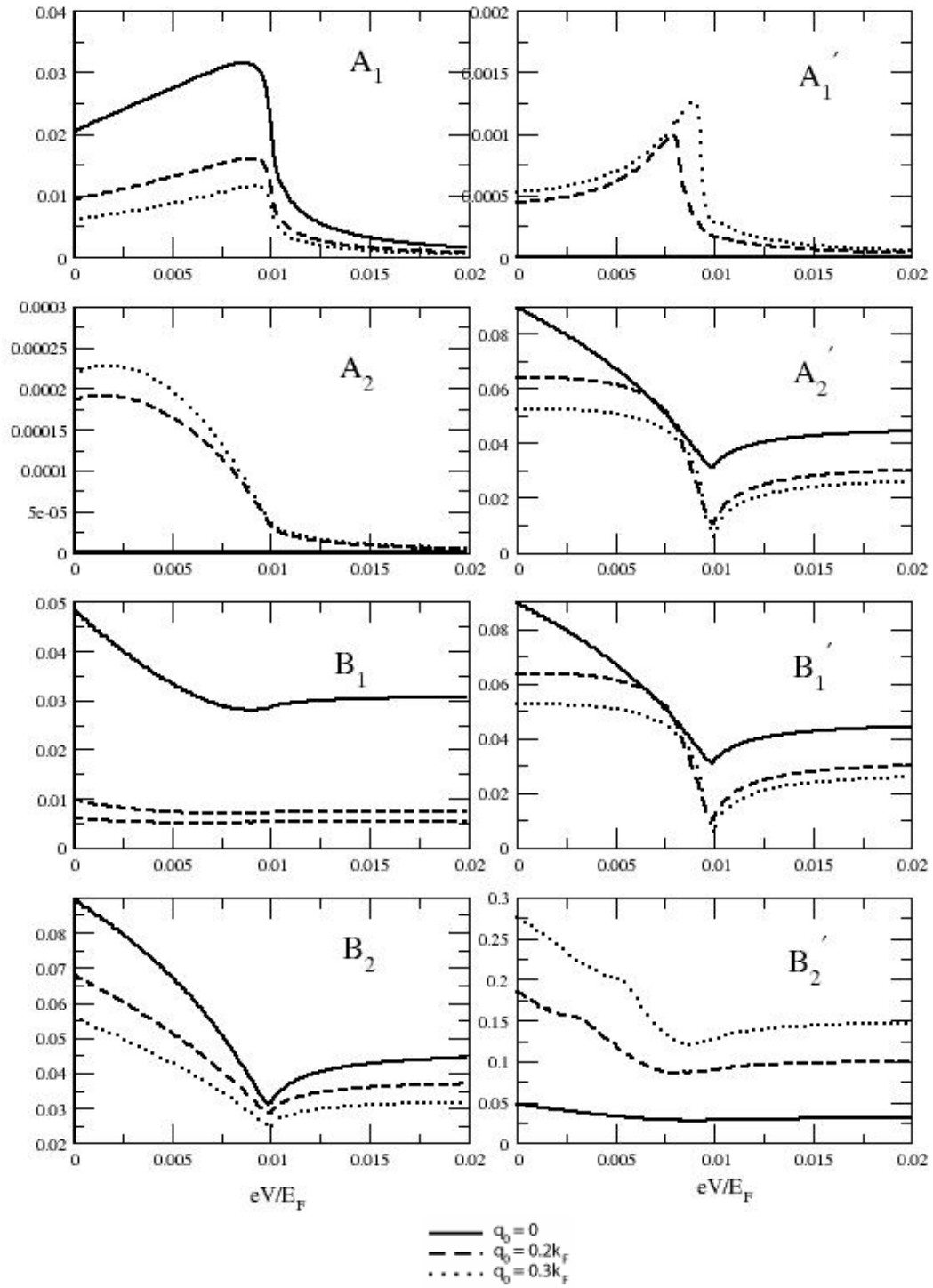
Angle Average of Tunneling Probabilities of case 2DEG/D Junction: $r_m = 10, z = 1$ 

Figure A10 Average tunneling probabilities of 2DEG/D junction (case1) where $r_m = 10, z = 1, \alpha = 0, \Delta = 0.01E_F$.

Angle Average of Tunneling Probabilities of case 2DEG/D Junction: $r_m = 10, z = 0$

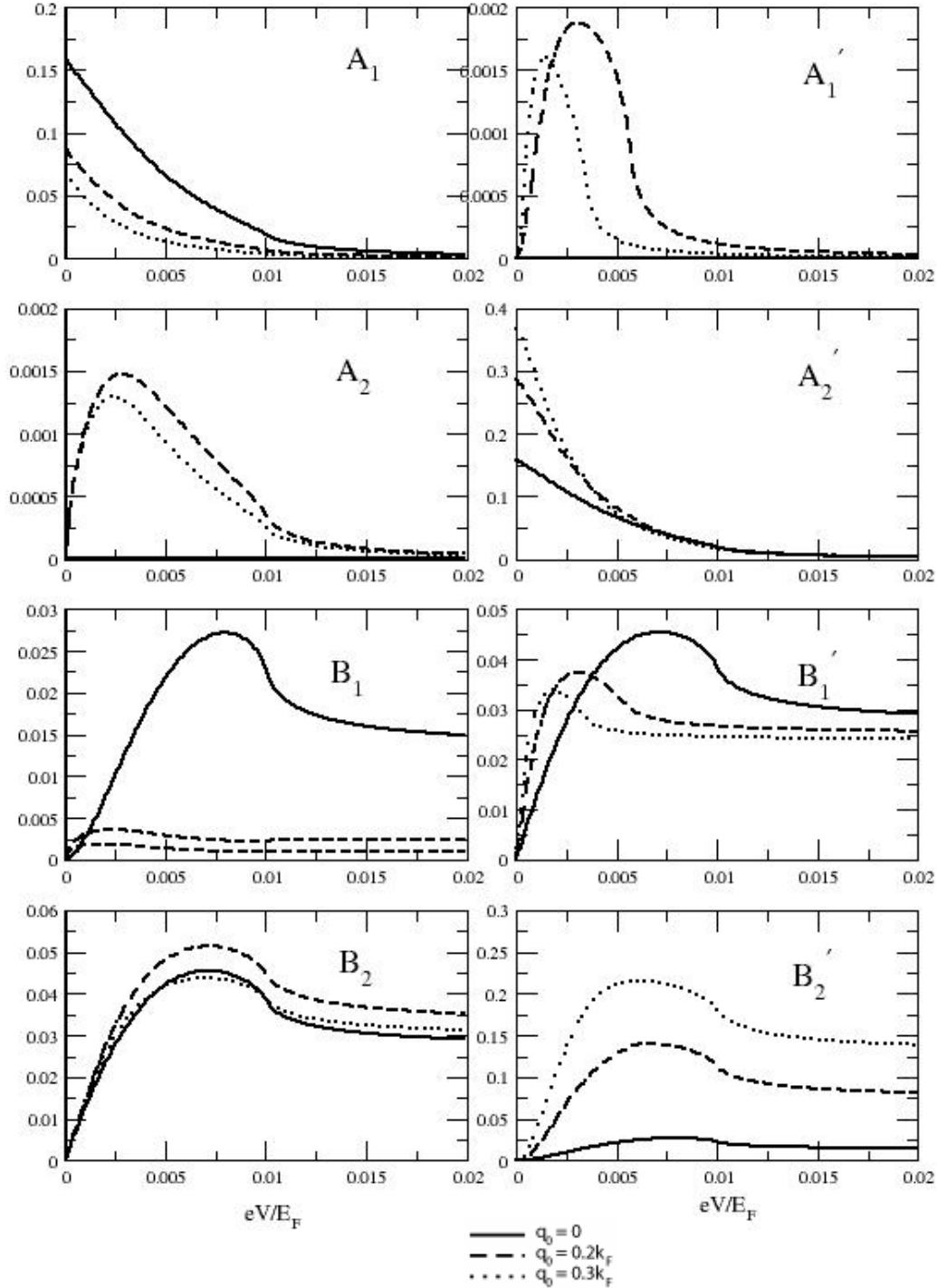
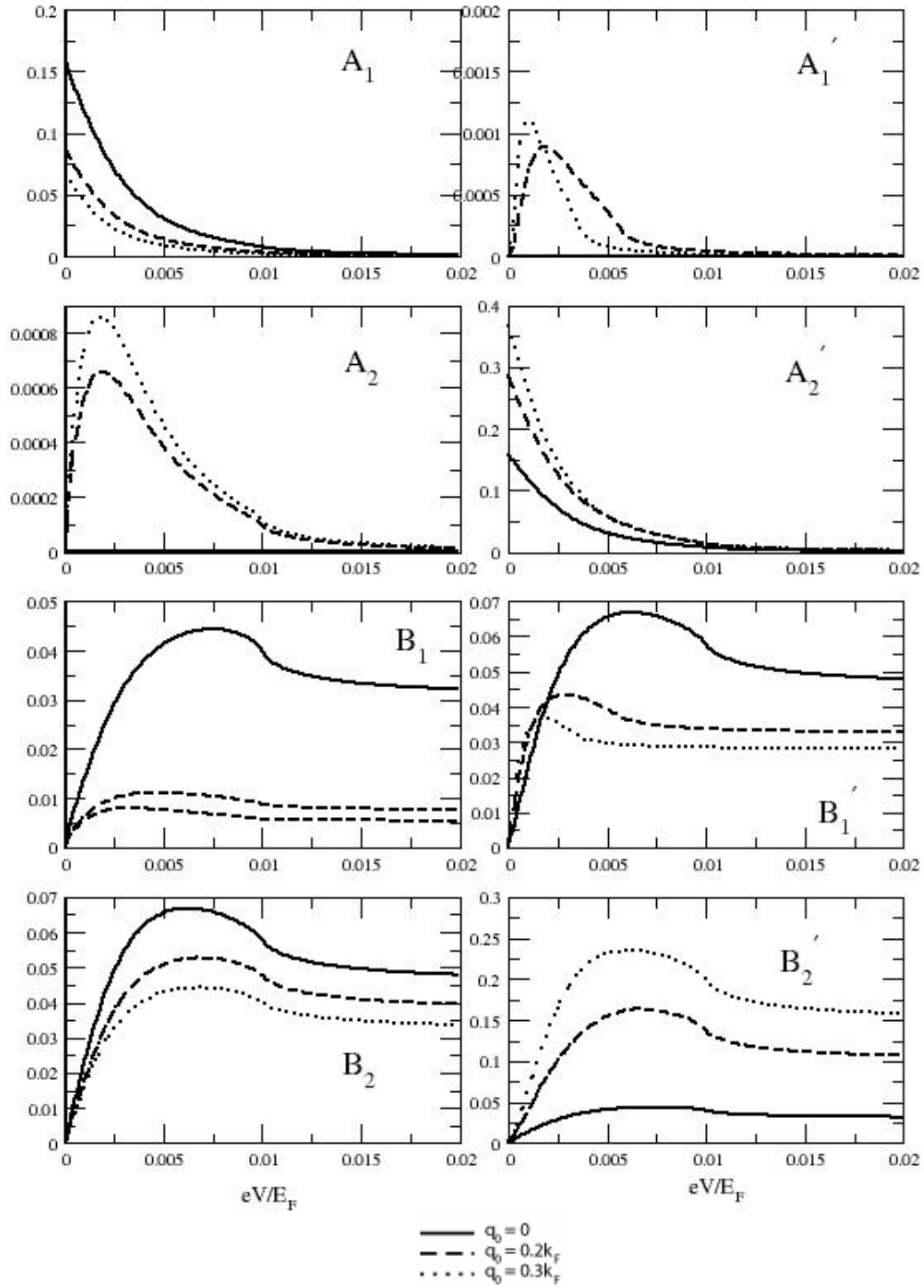


Figure A11 Average tunneling probabilities of 2DEG/D junction (case1) where $r_m =$

$$10, z = 0, \alpha = \frac{\pi}{4}, \Delta = 0.01E_F.$$

Angle Average of Tunneling Probabilities of case 2DEG/D Junction: $r_m = 10, z = 1$ **Figure A12** Average tunneling probabilities of 2DEG/D junction (case1) where $r_m =$

$$10, z = 1, \alpha = \frac{\pi}{4}, \Delta = 0.01E_F.$$

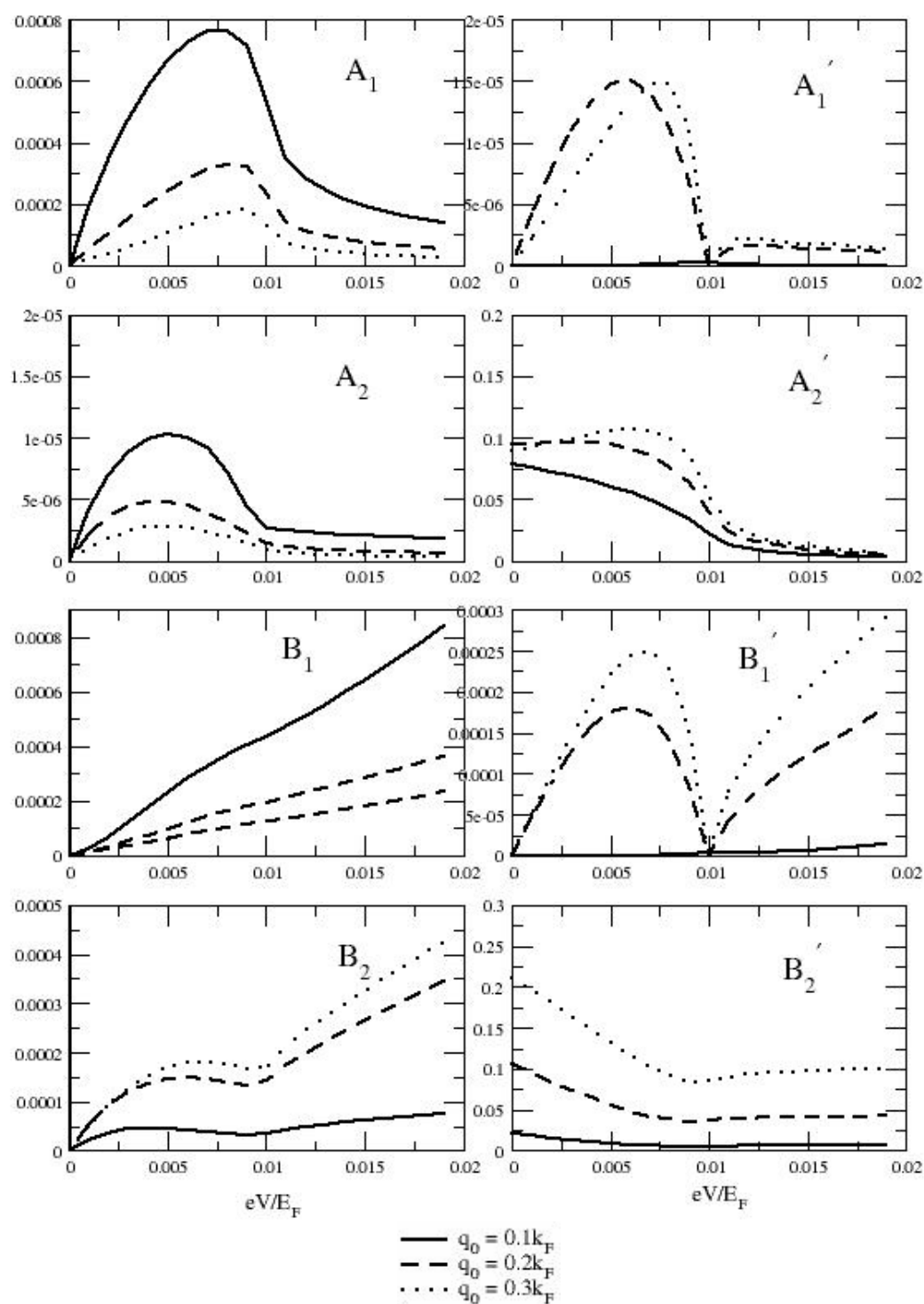
Angle Average of Tunneling Probabilities of 2DEG/D Junction: $r_m = 10, z = 0$ 

Figure A13 Average tunneling probabilities of 2DEG/D junction (case2) where $r_m = 10, z = 0, \alpha = 0, \Delta = 0.01E_F$.

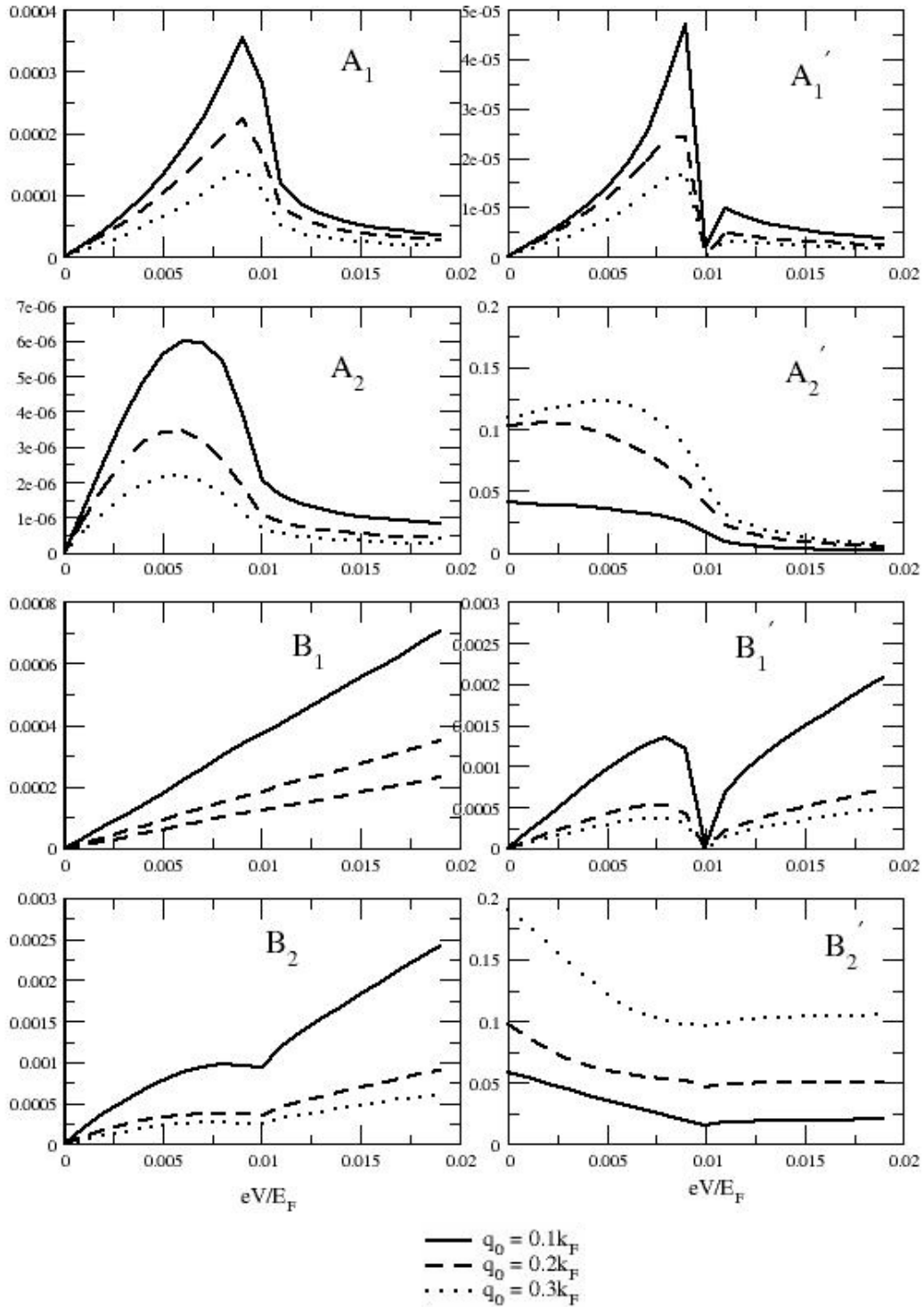
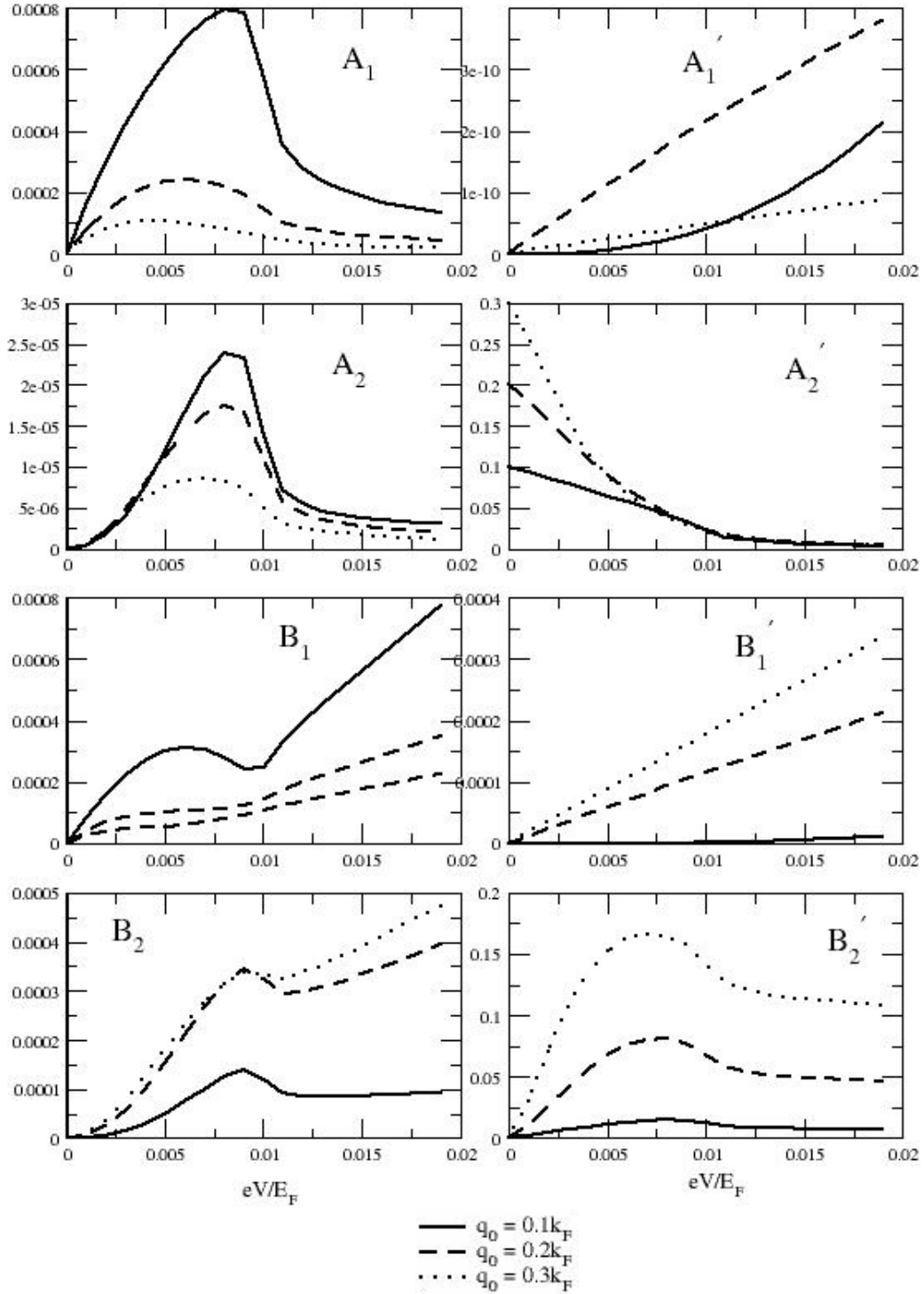
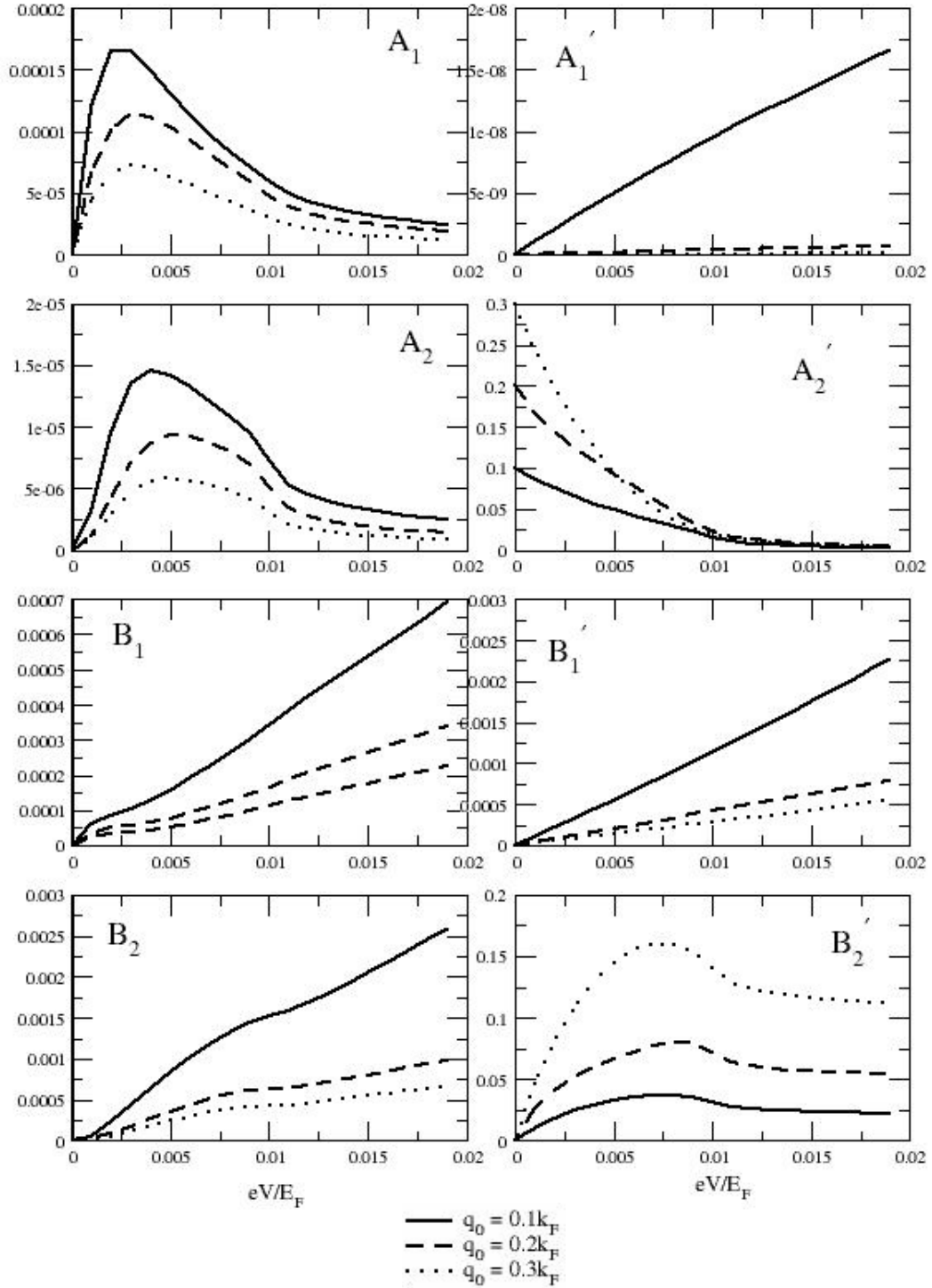
Angle Average of Tunneling Probabilities of 2DEG/D Junction: $r_m = 10, z = 1$ 

Figure A14 Average tunneling probabilities of 2DEG/D junction (case2) where $r_m = 10, z = 1, \alpha = 0, \Delta = 0.01E_F$.

Angle Average of Tunneling Probabilities of 2DEG/D Junction: $r_m = 10, z = 0$ **Figure A15** Average tunneling probabilities of 2DEG/D junction (case2) where $r_m =$

$10, z = 0, \alpha = \frac{\pi}{4}, \Delta = 0.01E_F.$

Angle Average of Tunneling Probabilities of 2DEG/D Junction: $r_m = 10, z = 1$ **Figure A16** Average tunneling probabilities of 2DEG/D junction (case2) where $r_m =$

$$10, z = 1, \alpha = \frac{\pi}{4}, \Delta = 0.01E_F.$$

CURRICULUM VITAE

Miss Benjamat Srisongmuang

Date of birth: 27 July 1976

Place of birth: Kalasin, Thailand

Nationality: Thai

Education

Academic year

1995-1998 Khon Kaen University, Khon Kaen, Thailand.

Bachelor of Science (Physics)

1999-2003 Khon Kaen University, Khon Kaen, Thailand.

Master of Science (Physics)